METAL ION BINDING ON RESUSPENDED SEDIMENT

METAL BINDING ON RESUSPENDED SEDIMENT

By

Susan Jane Fish, B.Sc.H, B.Ed.

A Thesis

Submitted to the School of Graduate Studies

in Partial Fulfilment of the Requirements
for the Degree

Master of Science

McMaster University

MASTER OF SCIENCE (1996)	MCMASTER UNIVERSITY
(Chemistry)	Hamilton, Ontario
TITLE:	Metal binding on resuspended sediment
AUTHOR:	Susan Jane Fish, B.Sc.H, B.Ed. (Queen's University)
SUPERVISOR:	Dr. Pierre Brassard
NUMBER OF PAGES:	xiii, 101

ABSTRACT

Natural organic matter (NOM) on the surface of resuspended particles influences the partition of metal ions between free dissolved organic matter (DOM), and the particulate species. It also affects the size distribution of flocs under agitation. Equilibrium between dissolved organic and particulate organic matter should, therefore, be an important indicator for predicting metal ion exchange.

We examined the exchange of cadmium along a pH edge and compared aqueous, organic, and particulate forms of the metal ion in reactors containing either settled or resuspended sediments. A pH edge profile between 3 and 8 shows two regions of speciation: above and below pH 6.2, which corresponds to a 1 : 1, H : Cd exchange. At low pH, cadmium remains in the free form when sediments are settled, but, upon resuspension, about half of it transfers to the dissolved organic and particulate forms. On the other hand, at high pH, all cadmium is particulate in both cases. In both cases there is also a release of DOM centred at pH 6.2, followed by readsorption at higher pH values.

The interesting finding is that cadmium binding on particles appears independent of the surge in DOM, as though cadmium is weakly bound to DOM and strongly bound to particles. We can assume that two types of organic matter exist, one dissolved, one particulate.

To fix size distribution, the sediment/metal ion mixture was put in a Couette flocculator and subjected to a uniform shear stress. Then, the partitioning of the metal ions between the solution and sediment phases was determined. A distribution coefficient, K_D was calculated for each metal ion. A correlation between log K_D and log K (hydrolysis constant) was apparent, and our data was consistent with the reported metal ion binding to both sediments and artificial surfaces. We envision that organic matter accumulating on the particle creates a polyelectrolyte domain responsible for greater binding capacity. We propose that an increase in metal ion binding with increasing particle size is due to this polyelectrolyte effect, where binding is governed by particle volume, and not surface area.

ACKNOWLEDGEMENTS

Dr. Pierre Brassard

Evadne Macedo
Sue Lantos
Tony Cervinka
Marie Bozzo
Paul Bodurtha

Dr. Hileman

Dr. Kramer and his group
Pam Collins
Jim McAndrew

Engineering Machine Shop - Yosh and Michael
Howard Kettleson
Karen Neumann

Family and friends

NSERC

LIST OF FIGURES

Introduction

Figure I: Collision function vs. particle size for a 25 micron particle (Tsai *et al*, 1987), p. 5.

Figure II: Flux of particle sizes in a water column, p. 8.

Chapter 1

Figure 1.1: A typical pH edge, demonstrating binding capacities for two different metal ions, p. 17.

Figure 1.2: Distortion of pH edge profile for cadmium adsorption on 1 g/L suspended sediments, p. 27.

Figure 1.3: Effect of drift on the cadmium (II) ISE for water and sediment solutions at 10^{-4} M cadmium, both with, and without, a dialysis membrane, p. 28.

Figure 1.4: Calibration without dialysis membrane, p. 30.

Figure 1.5: Calibration with the dialysis membrane, p. 32.

Figure 1.6: Sensitivity analysis for adjusted parameters in Table 1.1, p. 36.

Figure 1.7: Proton and cadmium 1 : 1 Langmuirian exchange, p. 37.

Chapter 2

Figure 2.1: Vacuum filtration vs. reverse filtration, p. 42.

Figure 2.2: Chapter 2 experimental flow diagram, p. 44.

Figure 2.3: Batch experiment results, p. 47.

Figure 2.4: Batch experiment results as combinations of the three pH divisions, and the suspension regimes, p. 48.

Chapter 3

Figure 3.1: The Couette flocculator (Burban and Lick, 1989), p. 56.

Figure 3.2: The Couette flocculator (cross-section and filtration ports), p. 58.

Figure 3.3: Effect of inner cylinder radius on maximum available shear stress for a 0.2 cm annulus, p. 59.

Figure 3.4: Image analysis configuration, p. 61.

Figure 3.5 - Figure 3.9: Chapter 3 experimental flow diagrams, pp. 62-67.

Figure 3.10: Typical particle size distribution from Couette flocculator, p. 69.

Figure 3.11: Floc size (μm)(●), and particle count (■), variations with time for a 1 g/L sediment suspension rotating at a shear stress of 2.2 dyne/cm^2, p. 70.

Figure 3.12: Floc size (μm) variations with shear stress (dyne/cm^2) and suspension concentration, p. 71.

Figure 3.13: Particle size distribution analysis by Hunt (15), Kavanaugh (16), and Filella (17) for a 1 g/L sediment suspension, p. 73.

Figure 3.14: Variation of 50 ppb metal ion cocktail B with time, p. 76.

Figure 3.15: Floc size (μm)(●), and particle count (■), variations with time for a 1 g/L sediment suspended in 500 ppb metal ion cocktail B, rotating at a shear stress of 2.2 dyne/cm^2, p. 78.

Figure 3.16: Floc size (μm) variations with rotation speed for a 1 g/L suspension, p. 79.

Figure 3.17: Comparison of floc size with and without metal ions present, p. 80.

Figure 3.18: Particle size distribution analysis by Hunt (15), Kavanaugh (16), and Filella (17) for a 1 g/L sediment suspension in 500 ppb of metal ion cocktail B, p. 81.

Figure 3.19: Change in free metal ion concentration with increasing floc size for a 1 g/L sediment suspension in 500 ppb of metal ion cocktail B, rotating at a shear stress of 2.2 dyne/cm^2, p. 82.

Figure 3.20: Log K_D versus first hydrolysis constant for metal ions in seawater, p. 84.

Future Work

Figure III: Proposed flow chart describing the procedure required to examine binding in a polyelectrolyte under varying size and ionic strengths, p. 89.

LIST OF TABLES

Table 1.1: Parameter optimization for cadmium adsorption profiles (Equation 3) as biased by electrode fouling, p. 33.

Table 3.1: Metal ion distribution coefficients, p. 83.

LIST OF ABBREVIATIONS

NOM . . . . . natural organic matter
DOM . . . . . dissolved organic matter
P . . . . . a sediment particle
W . . . . . weak cadmium binding organic matter
S . . . . . strong cadmium binding organic matter
ISE . . . . . ion selective electrode
DOC . . . . . dissolved organic carbon
ICP-MS . . . . . inductively coupled plasma - mass spectroscopy

[L] . . . . . fluid length unit
[l] . . . . . particle length unit
[t] . . . . . time unit
G . . . . . parameter representing shear coagulation [L^3 l^{-3} t^{-1}]
K_b . . . . . parameter representing Brownian coagulation [L^3 t^{-1}]
K_{ds} . . . . . parameter representing differential coagulation [L^3 l^{-4} t^{-1}]
S . . . . . parameter representing gravitational settling [L l^{-2} t^{-1}]
r . . . . . radius [l]
υ . . . . . tangential velocity [l t^{-1}]
ω . . . . . angular velocity [t^{-1}]

A . . . . . constant associated with Kavanaugh's (16) particle size distributions
β . . . . . constant associated with Kavanaugh's (16) particle size distributions

$d(d_p)$ . . . . . range of particle diameters
Δd_p . . . . . size interval
$n(d_p)$ . . . . . particle size distribution
N . . . . . number of particles in a particular size interval per unit volume of fluid
ΔT . . . . . time interval (min)

α_a . . . . . collision efficiency factor / stability factor
$\beta_{i,j}$, $\beta_{i,k}$ . . . . . collision frequency functions (cm^3 s^{-1})
Γ_{max} . . . . . total available surface site concentration (M)
μ . . . . . dynamic viscosity (g cm^{-1} s^{-1})
ν . . . . . kinematic viscosity (cm^2 s^{-1})
ρ_f . . . . . fluid density (g cm^{-3})
ρ_p . . . . . particle density (g cm^{-3})
τ_m . . . . . shear stress (dynes cm^{-2})

d_i, d_j, d_p . . . . . particle diameters (cm)
E . . . . . flux of particle volume through a size distribution
f . . . . . rotation frequency (s^{-1})
g . . . . . gravitational acceleration (cm s^{-2})
G . . . . . mean shear velocity gradient (s^{-1})
G_m . . . . . mean velocity gradient
H^+ . . . . . proton concentration
i, j, k . . . . . discrete particle size classes
k . . . . . Boltzman's constant (g cm K^{-1})
K . . . . . stability constant, hydrolysis constant
K_D . . . . . distribution coefficient (L g^{-1})
M_T . . . . . total exchangeable metal ion
n_i, n_j . . . . . number concentration (m^{-3})
R_1, R_2 . . . . . inner and outer cylinder radii (cm)
r^2 . . . . . correlation coefficient
T . . . . . temperature (K)
w_s . . . . . settling velocity (g cm^{-2})

TABLE OF CONTENTS

ABSTRACT iii

ACKNOWLEDGEMENTS iv

LIST OF FIGURES v

LIST OF TABLES viii

LIST OF ABBREVIATIONS iv

INTRODUCTION 1

Theory of the flocculation process 2

Binding theory 12

Thesis overview 14

CHAPTER 1: Development of the methodology to characterize metal ion/proton equilibrium between the sediment surface and the aqueous phase

1.1 Theory 16

1.1.1 pH edge titrations 16

1.1.2 Electrode response interference from NOM 18

1.2 Materials and Methods 19

1.2.1 Sediment samples 19

1.2.2 Solutions 20

1.2.3 pH edge titrations 21

1.2.3.1 Titration instrumentation and procedures 21
1.2.3.2 Electrodes 21
1.2.3.3 The membrane 22
1.2.3.4 Cadmium ISE exposure to sediment: procedures 22

1.3 Results and Discussion 24

1.3.1 Sediment samples 24

1.3.2 Titrations 25

1.3.2.1 Titration instrumentation and procedures 25
1.3.2.2 Cadmium ISE exposure to sediment 25

1.3.3 Effect of electrode drift on adsorption parameters 31

1.3.4 Sensitivity analysis 34

1.3.5 Proton consumption versus cadmium consumption 35

1.4 Conclusions 38

CHAPTER 2: Batch settling experiments: flocculation due to differential settling and pH variation

2.1 Theory 40

2.2 Materials and Methods 41

2.2.1 Humic acid extraction by reverse filtration 41

2.2.2 Batch experiment procedure 42

2.3 Results and Discussion 43

2.3.1 Validation of the reverse filtration technique 43

2.3.2 Batch experiment results 45

2.3.3 The model 46

2.3.4 Simplifying the model 49

CHAPTER 3: Metal ion binding during flocculation under uniform shear stress

3.1 Introduction 52

3.1.1 Design of the apparatus to control shear stress 52

3.2 Materials and Methods 57

3.2.1 The Couette flocculator 57

3.2.2 Floc aggregation/disaggregation analysis 60

3.2.3 Analysis of metal ion binding under shear stress 63

3.2.3.1 System calibration 63
3.2.3.2 Metal ion binding analysis 65

3.3 Results and Discussion 68

3.3.1 Calibration of the apparatus 68

3.3.2 Analysis of metal ion binding under shear stress 72

3.3.2.1 System calibration 74
3.3.2.2 Metal ion binding analysis 77

SUMMARY 87

FUTURE WORK 88

REFERENCES 90

APPENDICES 94

Metal Ion Binding on Resuspended Sediment

INTRODUCTION

The geochemistry of sediments is similar to that of soils. Many of the sediments from natural waters are made up of oxides, hydroxides, or aluminosilicate minerals. Commonly, these particles carry an electrical charge which is the sum of a structural charge and a variable charge. The structural charge is due to the aluminosilicate minerals and is always negative, while the variable charge is due to proton binding to the surface sites. The latter is pH-dependent.

Typically, sediment surfaces exposed to natural waters become coated with a tenacious layer of natural organic matter (NOM) which is mainly composed of humic substances. Humic substances are produced by biological degradation of plant and animal residues and are ubiquitous, existing in all soils, sediments, and natural waters. They are molecularly heterogeneous and no "pure" humic substance has ever been isolated. In general, they are anionic polyelectrolytes of low to moderate molecular weight. They contain both aromatic and aliphatic components and some are surface active (1). Carboxylic acid (-COOH) and phenolic (-OH) groups appear to be the major ionizable functional groups in the organic film as shown by titrations of ionizable surface functional groups (2). By convention, humic substances have been divided into three subfractions by operational definitions. Humic acids are humic substances soluble above pH 2, fulvic acids are soluble under all pH conditions, and humin is not soluble in water at any pH

value (3).

Natural particles typically are close to neutral charge, which allows coagulation to occur since the particles are not significantly repelled by each other and they collapse together. If the surface charge becomes significantly positive or negative, stability is conferred to the particles. Particles are not able to approach each other close enough to cause aggregation and they stay dispersed (4). NOM has been shown to dominate the surface chemistry of the particle it coats. If model particles ranging in surface charge from negative to positive are repeatedly exposed to organic material, the surface becomes increasingly more negative (3, 5 - 9). Generally, coated particles, no matter what the composition of the solid phase, exhibit a net negative charge. Divalent metal cations, (calcium, for example), have been shown to neutralize some of this negative charge, thus, allowing the particles to approach each other more closely, and to aggregate.

The adsorption of surface-active organic matter and divalent metal cations is a significant mechanism controlling the surface chemistry of natural particles. The surface characteristics of the particles will directly affect their interactions with each other during collisions (1).

Theory of the flocculation process

In nature, sediment particles present in natural waters are agitated by wind and currents. As a result, shear stress is applied to the particles and transport occurs. During sediment transport, particles collide with each other causing either aggregation or disaggregation via flocculation processes. Flocculation is a dynamic process where the

state of flocculation depends upon the rates of aggregation and disaggregation of colliding particles (10, 11). These rates depend on state variables such as fluid shear, sediment concentration, dissolved chemicals, salinity, pH, temperature, and the content levels of both organic matter and organisms (12, 13).

There are 3 physical processes of mass transport which result in particle collisions: Brownian diffusion, fluid flow, and differential sedimentation. Brownian diffusion is random motion of small particles brought about by thermal effects. The driving force is a function of Boltzman's constant (1.38×10^{-23} J/K) and temperature (K), and the resistive force is due to viscous drag on the diffusing particles. Transport by Brownian diffusion depends on thermal and viscous effects only and is not dependent on gravity. Particle transport is also affected by both laminar or turbulent fluid flow. Velocity gradients occur in flowing fluids causing particles which follow the motion of the fluid to move at different velocities. These gradients can cause interparticle contacts among particles suspended in the fluid. This type of particle transport depends on the mean velocity gradient in the fluid, G (s^{-1}). Resuspension of sediments by currents or wave action is an example of the effects of fluid flow. Vertical transport due to gravity occurs according to the buoyant weight of particles. Individual particle density causes them to settle at different rates. When large, dense particles collide with smaller or less dense ones, the process is referred to as differential settling/sedimentation.

Only a fraction of particles colliding with each other will stick and cause an increase in the floc size. The probability of cohesion is determined partly by forces between particles. The original collision rate theory is from Smoluchowski (14). He considers that

all particles move in straight lines until contacts occur between them, i.e., a rectilinear model. Smoluchowski develops mass transport coefficients or collision frequency functions ($\beta_{i,j}$, $\beta_{i,k}$) for each type of collision. The rate of aggregation to form a new particle size distribution depends on the sum of these collision functions, the collision efficiency factor (α_a), and the number concentration (n_i, n_j, m^{-3}) of the colliding particles. Equation 1 results from the assumption of conservation of volume.

$$\frac{dn_k}{dt} = \frac{1}{2} \sum_{i+j=k} \alpha_a \beta(i,j) n_i n_j - n_k \sum_{all\ i} \alpha_a \beta(i,k) n_i \qquad (1)$$

Discrete particle sizes of size classes are noted by i, j, and k. The first term on the right of equation 1 represents formation of particles of size "k" by aggregation of two smaller particles whose total volume is that of size "k". This is the coalesced sphere assumption, where pore volume of the aggregate is ignored. The second right-hand term represents the loss of particles of size "k" to form larger flocs by aggregation with particles of any other size. These two terms are equivalent to the change in the concentration of particles of size "k" with time (1).

Figure I shows the relative contribution of each type of mass transport or collision frequency function to the overall function when a 25 μm particle (typical of those in nature) collides with a range of particle sizes (10). The plot of β versus colliding particle size approximates the dominance of a coagulation mechanism over a particle size interval. It demonstrates that Brownian collisions remain insignificant for the considered

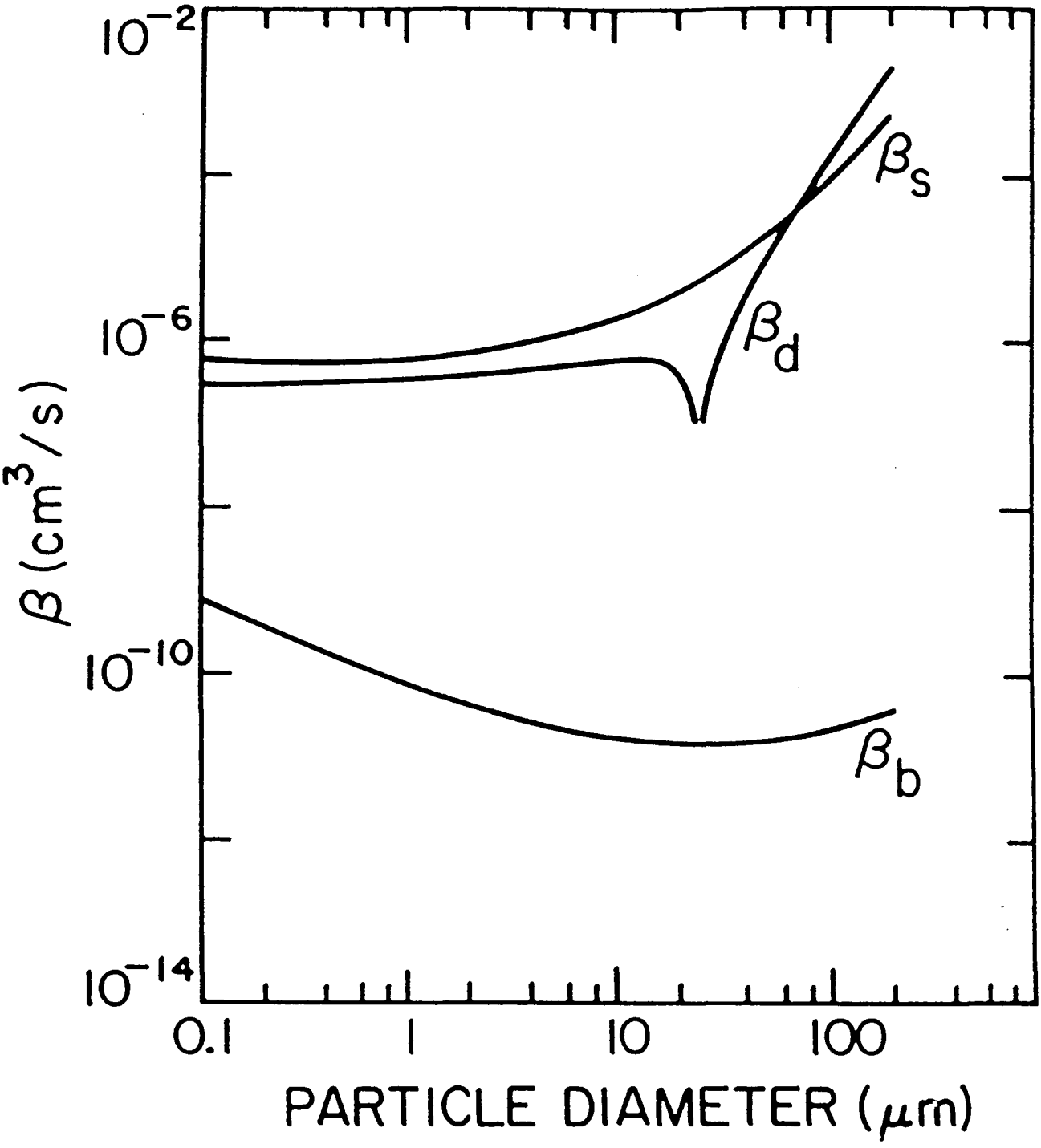

Figure 1: Collision function versus particle size for a 25 micron particle (Tsai *et al*, 1987).

particle size range, since the β_B contribution is relatively low (about 10^{-10}). Shear collisions prevail for the most part ($\beta_S = 10^{-6}$ to 10^{-4}), and only after the test particle starts colliding with particles greater than its own size do contributions due to differential settling dominate.

Smoluchowski's mass transport coefficients for the three transport processes are as follows (10):

Brownian

$$\beta_{ij} = \frac{2}{3} \frac{kT}{\mu} \frac{(d_i + d_j)^2}{d_i d_j} \qquad (2)$$

Fluid shear

$$\beta_{ij} = \frac{G}{6} (d_i + d_j)^3 \qquad (3)$$

Differential settling

$$\beta_{ij} = \frac{\pi g}{72\mu} \frac{(\rho_p - \rho_f)}{\rho_f} (d_i - d_j)^2 (d_i^2 - d_j^2) \qquad (4)$$

Symbol identification is noted below.

k = Boltzman's constant (g cm K^{-1})	T = temperature (K)
μ = viscosity (g cm^{-1} s^{-1})	d_i, d_j = particle diam. (cm)
g = gravitational accel. (cm s^{-2})	ρ_p= particle density (gcm^{-3})
G = mean shear velocity gradient (s^{-1})	ρ_f = fluid density (gcm^{-3})

Smoluchowski's model makes two main assumptions: rectilinear motion and coalesced spheres. Hydrodynamic interactions and short range forces are neglected by the rectilinear model which, if considered, would reduce the frequency of collision from that predicted by Smoluchowski's equations. If it is assumed that particle volume is conserved upon collision, the actual collision rate is underestimated. During coagulation,fluid would be incorporated into the pores which would increase the effective target volume available for collisions. Together, they produce opposite effects on aggregation rates. With further analysis, it has been suggested that Smoluchowski's equations produce a reasonable representation of the initial contact rates in laboratory studies where monodisperse suspensions are used (3). For natural polydisperse suspensions, the model deviates from the observed results. The parameters are then defined operationally. Successful fittings are obtained assuming tertiary collisions instead of binary collisions (13).

Only a fraction of collisions will result in aggregation. The adsorption of humic substance onto the particle surface has been shown to produce colloidal stability, while divalent metal cations in natural waters destabilize colloids. These patterns are often observed but, as of yet, have not been well explained. Typically, the colloidal stability of

suspended particles is defined by a sticking, or stability factor, α_a:

$$\alpha_a = \frac{\textit{rate at which particles attach}}{\textit{rate at which particles collide}} \qquad (5)$$

The stability factor is described by the ratio of the collision rate producing aggregates to the total rate at which collisions occur by all three types of mass transport. If all collisions are unsuccessful, $\alpha_a = 0$; if all collisions result in aggregation, $\alpha_a = 1$. Both attachment and collision rates can be determined experimentally to give values for α_a. They may be estimated by use of mass transport theories for special cases. The accuracy of these estimations depends on the mass transport process used and the experimental conditions defined (2).

As an example, Hunt (15) considers a water column with an influx of particles of certain size, due to aggregation processes, and an outflux of that size due to sedimentation (See Figure II).

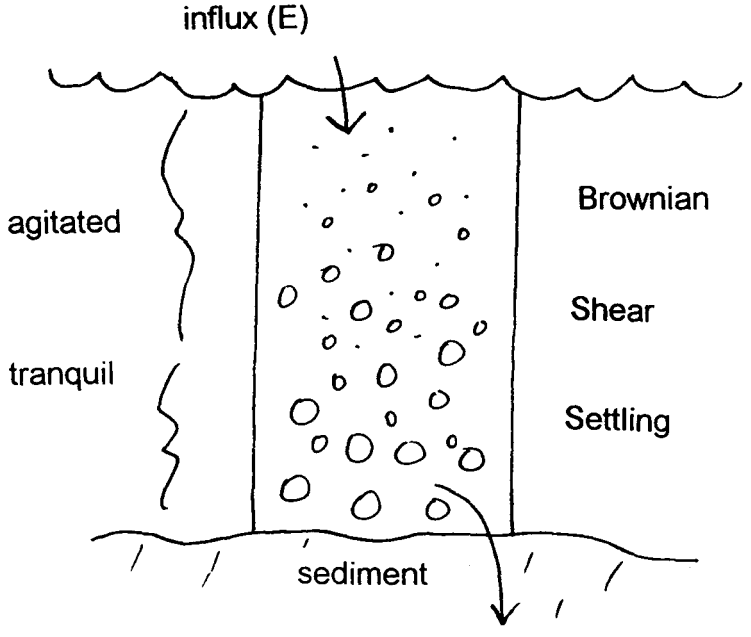

Figure II: Flux of particle sizes in a water column.

The flux is governed by Stoke's settling:

$$\frac{g}{18v}\left(\frac{\rho_p - \rho_f}{\rho_f}\right) d_p^2\, n(d_p)d(d_p) \qquad (6)$$

He assumed only one coagulation or sedimentation mechanism dominates over a particular range of particle size: Brownian (< 1 μm), shear (1 to 100 μm), or differential settling (>100 μm). A steady state assumption is made which implies a constant flux of particle volume through the distribution that is equal to both the rate of formation of small particles and to the rate of large particle removal by sedimentation. For each small interval of particle size, the rate of particle volume transferred into the size interval is balanced by either the volume coagulated from the interval or the particle volume lost from the fluid volume by sedimentation. Hunt (15) also assumes that the particle size distribution is a function of the following six variables: particle diameter (d_p), flux of particle volume through the distribution (E), parameters representing Brownian coagulation (K_b), shear coagulation (G), differential-sedimentation coagulation (K_{ds}), and gravitational settling (S). The following coagulation and sedimentation expressions were obtained from the constants found in Smoluchowski's β equations and Hunt's sedimentation flux equation:

Brownian

$$K_b = \frac{kT}{\mu} \qquad [L^3 t^{-1}] \qquad (7)$$

Shear

$$G \qquad [L^3 l^{-3} t^{-1}] \qquad (8)$$

Differential sedimentation:

$$K_{ds} = \frac{g}{v}\left(\frac{\rho_p - \rho_f}{\rho_f}\right) \qquad [L^3 l^{-4} t^{-1}] \qquad (9)$$

Settling:

$$S = \frac{g}{v}\left(\frac{\rho_p - \rho_f}{\rho_f}\right) \qquad [L l^{-2} t^{-1}] \qquad (10)$$

The parameters for differential sedimentation coagulation and settling have the same grouping of constants but different units because differential sedimentation is second order in the particle size distribution while gravitational settling is first order in the size distribution. The resulting particle size distribution has the following functional form:

$$n = n(d_p, E, K_b, G, K_{ds}, S) \quad (11)$$

For each range of particle size where one coagulation mechanism or gravitational sedimentation is dominant, Hunt used dimensional analysis to group the variables into a unique non-dimensional expression. The resulting particle size distributions for gravitational settling and for each coagulation mechanism were all of the following general form:

$$n(d_p) = Ad_p^{-\beta} \quad (12)$$

and,

$$n(d_p) = \frac{\Delta N}{\Delta d_p} \quad (13)$$

where, Δ N is the number of particles with a diameter in the size interval Δ d_p per unit volume of fluid and A and β are constants. Thus,

$$\frac{\Delta N}{\Delta d_p} = Ad_p^{-\beta} \quad (14)$$

It has been shown that this hyperbolic power law relationship characterizes a large number of particulate systems, including natural and waste water (16, 17). If the log of the number of particles with a diameter in the size interval per unit volume of fluid is plotted versus the log of that particle size, the resulting slope corresponds to the β constant from equation

12. In several cases, β values have been equated to the dominant collision types (15, 16, 17).

Hunt, Kavanaugh, and Filella (15, 16, 17) studied freshwater, waste water, and ocean water sediments to determine the major source of collisions in sediment suspensions. Kavanaugh (16) examined particles larger than one micron that are found in several low ionic strength environments, and found values of β ranging from 1.8 to 4.5 for these suspensions. He suggests that extrapolation of the power law function below sub micron sizes is not reasonable. This type of analysis will be used to assess our particle size distributions.

Binding theory

Macroscopically, sediment can be considered as a weakly acidic material in equilibrium in solution. To characterize the binding of protons and metal ions on a sediment surface, a sediment suspension, spiked with a known concentration of metal ion, is titrated with either base or acid to increase or decrease the pH in constant steps, and at a constant time interval. The free metal ion concentration at each step is measured and plots of its value *versus* pH are prepared. These are identified as "pH edge" titrations. From the results of pH edge titrations, it has been determined that adsorption on surfaces is typically a Langmuirian exchange between protons and free metal ions. Fu and Allen (18) tested adsorption models based on both 1:1 and 2:1 exchanges and found the predominant sites to follow a 1:1 exchange. Ignoring electrostatic terms, Fu *et al* (18)

found correlation coefficients ranging from 0.993 to 0.999 for four different sediment types. Bourg and Mouvet (19) also found predominantly 1:1 exchanges for copper (II), zinc (II), and cadmium (II) ions. Also ignoring electrostatic terms, we therefore assume:

$$=SOH + M^{2+} \rightleftharpoons =SOM^{+} + H^{+}$$

where: (15)

$$K = \frac{[H^{+}][SOM^{+}]}{[M^{2+}][SOH]}$$

The resulting Langmuirian profile for adsorbed metal ion is as follows:

$$\Gamma = [M_T] - [M^{2+}] = \frac{\Gamma_{MAX}\,[M^{2+}]}{\frac{[H^{+}]}{K} + [M^{2+}]} \qquad (16)$$

where Γ_{max} is the total available surface site molar concentration, K is the stability constant, $[M_T]$ represents total exchangeable metal ion, H^+ is the proton concentration, and Γ is bound metal. A Levenberg-Marquard minimization method of non-linear curve fitting can be used to obtain optimized values for a binding constant for metal ion adsorption from the resulting pH edge titrations.

Typically, surface binding models have been used to explain the affinity of metal ions to sediments. Brassard *et al* (20) have shown a large contribution of measured binding to a sediment surface to be due to a Donnan type domain, which indicates that two types of binding occur on particles: an ampholytic surface site (21) and a polyelectrolyte

domain (22, 23). Consider a polyelectrolyte to be a charged domain created by a matrix of active sites. The accumulation of charge inside the polyelectrolyte domain creates a Donnan potential relative to the bulk solution outside. The diffusion of protons and metal ions to the organic matter inside the domain, not to the surface, determines the apparent binding constant, K. If the amount of organic matter in the domain increases, both the volume, and the number of binding sites increase. It follows that more binding will occur with an increase in volume, and not with an increase in surface area (22, 23).

Thesis overview

The objective of this study is to evaluate the hypothesis that metal ion binding on a sediment surface is influenced by particle aggregation and disaggregation.

Chapter one describes experiments designed to determine the type and extent of binding that occurs between metal ions and the sediment. Problems associated with using ion-selective electrodes (ISE) in sediment solutions to measure the free metal ion concentration are resolved, because the very process by which organic matter coats particles is also responsible for fouling on the surface of an ISE.

The remainder of the thesis describes the experiments designed to test the hypothesis that changes in a particle size distribution will affect metal ion binding. Chapter two deals with size distribution changes during settling and resuspension. The approach is to determine the difference in metal and DOM partitioning between a settled and a resuspended sediment.

Chapter three deals with experiments designed to measure changes in metal ion

binding during flocculation of a sediment suspension mixed with a metal ion cocktail subjected to a uniform shear stress. The partitioning of each metal ion species between the solution and sediment phases was determined by ICP-MS.

Results of studies on metal ion binding during flocculation suggest that binding is more affected by the volume of the particle, rather than its surface, as would be the case if only surface exchange took place. The effect of a volume controlled binding means that large natural particles can also play an important role as accumulator of metal ions and that the apparent binding results from penetration of the metal ion into the particles, as would be the case in a polyelectrolyte domain.

CHAPTER 1

DEVELOPMENT OF THE METHODOLOGY TO CHARACTERIZE METAL ION/PROTON EQUILIBRIUM BETWEEN THE SEDIMENT SURFACE AND THE AQUEOUS PHASE

(submitted to Talanta: Chemical Sensors)

1.1 THEORY

1.1.1 pH Edge Titrations

A pH edge titration is often performed to characterize the equilibrium between protons and metal ions on a sediment surface and the aqueous phase. As described, a sediment suspension containing a known concentration of metal ion, is titrated with either strong acid or strong base over the full pH range in constant steps, and at a constant time interval per step. The pH and the free metal ion concentration are measured with ion selective electrodes (ISE). As the total metal ion concentration remains constant, the bound metal ion is determined by difference. The extent of metal ion binding tends to increase with pH, with an inflection dependent on the binding capacity of the substrate. A typical pH edge for two different metal ions follows:

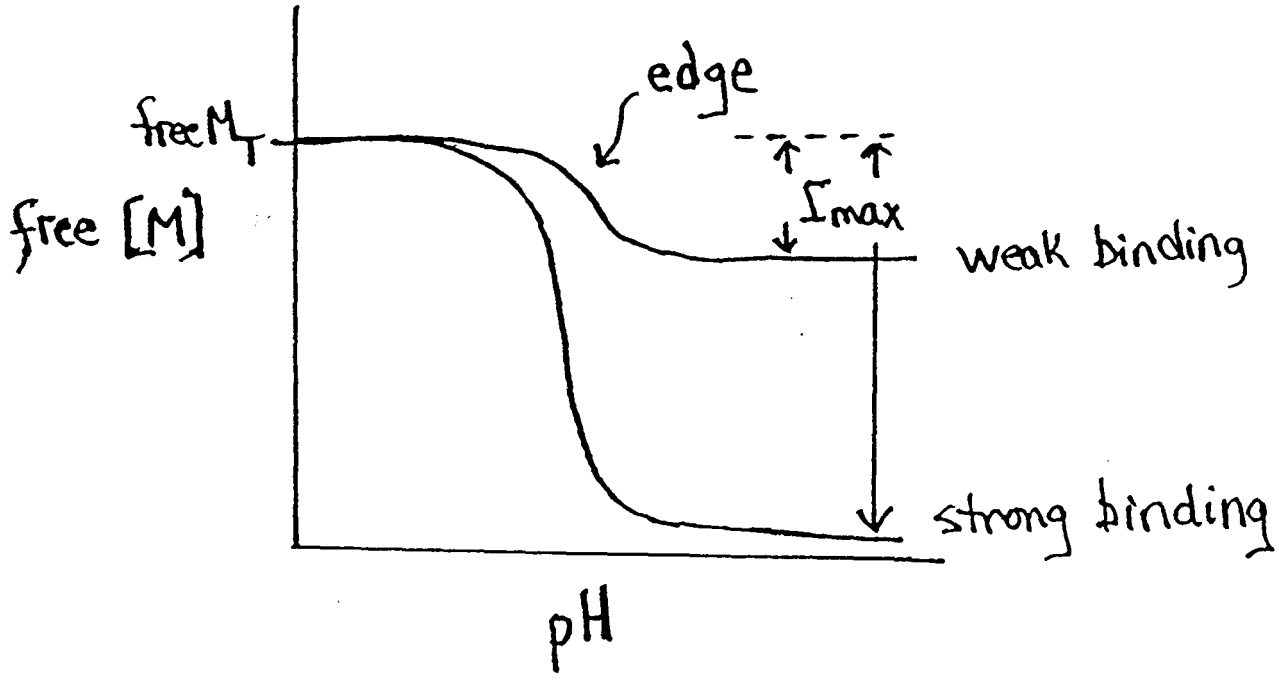

Figure 1.1: A typical pH edge, demonstrating binding capacities for two different metal ions.

For the following experiments, cadmium (II) was the chosen metal ion because it is easily detectable with an ISE, minimal hydroxide formation occurs, and it is of environmental interest because of its toxicity. Previous studies have shown that organic matter causes biases in ISE output, possibly in a manner similar to the coating of natural particle surfaces (1). These difficulties need to be addressed in order to measure the free metal ion levels in sediment suspensions, as this is the basic analysis tool for this experimental work.

1.1.2 Electrode Response Interference From NOM

The interference of organic matter with electrode response is not a new phenomena. In 1931, Heyrovsky developed the "adsorption analysis" technique, which takes advantage of the natural adsorption of organic species on to the surface of a mercury electrode. This adsorption of natural surface-active organic species suppresses the streaming maxima around a mercury drop electrode, and can be quantified. Some difficulties with this technique were noted by Pleše and Zutić (24), who attributed irregular oscillations in polarographic maxima to collisions of unsaturated surfactant aggregates with the mercury electrode/aqueous solution interface.

More recently, Ochs *et al* (25) studied the extent of adsorption of humic substances onto a hydrophobic mercury electrode surface by measuring directly the change in double layer capacitance due to adsorption. They determined that humic substances adsorbed significantly to both hydrophobic and hydrophillic surfaces, over a pH range. It was suggested that the adsorbed material could influence the chemical characteristics and reactivity of a surface and, therefore, its affinity for metal ions.

In general, a cadmium ISE responds to other ions in solution, including mercuric, bismuth and sulphide ions. More specifically, a silver sulphide based ISE will undergo ion exchange reactions in the presence of light which causes silver halide crystal growth on, and out of the membrane (26). The results from scanning electron microscopy experiments have been interpreted as silver on the active surface. This metallic silver leads to silver sulphide or silver oxide deposits on the electrode (27). ISE responses have also been found to be affected by the presence of humic substances in solution although

the exact nature of the contamination is uncertain.

With the advent of automatic titrators for pH edge titrations, constant monitoring of the solution by each ISE is required. Since the electrodes are not removed between readings, no re-calibration is possible and some drift or fouling, due to contact with humic substances, is inevitable. These interferences can cause significant bias in the response. This bias could be removed by preventing natural organic matter (NOM) from contacting the electrode surface and, at the same time, allowing metal ions to react with the electrode.

We present here a series of experiments to evaluate the hypothesis that a dialysis membrane can be used as a shield to isolate the electrode surface from contamination by NOM of high molecular weight. This approach is similar in concept but opposite in application from using dialysis membranes to retain enzymes near the electrode surface, as was done recently in the development of enzyme specific electrodes (28). This is followed by a determination of the extent of binding of cadmium (II) ions to Coote's Paradise sediments, and the effect that ISE drift and fouling have on model parameters.

1.2 MATERIALS AND METHODS

1.2.1 Sediment Samples

Surficial sediments from Coote's Paradise (Cootes sediments) were collected with a square dredge from the deck of a scow in the western part of Hamilton Harbour at a depth of less than 3 meters. The shallow depth of the embayment and strong winds

maintain oxic conditions year round. Cootes sediments consist of erosion debris, mostly clays, coated with a small layer of organic matter arising from the very active algal and bacterial populations. Previous work on these sediments and samples from other locations in the harbour are given in Brassard *et al.* (29). Loadings in Coote's Paradise come mainly from creek erosion (47050 kg/day in 1987) and farming operations.

Surficial sediments were stored in polyethylene bottles at 4°C until decanted. Fifty grams of raw sediment were diluted in 500 mL water, stirred vigorously and then allowed to settle for 1 min. The top 1.5 cm were collected. The volume was replaced with water and the process repeated until approximately 1 L of suspension was collected. The particle concentration as mass/volume was determined by filtering an aliquot through a 0.45 μm filter (Millipore) and drying the filter and collated solid to constant mass at 80°C until it reaches constant weight. Set point concentrations were prepared by performing appropriate dilutions of this stock. Electrophoretic light scattering and image analysis were used to confirm that calculations from Stoke's settling equations accurately predict the size distribution of the collected suspension.

1.2.2 Solutions

Barnstead Nanopore deionized distilled water was used to prepare or dilute solutions as required. 0.1 N HCl and 0.1 M NaOH standard solutions were prepared from BDH standards. The ionic strength of the solutions was adjusted with analytical reagent grade sodium nitrate (Mallinckrodt Chemical Work). 0.1 M cadmium nitrate (Fisher Scientific) was prepared by dissolving the hydrated salt in deionized water.

1.2.3 pH Edge Titrations

1.2.3.1 Titration instrumentation and procedures

All titrations were done under CO_2 free water saturated air, obtained by passing feed instrument air through an ascarite column, followed by a water wash bottle. The reactor consisted of either a 120 mL polyethylene (PE) beaker or a 50 mL PE centrifuge tube. A plexiglass or centrifuge tube lid held reference and selected ISE electrodes along with the tubing required for adding titrant and CO_2 free air. This method allowed rapid insertion into and removal of electrodes from the reactor, which minimized exposure to ambient CO_2.

The following procedure was followed for all titrations. First, the electrode assembly was calibrated against standard buffers immediately before the titration. The titration vessel was then filled with the titration solution and lowered into a constant temperature jacket (25°C) held over a magnetic stirrer. The titration was carried out after a 10 minute equilibration time. After recalibration, blank titrations without cadmium and/or sediment followed.

The titration profile was controlled by a computer driven titrimeter (Tanager Scientific Systems, model 8901). Equal 0.1 pH intervals, based on estimates of the buffer capacity obtained from the previous titration point, were selected.

1.2.3.2 Electrodes

The cadmium (II) ISE membrane was formed by thoroughly blending an equimolar

ratio of CdS and Ag_2S powders under argon. A 6 mm die was loaded with this blend and subjected to 8000 kg cm^{-2} pressure (30, 31). A temperature controlled jacket held the die at 150 ± 5 °C during a 16 hour curing period. The resulting pellet was mounted at the end of a glass tube and sealed with a thermoplastic sleeve. A strip of platinum mounted at the end of a small spring established electrical contact between the inner surface of the pellet and a copper wire.

The cadmium (II) ISE was polished before every use with 1.0 µm followed by 0.5 µm Al_2O_3 powder on a felt pad. It was calibrated both automatically, and manually with standard $Cd(NO_3)_2$ solutions, ranging from $10^{-5.5}$ M to 10^{-3} M. A Radiometer pH glass electrode and Fisher Scientific Calomel reference electrode were calibrated with standard buffers before every use.

1.2.3.3 The dialysis membrane

Dialysis tubing from Armin Plastics, with a molecular weight cutoff of 12000 to 14000 daltons, was cut into 3 inch lengths and boiled in deionized H_2O for 30 min. The wet tubes were slit open and stored in deionized H_2O until needed. After cleaning the electrode, a square of tubing was pulled tightly over the end of the cadmium electrode and an O-ring was rolled over the end, along the shaft, up to the edge of the tubing to hold the membrane in place.

1.2.3.4 Cadmium ISE exposure to sediment: procedures

The response of the electrode, with and without membrane protection, was

examined under three operational conditions: 1) a pH edge titration where the amount of metal ion adsorbed on the sediment was measured over a range of pH conditions; 2) drift of electrode potential with time due to NOM accumulation on the surface; 3) offset in Nernstian calibration due to NOM accumulation.

1) For pH edge experiments, 98.9 mL of 1.1 g L^{-1} sediment were brought to about 10^{-4} M cadmium (II) and 0.05 M KCl. The resulting suspension (100 mL) was brought to pH 3 by addition of 0.1 N HCl. The mixture was equilibrated in the titration reactor for 30 min in presence of precalibrated ISE electrodes. Titration commenced with addition of 0.1 M NaOH at equal 0.1 pH and time intervals until pH 10.

2) Eight experiments were performed in order to determine electrode drift. In each case, an ionic strength of 0.01 M $NaNO_3$ and a pH of 4.5 were maintained. Suspensions containing 1 g L^{-1} sediment were monitored, both with and without 10^{-4} M cadmium (II), and both with and without membrane protection. Control solutions containing deionized H_2O in place of the sediment suspension were also monitored under the same conditions.

3) For offset in Nernstian calibration, the electrode was placed in a sediment solution, prepared as described above, and the suspension was adjusted to a particular pH, ranging from 4 to 6. This range corresponds to the greatest deviation in electrode response from the edge experiments. The total exposure time ranged from 0 to 3 hours. The "fouled" electrode was then placed in a series of cadmium (II) standard solutions at the same pH

as the sediment and the cadmium ISE responses were measured. A similar series of experiments were performed with the cadmium (II) electrode covered with the membrane.

1.3 RESULTS AND DISCUSSION

1.3.1 Sediment samples

A settling procedure was designed to remove the coarse particulates which was a necessary step to prevent grinding in the reactor and wear of electrode surfaces. Calculations from Stoke's settling equations predict the size distribution of the collected stock suspension to be less than 16 μm.

The hypothesis that Stoke's settling equations can be used to predict average particle size of our suspensions was tested with two particle size analysis techniques, namely, light scattering and image analysis. A sediment solution was allowed to settle for 370 minutes and the supernatant was collected to a depth of 5.5 cm. Assuming a particle density of 2.65 g cm^{-3}, Stoke's equation (See equation 17) predicts an average particle size of 1.7 μm. Similar samples were analyzed by electrophoretic light scattering (Coulter Delsa 440) (1.5 μm) and image analysis (1.8 μm).

$$d^2 = \frac{18\ \mu\ w_s}{g\ \Delta\rho} \qquad (17)$$

where w_s = settling velocity (g cm^{-2})

1.3.2 Titrations

1.3.2.1 Titration instrumentation and procedures

The dialysis membrane arrangement is stable and the membrane could maintain a tight contact with the membrane surface for a week. The drift of the pH and reference electrodes, when exposed to sediments, was examined and no significant deviations occurred. After reaching a steady reading within minutes, the reading remained within ± 0.05 pH units for over 24 hours. Because of this, no membrane was used to protect the pH or reference electrode.

Because titration profiles for the blanks did not necessarily fall on the same pH points as the analyte, blank titration data were interpolated to the corresponding value of the analyte using a cubic spline method. The difference between analyte and interpolated blank titrant addition at the same pH values yielded charge excess in the suspension.

1.3.2.2 Cadmium ISE exposure to sediment

1) At low pH, sediment in suspension exists in a protonated form. As the pH of a sediment and metal ion suspension increases, protons on the sediment exchange with metal ions in solution and the total free metal ion concentration should decrease. Our results, however, showed that the free cadmium ion concentration increased with pH during a pH edge titration and suggested that more cadmium ions were present in the

system than was originally added (Figure 1.2). The additional cadmium ion could not have come from the sediment since Inductively coupled plasma - Mass spectroscopy (ICP-MS) analysis of the sediment indicated a cadmium content at 14 μg g^{-1} (29). If taken into solution, this would result in a concentration increase of 0.0485 μmol L^{-1}, which is significantly less than the 10^{-4} M apparently added to the system. Furthermore, a control experiment without added cadmium ion resulted in a similar increase in electrode potential over the same pH range, indicating electrode bias. Figure 1.2 demonstrates that as the time between titrant additions increases, the total titration length and electrode exposure time increase. An increase in bias is demonstrated by the increase in the apparent level of cadmium with an increase in time interval.

2) There are two distinct alteration processes occurring at the membrane surface. The first one is probably oxidation of the exposed surface and occurs any time the electrode is exposed to oxygen in water or air (27). This is shown as the lower curves of Figure 1.3 which have a drift value of 4.6 mV hr^{-1}. Also, the drift rate is constant in time and has increased to 6.4 mV h^{-1} when the cadmium ion concentration is increased 10 fold. This is shown by comparison of the lower and upper curves of Figure 1.3.

The second process arises from exposure of the electrode to NOM. In Figure 1.3, both solutions with and without sediments containing 10^{-4} M cadmium show a linear increase in electrode response at 11.5 mVh^{-1} and 4.6 mV h^{-1}, respectively. In the sediment suspension, the drift is more extreme, the difference owing entirely to the presence of NOM. Drift due solely to NOM is estimated to be 6.9 mV h^{-1} by comparison

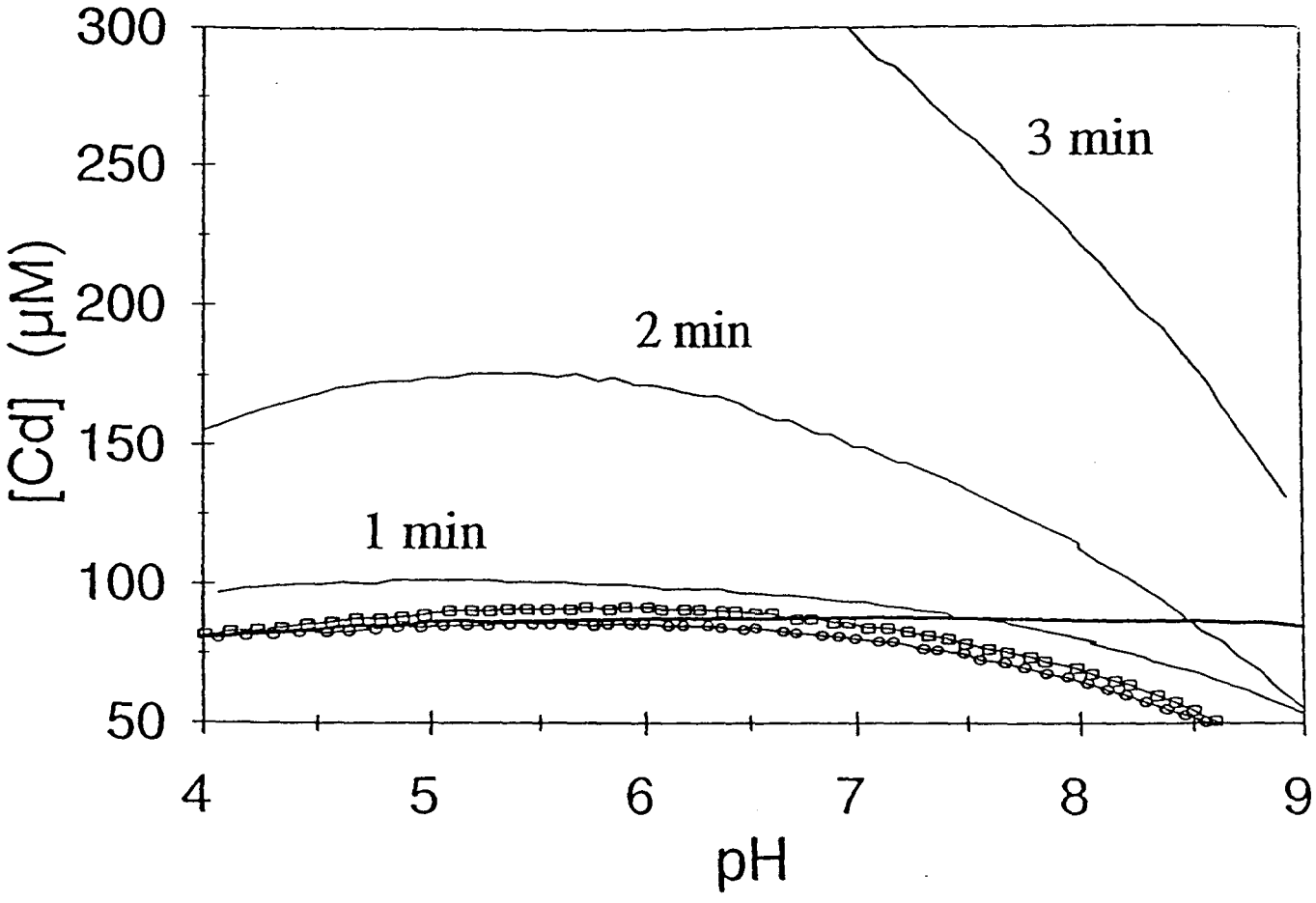

Figure 1.2: Distortion of pH edge profile for cadmium ion adsorption on 1 g/L suspended sediments. Titrations were done with both an unprotected, and a membrane protected electrode. Thin lines: unprotected electrode at the indicated time interval between titrant additions. Symbols: membrane protected electrode at [O], 2 min, and [□], 5 min intervals. The thick line is a control without sediments, with a membrane. Parameter optimization for Langmuir fit is shown in Table 1.1.

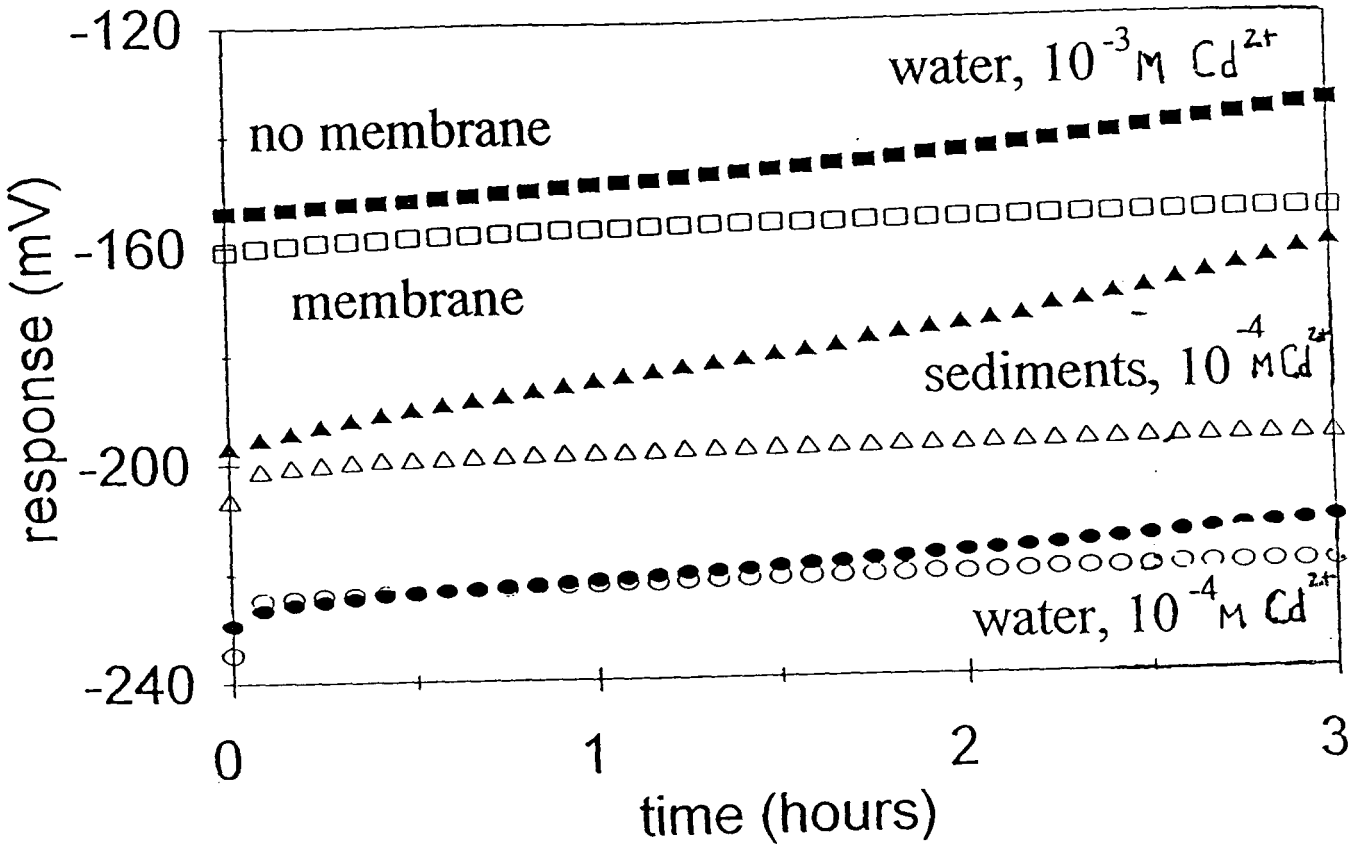

Figure 1.3: Effect of drift on the cadmium (II) ISE for water and sediment solutions at 10^{-4} M cadmium (II), both with, and without a dialysis membrane. [●] water blank with no membrane; [○] water blank with the membrane; [▲] sediment suspension with no membrane; [Δ] sediment suspension with the membrane; [■] 10^{-3} M cadmium (II) standard with no membrane; [□] 10^{-3} M cadmium (II)standard with the membrane. The data for the 10^{-4} M cadmium (II) water blank was shifted by -30 mV for graphic clarity.

with the water control. Since this drift rate difference disappears when the membrane is in place, the interference to the electrode surface can be attributed to colloidal NOM, above the 12000-14000 MW cut-off of the dialysis tubing. Organic matter of lower molecular weight may pass through the membrane, but has no noticeable effect on the electrode surface.

If we assume that the electrode surface is an adequate model for the surface of a resuspended natural sediment particle, it follows that only large molecular weight NOM, presumably humic acids, can significantly alter surface properties of aquatic suspensions. The NOM of lower molecular weight would thus have no effect. Coatings of NOM on suspended particles are recognized as an important agent controlling metal ion exchange with the bulk solution and in controlling surface charge (2, 6, 32).

Generally, the membrane appears to reduce significantly the drift due to oxidation and NOM fouling. We do not know how this occurs. It could reduce the rate of oxidation by creating a pocket around the surface, where diffusion of oxidizing materials to the electrode membrane surface would be reduced. It is also unclear what kind of binding occurs between the organic matter and the surface but the fact that only colloidal substances have an effect suggests that NOM could act as a surfactant on natural particles.

3) If organic matter is affecting the surface of the electrode, the Nernstian response could be affected as well. Figure 1.4 demonstrates the degradation of the Nernstian response after exposing the cadmium (II) ISE to sediment for extended periods of time, without membrane protection. Slope and intercept values are presented in Appendix A.

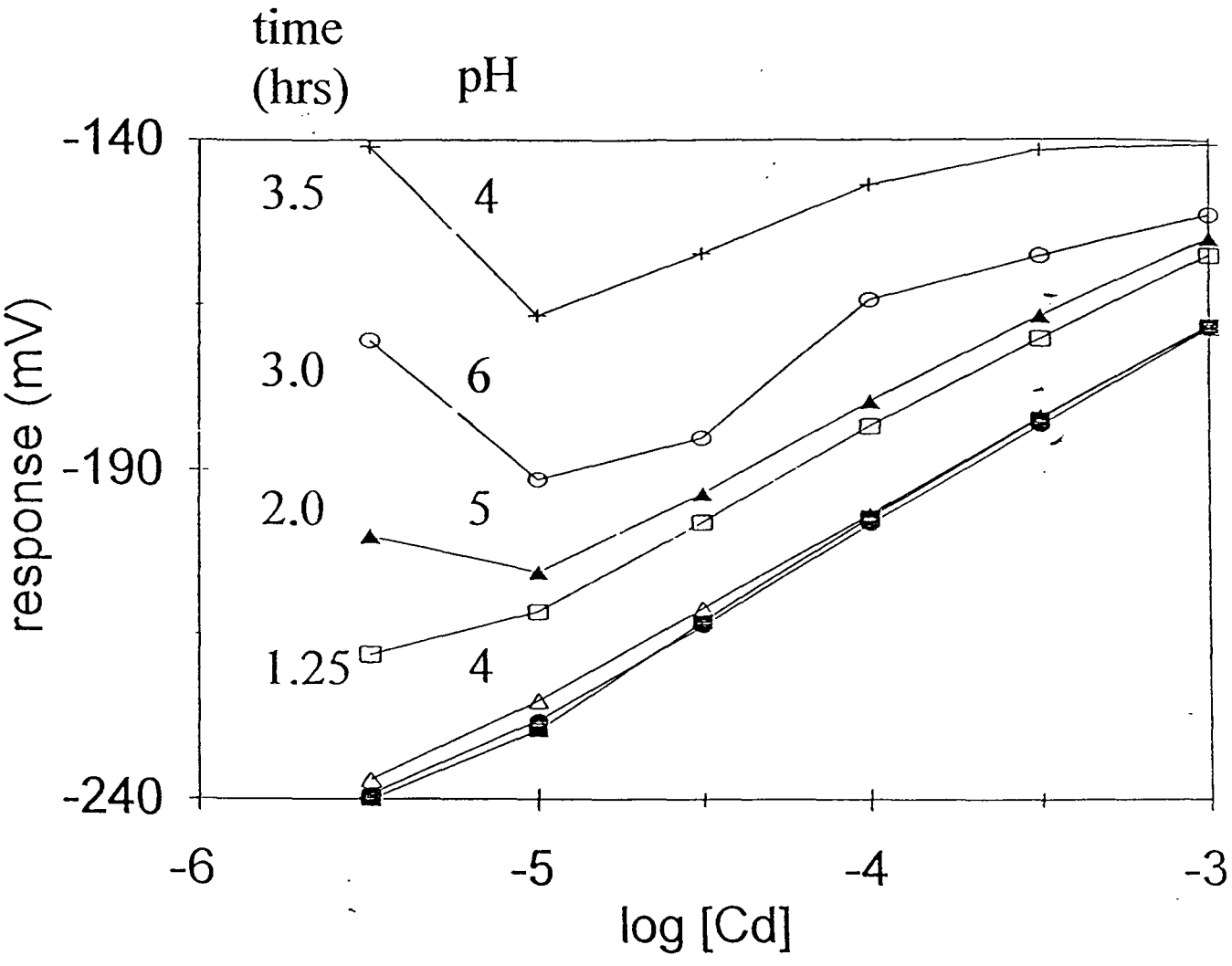

Figure 1.4: Calibration without dialysis membrane. Exposure conditions: [+] pH 4, 3.5hr exposure; [○] pH 6, 3 hr exposure; [▲] pH 5, 2 hr exposure; [□] pH 4, 1.25 hr exposure; [●] natural pH, 5 min exposure; [Δ] no exposure, with membrane; [■] no exposure, no membrane.

As both exposure time and pH increase, the deviations from the expected Nernstian response increase. In contrast, Figure 1.5 demonstrates that the membrane prevents this deviation from Nernstian response. The slope is the expected 30 mV per decade change in cadmium (II) concentration.

1.3.3 Effect of Electrode Drift on Adsorption Parameters

Electrode drift during a continuous pH edge titration can introduce unaccounted for biases in metal ion concentration which leads to erroneous parameter estimation. As noted in the Introduction, adsorption on sediment surfaces is generally a Langmuirian exchange between protons and free metal ions. This is shown in reaction 15 and equation 16.

Of interest is how the Langmuirian function (Γ) is distorted when we introduce a drift in the measurement of the free metal ion concentration. To do so, Equation 16 is rearranged as follows:

$$[M^{+2}] = [M_T] - \frac{\Gamma_{MAX}[M^{2+}]}{\frac{[H^+]}{K} + [M^{2+}]} \qquad (18)$$

We then use equation 18 to evaluate the pH edge titration data of suspended sediments (from Figure 1.2), for each condition of time interval, under an increasing time interval, and for both membrane free and membrane protected electrode conditions. Non-linear curve fitting (Levenberg-Marquard minimization method) was used to obtain optimized values for

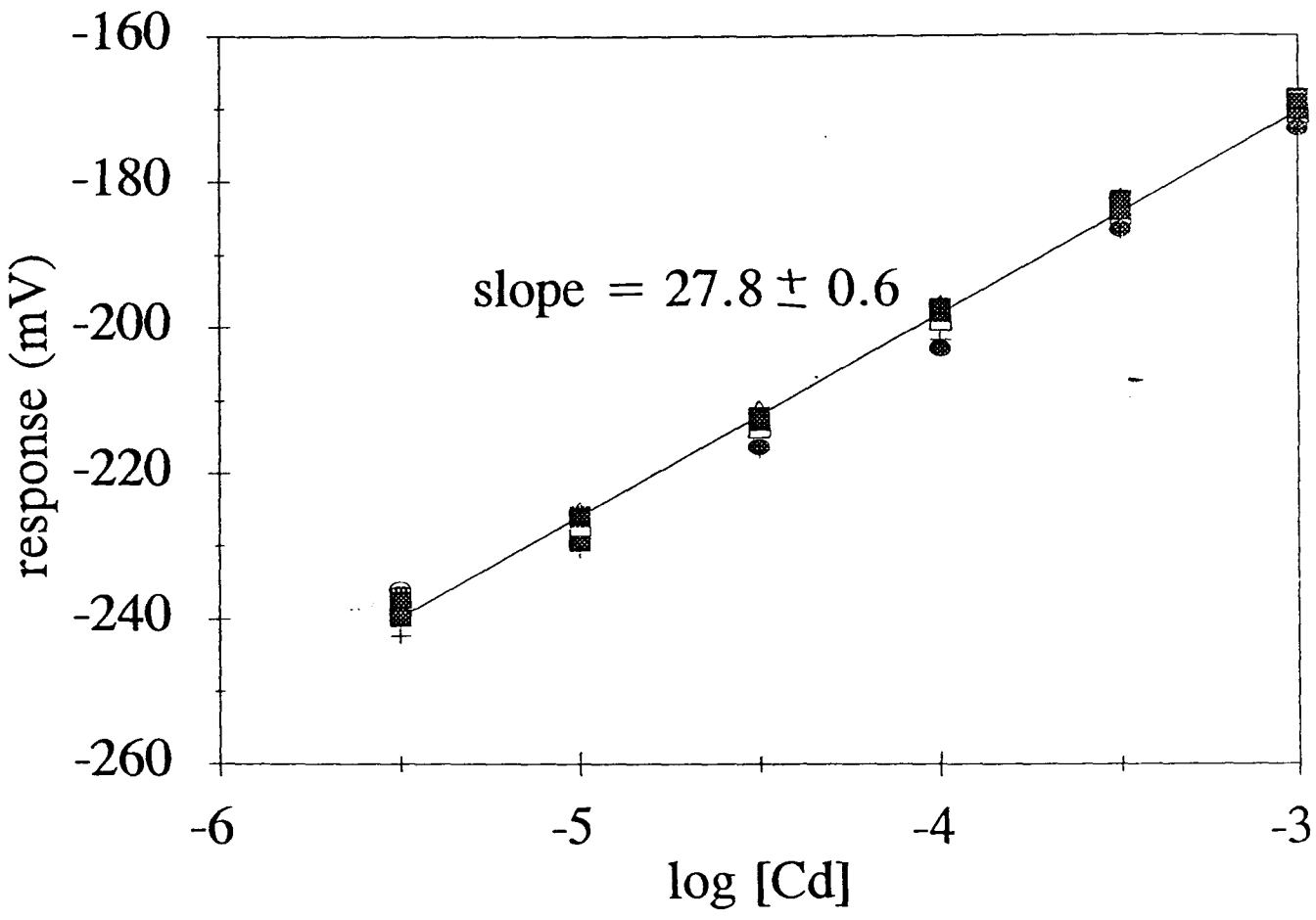

Figure 1.5: Calibration with the dialysis membrane. Exposure conditions: [■] no exposure, no membrane; [●] no exposure, with membrane; [▲] pH 4, 2 hrs; [+] pH 4, 0.5 hrs; [□] pH 6, 1.25 hrs; [○] pH 6, 3.5 hrs; [Δ] pH 5, 2 hrs.

Table 1.1: Parameter optimization for cadmium adsorption profiles (equation 3) as biased by electrode fouling. ΔT, time interval between titrant addition (min) for a fixed pH change of 0.1 units; Fit, overall goodness of fit expressed in percent deviation from data; M_T, total cadmium concentration (M); Γ_{MAX}, total available surface sites (M); pK, stability constant for 1:1 exchange between proton and cadmium; r^2 correlation coefficient. Values in parenthesis show percent uncertainty. No binding occurs in the control, therefore there are no pK values.

ΔT	Fit %	M_T $x10^{-5}$	Γ_{max} $x10^{-5}$	pK	r^2
control					
1		**8.6 (0.2)**	**0**		
with membrane					
2	**1.76**	**8.4 (0.1)**	**6. (1.1)**	**4.2 (.1)**	**.992**
5	**2.96**	**8.9 (0.3)**	**8. (2.7)**	**4.4 (.2)**	**.978**
without membrane					
1	**1.71**	**10.0 (0.2)**	**5. (1.1)**	**4.1 (.2)**	**.987**
2	**3.53**	**17.0 (0.6)**	**13. (3.2)**	**4.1 (.2)**	**.982**
3	**37.8**	**40 (12)**	**40. (44)**	**4.5 (2)**	**.732**

$[M_T]$, Γ_{MAX} and K (Table 1.1). Figure 1.2 shows that a greater time interval between titrant additions increases the duration of titration and, therefore, allows a greater bias due to

fouling. Thus, although the unprotected electrode at three minute time interval shows distorted estimates for M_T (Table 1.1 - $M_T = 4 \times 10^{-6}$), the protected electrode can still match the control at five minute intervals ($M_T = 8.9 \times 10^{-5}$ and $M_T = 8.6 \times 10^{-5}$, respectively). The results are consistent with Figures 1.4 and 1.5, which demonstrate that the membrane protected electrode prevents a deviation from the expected Nernstian response of 30 mV per decade.

Fu and Allen (18) also determined K and Γ_{MAX} values for sediment samples. In spite of our lower sediment concentration (1 g L^{-1} vs. 50 g L^{-1}) , K and Γ_{MAX} in this experiment are both greater by about two orders of magnitude than the samples analyzed by Fu and Allen (18). We attribute this difference to the air-drying step they used to remove reduced materials. We think that drying of the sediment could have decomposed some of the organic matter and/or forced the floc structure of the sediment particles to collapse. This would cause a reduction in the available surface sites for metal ion binding.

1.3.4 Sensitivity analysis

Adjustment of parameters by the Levenberg-Marquard method returns a sensitivity analysis useful for determining the pH range where a particular parameter is dominant. Sensitivity is expressed as a dimensionless ratio of the change in the function over its initial value (Equation 18) resulting from a unit change in the value of the parameter. Each parameter is studied one at a time. The binding function is essentially dominated by estimates for total metal ion concentration at pH values lower than the binding constant.

Past this point, its influence decreases somewhat and the other two parameters increase in influence only at a pH near 9. However, the titration would lose its value at that point since the precipitation of cadmium hydroxides becomes a factor. Figure 1.6 nevertheless shows why large uncertainties in Γ_{MAX} and K (Table 1.1) can still arise in spite of a good overall fit. This analysis exemplifies the false security in using goodness of fit or correlation as sole indicators of the suitability of a parameter.

1.3.5 Proton consumption versus cadmium consumption

Figure 1.2 depicts the binding of cadmium (II) to the sediment surface, but it does not give information about proton consumption over the pH range. In order to see how protons and cadmium ions interact, we examined proton consumption *versus* cadmium consumption for our pH edge titration data, both with and without sediments, at a 10^{-4} M cadmium ion concentration. The number of protons required to bring water to the same pH point as the sediment suspension were determined from the blank titrations and removed. An example is presented in Figure 1.7. Two regions are apparent. A is a region of proton consumption, independent of cadmium binding. We presume that the added protons cause organic acid structure changes. Region B has a slope of -½ which indicates that the total consumption is 2 protons for 1 cadmium ion. Regions A and B appear to represent two different conditions, or types of sites. Previously, the pH data was fitted to a 1 : 1 Langmuirian exchange between protons and cadmium, so we postulate that, in addition to the metal ion exchange site, there is also a proton binding site. This indicates

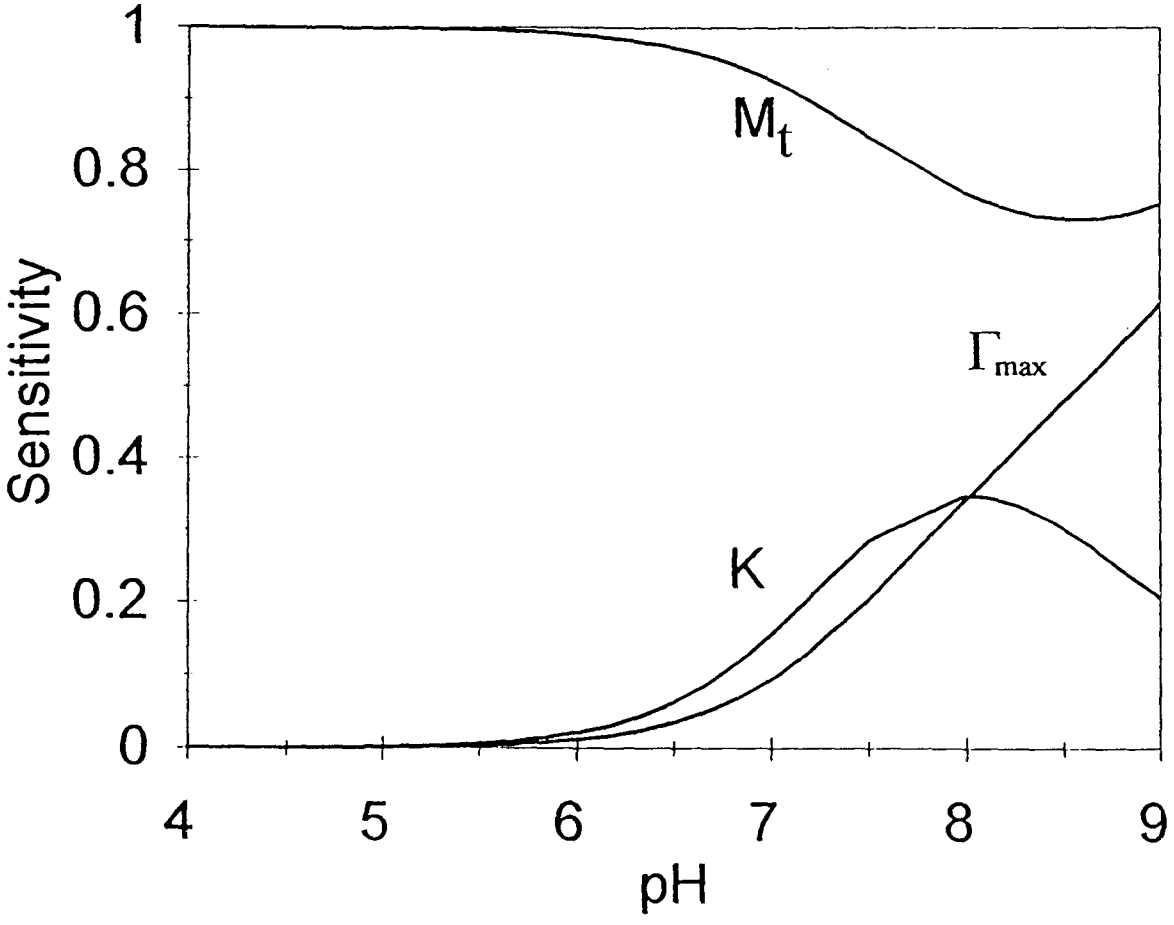

Figure 1.6: Sensitivity analysis for adjusted parameters in Table 1.1. The curves shown here are for a run of 2 minute time interval, without membrane. M_T, total cadmium concentration (M); Γ_{MAX}, total available surface sites (M); K, stability constant for 1:1 exchange between protons and cadmium.

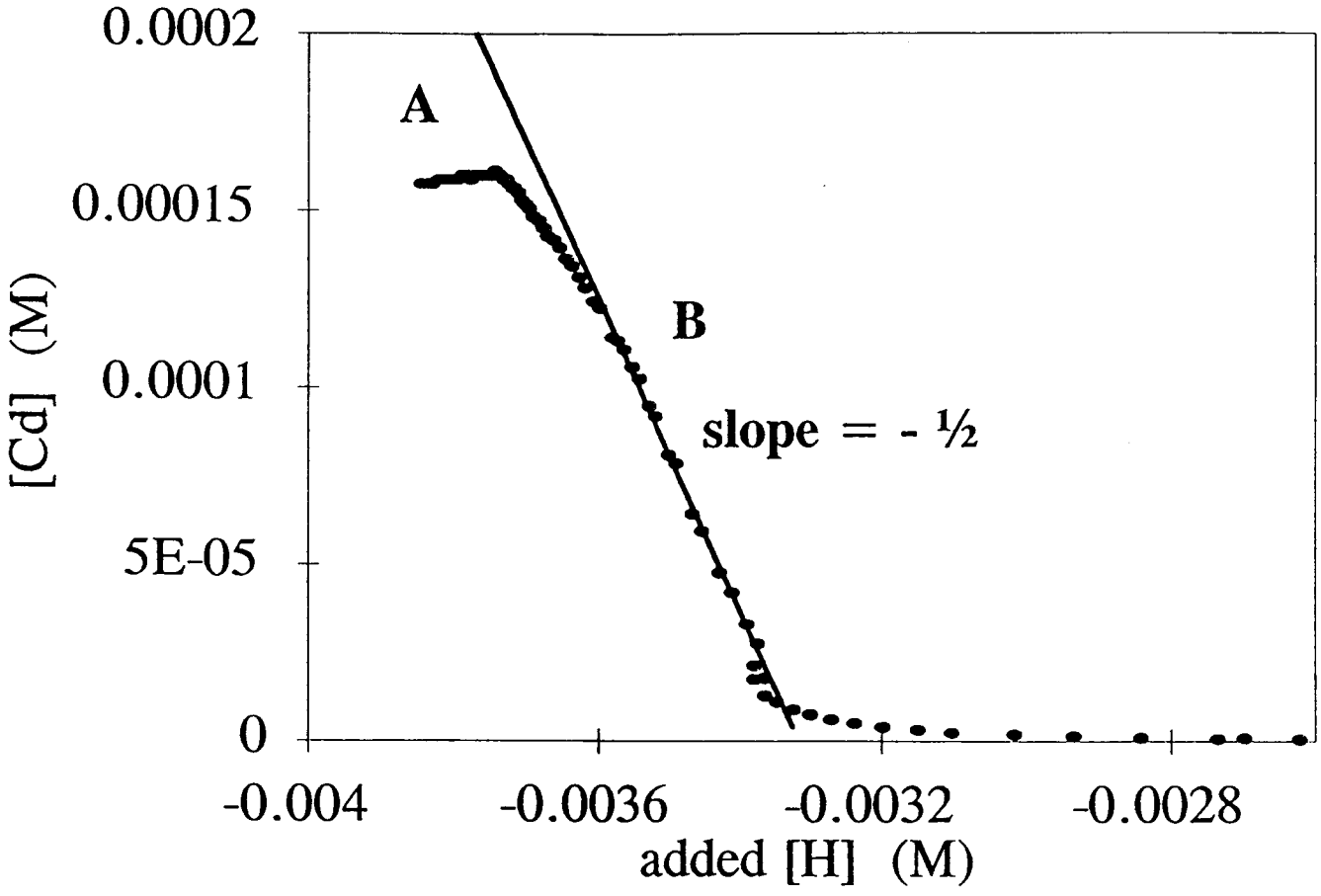

Figure 1.7: Proton and cadmium 1 : 1 Langmuirian exchange. Two regions are found. Region A represents proton consumption, independent of cadmium binding. Region B has a slope of -½, which indicates a total consumption of 2 protons for 1 cadmium.

that the following equations should be considered when developing a binding model:

On the particle surface	$P \equiv DOM - Cd^{+} + H^{+} \rightleftharpoons P \equiv DOM - H + Cd^{2+}$ $P \equiv DOM - H \rightleftharpoons P \equiv DOM^{-} + H^{+}$
In solution	$DOM - Cd^{+} + H^{+} \rightleftharpoons DOM - H + Cd^{2+}$ $DOM - H \rightleftharpoons DOM^{-} + H^{+}$

Potentially, cadmium ion and proton exchange could occur on the surface of dissolved organic matter, either attached to the particle surface, or in solution. Similarly, proton binding could occur with the dissolved organic matter on the particle surface or in solution.

1.4 CONCLUSIONS

Metal ion binding studies using ISE electrodes as indicators of free metal ion are biased by a drift in potential probably caused by oxidation of the surface and by NOM coating the surface. The drift increases linearly in time and causes serious distortions to estimates from binding models. Effects are small if the electrode is inserted in the

suspension only for short periods of time, and if regularly cleaned and calibrated between measurements.

The impact is severe when the electrode is part of an automated titration procedure since recalibration and cleaning are no longer possible. In this case, the use of a membrane to protect the electrode surface reduces both kinds of drift. The membrane probably prevents the first kind by hindering the flow of oxidant from the bulk solution to the electrode surface. In the second case, the membrane protects the electrode surface from contact with the high molecular weight colloidal fraction. The low molecular weight NOM has no effect and, presumably, does not coat the surface. By analogy, results suggest that only organic matter greater than 12000-14000 daltons in size would be found on the surface of natural aggregates.

pH edge titrations were used to characterize binding sites for a constant particle size distribution. Two different site types were identified: a proton binding site and a cadmium - proton exchange site. It is expected that these two types of sites may exist on DOM both attached to a particle and free in solution.

We are interested in characterizing metal ion binding during conditions in which the particle size distribution changes. In the natural environment, storms and wind shear cause resuspension, settling and shear of surface sediments. Two significant causes of aggregation and disaggregation in natural waters are differential settling and shear.

Chapter 2

BATCH SETTLING EXPERIMENTS: FLOCCULATION DUE TO DIFFERENTIAL SETTLING and pH VARIATION

2.1 THEORY

There are three causes of collisions during sediment transport: Brownian motion, differential settling, and fluid shear. Previously, Tsai *et al* (10) showed Brownian collisions to be insignificant over the particle range of interest, leaving differential settling and fluid shear as the two significant causes of particle collisions in the natural environment.

As mentioned, collisions due to differential settling occur because particles of differing density or size fall at different rates and collide with each other. Since agglomeration produces particles of larger size and lower surface area, the available surface charge and the number of available binding sites will decrease. Upon resuspension, the available surface area should increase again, along with the available binding sites.

It is also important to examine the binding or release of organic matter during the flocculation process. The pH edge titrations described previously identified two types of binding sites: proton binding and metal ion (cadmium ion) binding. This indicates the possible existence of 2 types of organic matter, one of which binds cadmium ions.

The following experiments compare the partitioning of cadmium ions between the bulk solution and dissolved organic matter in both settled and resuspended sediment suspensions.

2.2 MATERIALS AND METHODS

2.2.1 Humic acid extraction by reverse filtration

Vacuum filtration is commonly used to separate solid and liquid phases, however the process produces a relatively high shear from the suction at the membrane. When separating sediment flocs from the liquid phase, care must be taken not to break them. Ideally, by decreasing the suction pressure at the membrane interface the shear is decreased during separation. A reverse filtration technique provides this decreased shear. Contrary to vacuum filtration, where the sample is placed in the filter, reverse filtration involves placing the filter into the sample.

The head of a 10 mL plastic syringe was cut off with a lathe and a 0.2 μm Nuclepore membrane was fixed in place with silicon glue. A hole, sized to receive the cylinder snugly, was cut in the lid of a 150 mL plastic urine cup and the cylinder was glued in place such that the distance between the membrane and the cup bottom was the same for all cups when the lid was closed. When the cup was filled, a low shear filtration occurred, due to the pressure difference caused by the difference in fluid level inside and outside the syringe (See Figure 2.1).

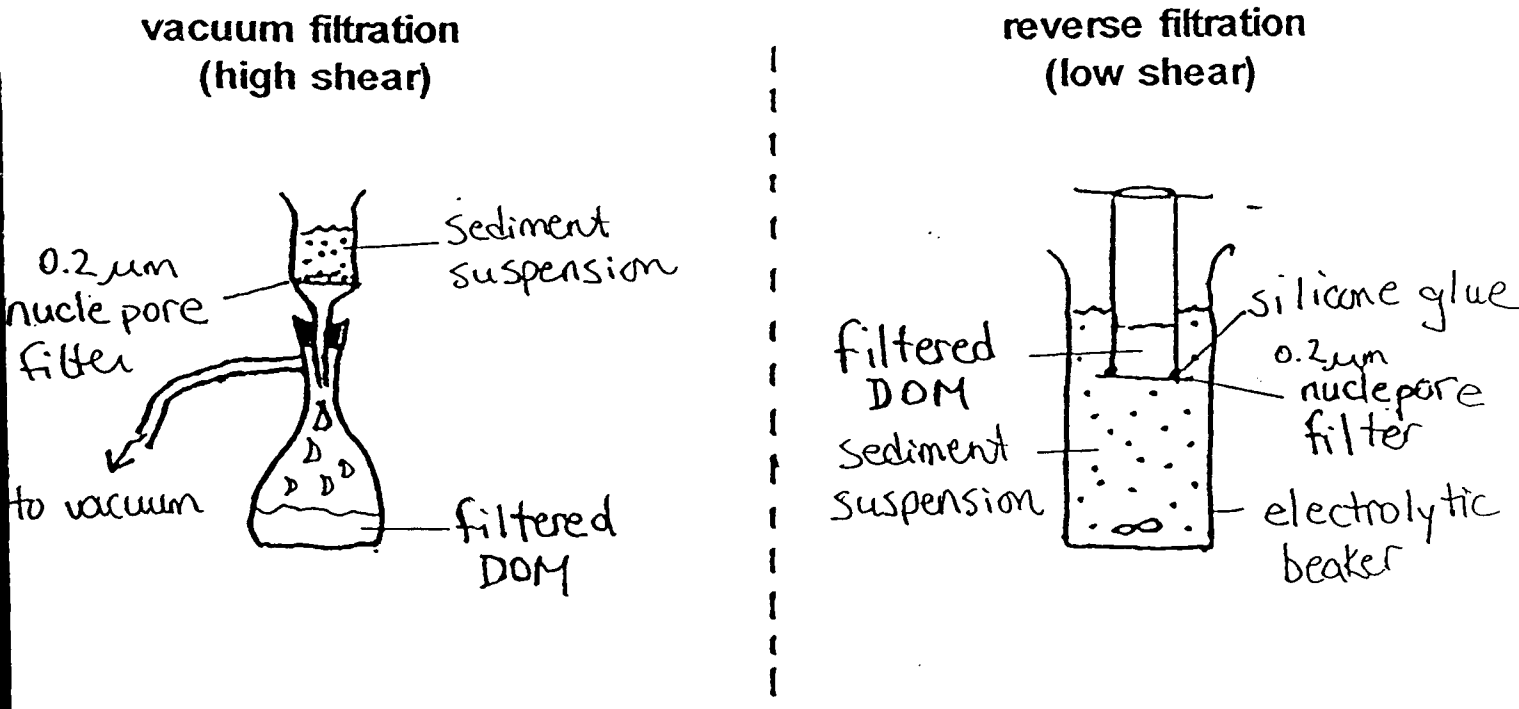

Figure 2.1: Vacuum filtration *versus* reverse filtration

2.2.2 *Batch experiment procedure*

We examined the exchange of Cd along a pH edge and compared the three forms of the metal ion in reactors containing either settled or resuspended sediments. Free aqueous cadmium (Cd^{2+}) is detected by an ion-specific electrode. Dissolved organic cadmium and particulate cadmium are differentiated by filtration through a 0.2 µm nuclepore membrane. This operationally defines particulate cadmium as that bound to

particles greater than 0.2 μm and dissolved organic cadmium as that attached to particles or colloids which pass through the 0.2 μm membrane.

The basic procedure used for the batch settling and resuspension experiments is presented in Figure 2.2 in a flow chart. Two sets of sediment suspension samples and blank solutions were prepared. All samples and blanks were prepared with a fixed ionic strength and spiked with cadmium. Each set was acidified over a pH range from 3 to 8, mixed well and allowed to settle for 24 hours. After settling, the first set was resuspended for 8 hours and the second set was decanted. The pH and cadmium ion concentration were then measured with electrodes for every sample. Finally, an aliquot of the supernatant was collected by reverse filtration for DOC analysis and cadmium (II) analysis by AAS. Further details are available in Appendix B.

2.3 RESULTS AND DISCUSSION

2.3.1 Validation of reverse filtration method

The filtrates collected by this technique were compared to those collected from a conventional (0.2 μm nuclepore) vacuum filtration for both settled and resuspended filtrates. The fluid level difference in the cups corresponds to a pressure of about 25 mm Hg, which is low compared to vacuum pressure of 760 mm Hg. Vacuum filtration creates a high shear environment, which is more likely to break apart flocs and extract more organic material as the solution is pulled through the sediment in the filter cup. UV

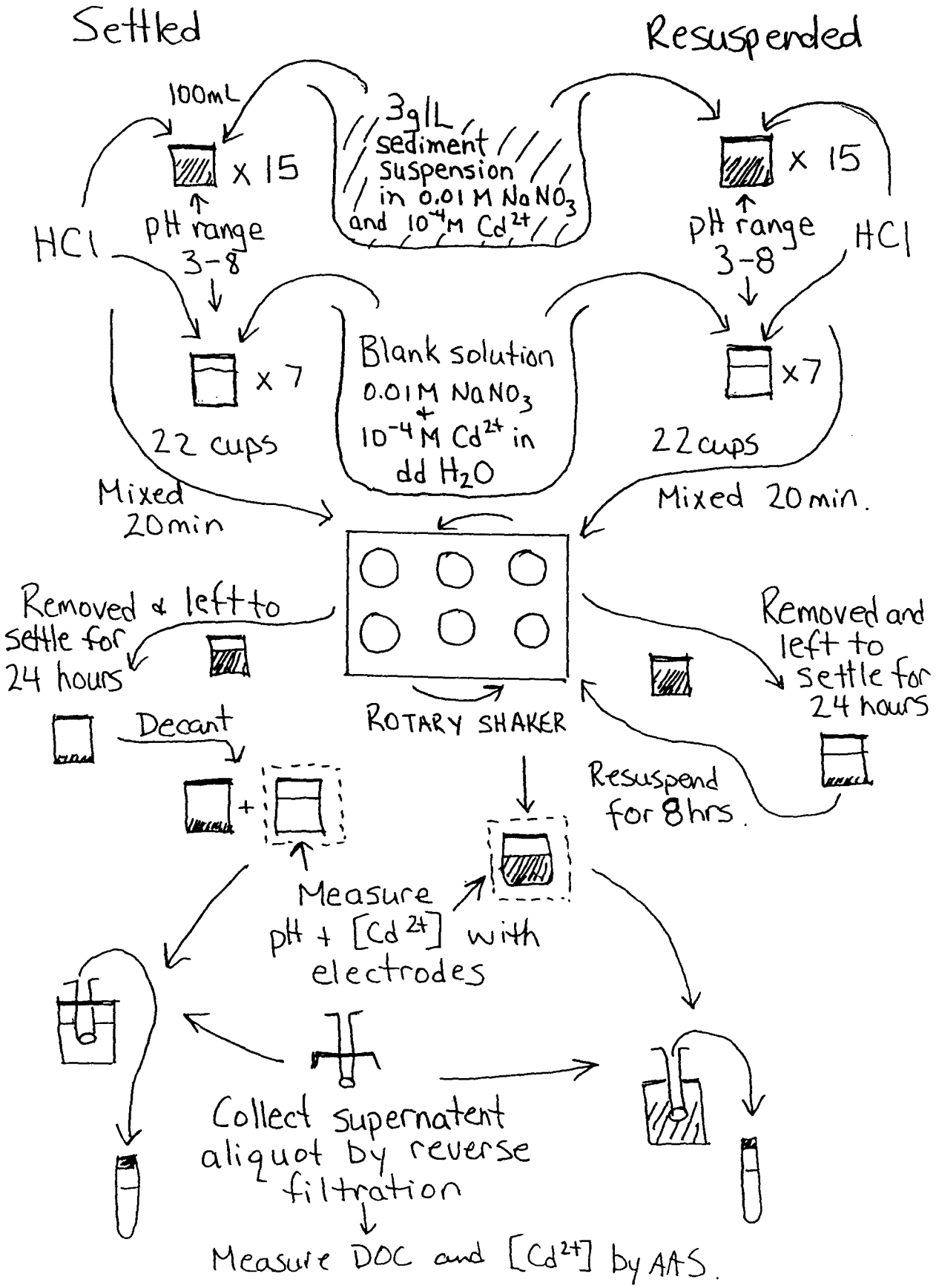

Figure 2.2: Flow diagram for the batch experiment procedure.

adsorption at 190 nm was used as an indicator of DOC concentration. Overall, vacuum filtration caused extraction of DOC up to eight times the concentration obtained using reverse filtration. The fact that more organic material could be extracted from the sediments indicates that up to eight times as much DOM resides on the particles than in solution. It is therefore necessary to ensure that floc integrity is maintained during organic matter collection.

2.3.2 Batch experiment results

Atomic adsorption spectroscopy measures all cadmium which passes through the 0.2 μm membrane, ie. both free and organic cadmium. The actual amount of organic cadmium is, thus, the difference between the AAS and the ISE readings. Similarly, the difference between the total cadmium added to the system and the AAS readings determines the particulate cadmium level. The particulate cadmium was not analytically determined because it would have required separating the particulate from the suspension by filtration. As we have shown, filtration creates a bias which would have been too large to accurately determine the particulate cadmium ion concentration. Since a total mass balance could not be accurately determined, the particulate cadmium ion concentration was determined by difference.

Results of previous titrations of reverse filtered humics indicated that very little cadmium binding occurred with the free organic material in solution. The fact that cadmium binds to particulate matter coated with NOM suggests that two types of organic matter may exist, one which prefers to bind to cadmium, one which does not. These will

be referred to as strong and weak organic matter, respectively.

The pH edge profiles between pH 3 and pH 8 show three regions of speciation: below, at, and above pH 6.2, for each of the settled and resuspended conditions (Fig. 2.3). At low pH, cadmium remains in the free form (Figure 2.3c) when sediments are settled, but upon resuspension, about one third of it transfers to the DOM in solution (Fig. 2.3b). In both the settled and resuspended cases, there is a release of DOM centred at pH 6.2 (Fig. 2.3d), which coincides with the one-to-one H : Cd Langmuirian exchange defined previously (See Chapter 1). Above pH 6.2, all cadmium and excess DOM become particulate (Fig. 2.3a).

The interesting finding is that the onset of cadmium binding on particles occurs during the surge in DOM at pH 6.2, as though a release of weak organic matter is required for cadmium to bind to the particle.

2.3.3 The model

As described, the results can be condensed into a model based on the combinations of the three pH divisions, and the two suspension regimes, resulting in six defined states (Fig. 2.4). At low pH in the settled condition (Fig. 2.4a), the particles are coated with both weak and strong organic matter. The presence of DOM (Fig. 2.3d) indicates that some weak organic matter is in solution since the majority of the cadmium added to the system remains free (Fig. 2.3c).

Since DOM does not change on resuspension (Fig. 2.3d), the strong organic matter on the particle must exchange with the weak organic from solution (Fig. 2.4b). The free

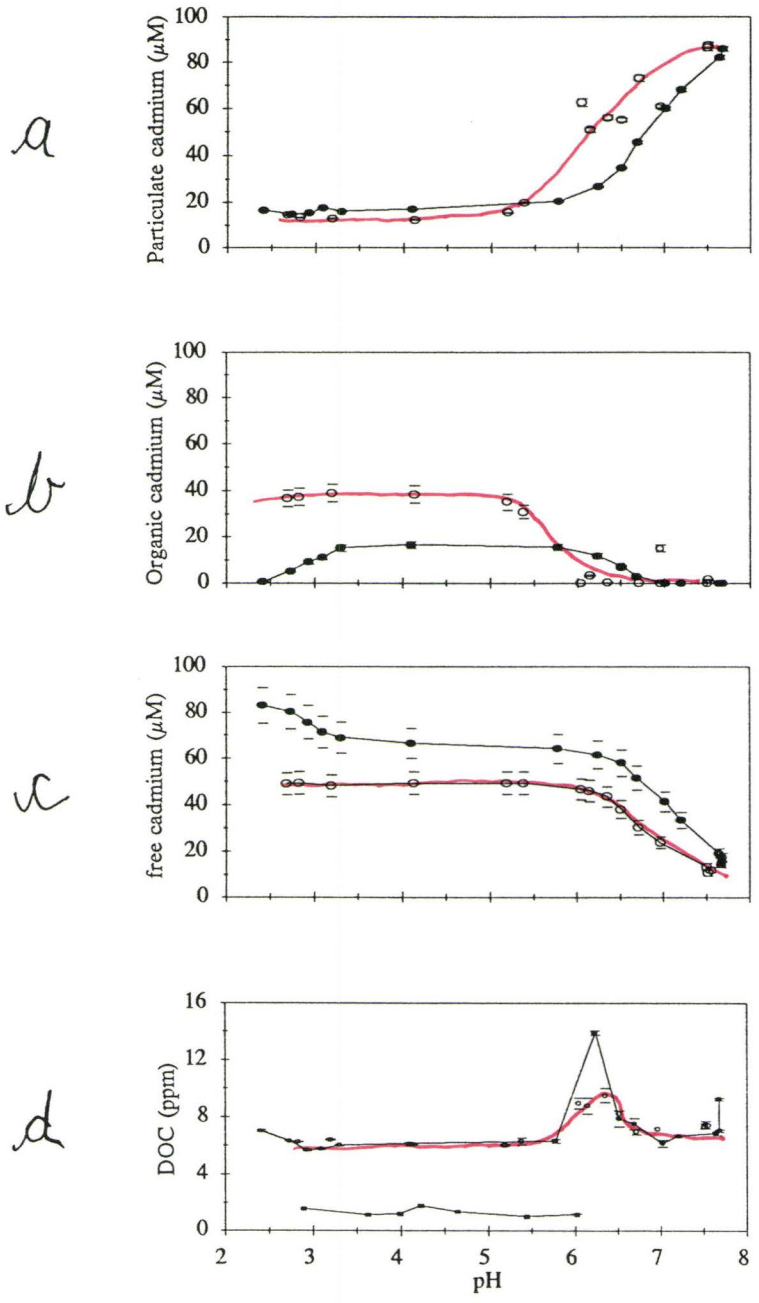

Figure 2.3: Batch experiment results. ●, settled data, ○, resuspended data; (a), particulate cadmium; (b), organic bound cadmium; (c), free cadmium; (d), dissolved organic carbon (DOC): ●, ○ - data; ■, □ - blanks.

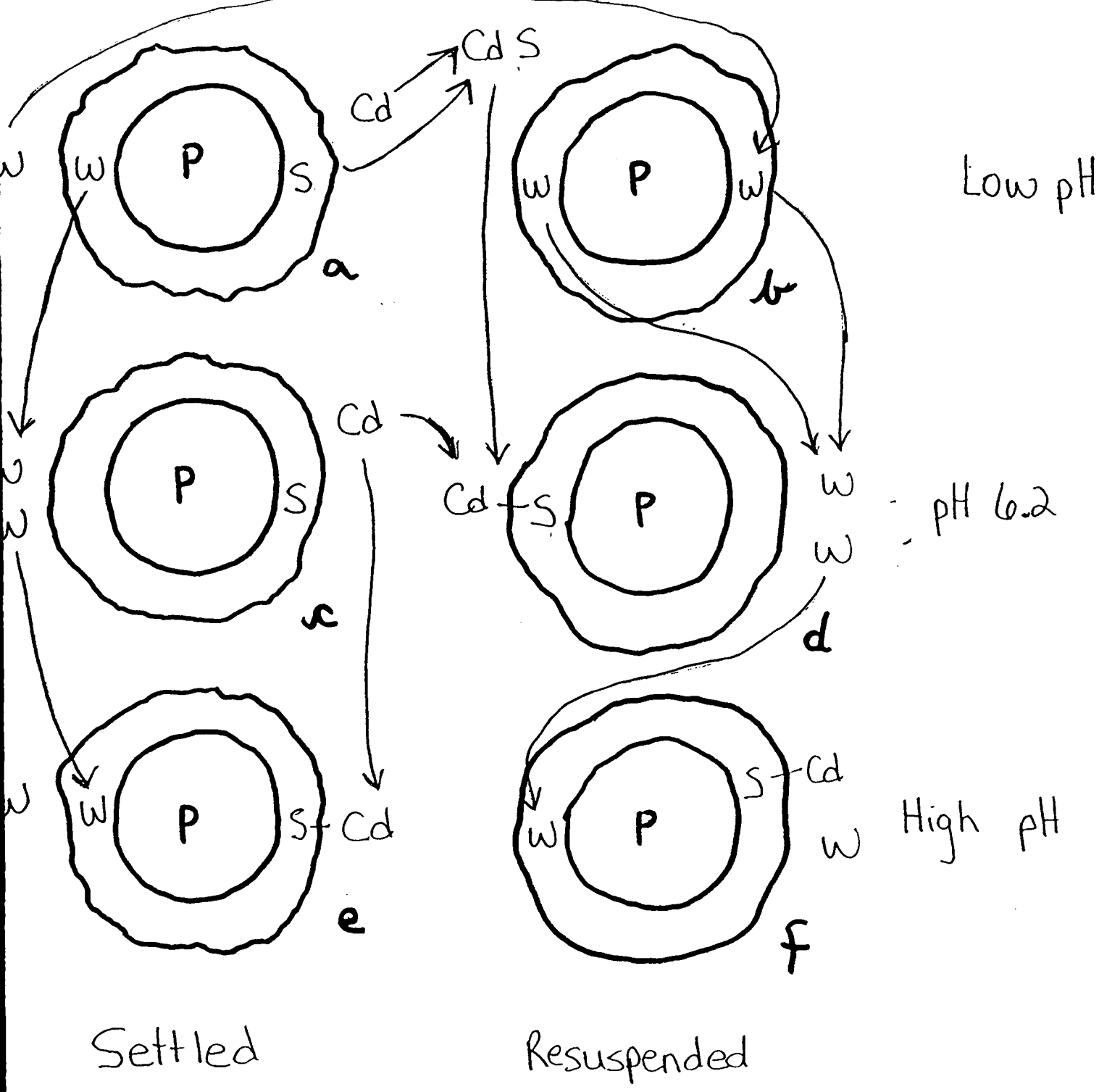

Figure 2.4: Batch experiment results as combinations of the three pH divisions, and the suspension regimes. (a) low pH, settled; (b) low pH, resuspended; (c) pH 6.2, settled; (d) pH 6.2, resuspended; (e) high pH, settled; (f) high pH, resuspended.

cadmium in solution binds with the organic matter released from the particle, causing a loss in free cadmium (Fig. 2.3 b, c).

With an increase to pH 6.2 in the settled condition (Fig. 2.4c), free metal ion remains the same (Fig. 2.3c) and a peak in the DOC level occurs (Fig 2.3d), suggesting that weak

organic matter from the particle is released into solution.

Once resuspension occurs (Fig. 2.4d), the free metal ion starts attaching to the particle to produce particulate cadmium (Fig. 2.3a). There is still a relatively higher amount of DOC than the previous low pH condition (Fig. 2.3d), indicating that the weak organic binding sites remained in solution upon resuspension.

In both the settled and resuspended conditions at high pH (2.4 e, f), no organic cadmium remains in solution (Fig. 2.3b), and particulate cadmium becomes dominant (Fig. 2.3a). In addition, the DOC level drops to its original level (Fig. 2.3d).

2.3.4 Simplifying the model

Although this model fits our results, a simpler explanation is desirable. I propose that the two operationally defined organic matter types represent two different properties of the same substance.

In the past, several electrostatic models have been proposed to describe the electric double layer of charged surfaces and the binding which occurs at the surface. For example, since particles in nature are coated with negatively charged NOM, positive counter-ions are attracted which form a firmly attached layer around the particles, referred

to as the Stern Layer. As more positive ions are drawn towards the negative surface, they are repelled by the positive Stern layer. An equilibrium results when the counter-ion concentration balances the negative co-ions in the surrounding solution, this region being the diffuse layer. Together, the Stern and diffuse layers result in the double layer model (4, 33, 34, 35). Schindler and Stumm (21) suggest that the main reactive group on particle surfaces are hydroxyl groups, S-OH, which when deprotonated, exhibit Lewis base behaviour. Adsorption of metal ions on the surface is described as competitive complex formation with one or two hydroxyl groups. pH controls the extent of adsorption and the type of double layer on the surface determines the species obtained and their stability. Using a constant capacitance model Schindler found "significant correlation" between experimental and model data which indicates that the surface complexation model is appropriate.

However, Marinsky (22) noted that, of five electrostatic models proposed to describe an electric double layer, each model could represent the data well, but the values of corresponding parameters in all five models were not comparable. This indicated that the models were of appropriate mathematical form, but did not provide an accurate physical description of the surface-solution interface (22). Marinsky considered humic acids to be rigid and hydrophilic and also to behave as a polyelectrolyte.

If a polyelectrolyte is considered to be a charged domain, created by a matrix of active sites, both the volume, and the number of binding sites will increase if the amount of organic matter in the domain increases. More binding will occur with an increase in volume, and not with an increase in surface area (22, 23).

Brassard *et al* (20) identified an ampholytic surface site (21) and a polyelectrolyte domain (22, 23) in sediment particles. Suspended particles in natural water exchange protons according to two important mechanisms which can be related to their visible structure. Binding on surfaces imprisoned in the organic matrix accounts for 1/3 to 1/2 of the total binding capacity while the rest is caused by a polyelectrolyte sorption in the interior of the particle.

I thus propose that metal ion binding increases with the size of organic colloids. As agglomeration occurs, the organic material acquires a polyelectrolyte property with a greater affinity for metal ions. The build up of the organic material to produce the polyelectrolyte effect could occur either in solution by collision processes (eg Fig. 2.4a to 2.4b), or on the particle surface (eg Fig. 2.4f). Past a certain pH point, the colloid has a greater affinity for the particle.

The DOM surge is explained by the pH dependent coagulation of humics. At low pH, coagulation is promoted by protonation, which reduces charge on the surface, and agitation, which increases collision rates (See introduction). This produces colloids larger than a 0.2 micron diameter. As pH increases, colloids decrease in size and eventually appear in the dissolved phase at pH 6.2, when they are less than 0.2 microns in size. After pH 6.2, there is dispersion of organic colloids and accumulation on the particle surface.

Chapter 3

METAL ION BINDING DURING FLOCCULATION UNDER UNIFORM SHEAR STRESS

3.1 INTRODUCTION

A polyelectrolyte model has been proposed to explain the binding of metal ions to sediments during settling and resuspension. According to Smoluchowski (14), shear stress is also a major cause of flocculation. The following describes the design of the apparatus required to obtain a uniform shear stress to measure flocculation rates and metal ion partitioning with the sediment.

3.1.1 Design of the apparatus to control shear stress

Fluid shear is transmitted to the water column and shallow sediments by waves at the surface. The resulting mixing of the water column drives processes of aggregation and disaggregation of suspended particles.

Adequate control of Smoluchowski's three collision functions (Equations 2, 3, and 4) is required to fix the particle size distribution. The first two functions of Brownian collisions and differential settling are dependent on state variables, but, to produce a definable fluid shear requires a laminar, two-dimensional flow in order to define the velocity gradient and thus shear stress.

Theoretically, this is obtainable with a liquid contained between two infinite parallel plates; practically, it is done with concentric cylinders, one or both rotating. The flow produced between them is called a Couette flow.

The velocity distribution in the fluid between two plates is found by integrating Navier-Stokes equations (12). For a radius, r to any point in the annulus, with tangential velocity, u and angular velocity, ω (where u = ωr), a steady uniform flow in the direction rotation is represented by the Navier-Stokes equations as:

$$\frac{du}{dr} + \frac{u}{r} = constant \qquad (19)$$

By integrating and setting $u = \omega_1 \cdot R_1$ for $r = R_1$ (radius of inner cylinder) and $u = \omega_2 \cdot R_2$ for $r = R_2$ (radius of outer cylinder) as boundary conditions, the distribution over the annulus becomes:

$$u = \frac{\omega_2 R_2^2 - \omega_1 R_1^2}{R_2^2 - R_1^2} r + \frac{(\omega_1 - \omega_2) R_1^2 R_2^2}{R_2^2 - R_1^2} \frac{1}{r} \qquad (20)$$

which gives

$$\frac{du}{dr} = \frac{\omega_2 R_2^2 - \omega_1 R_1^2}{R_2^2 - R_1^2} - \frac{(\omega_1 - \omega_2) R_1^2 R_2^2}{R_2^2 - R_1^2} \frac{1}{r^2} \qquad (21)$$

and

$$\frac{U}{r} = \frac{\omega_2 R_2^2 - \omega_1 R_1^2}{R_2^2 - R_1^2} + \frac{(\omega_1 - \omega_2)\, R_1^2\, R_2^2}{R_2^2 - R_1^2}\,\frac{1}{r^2} \qquad (22)$$

The mean velocity gradient (G_m) over the annulus width, $R_2 - R_1$, must take into account the rotation of the whole apparatus which does not generate shear stress. G_m is given by averaging the difference between the velocity gradient and the rotation of the whole apparatus:

$$G_m = \frac{1}{R_2 - R_1} \int_{R_1}^{R_2} \left(\frac{du}{dr} - \frac{U}{r} \right) dr \qquad (23)$$

In our case, only the outer cylinder rotates and $\omega_1 = 0$:

$$G_m = \frac{2\omega_2 R_1 R_2}{R_2^2 - R_1^2} \qquad (24)$$

Typically, the maximum shear stress occurring in the natural environment is about six dynes cm^{-2} (10). This represents the equivalent of a severe storm. The generation of suitable shear gradients is done by proper selection of drive mechanism and cylinder size. If the cylinders get too small in diameter, they rotate too fast and centripetal forces become significant. The annulus width also affects velocity gradient range and flow stability. A narrow annulus is preferred since smaller shear variations occur. Taylor (36) predicted that a two-dimensional flow is stable at higher shear stresses if only the outer cylinder is

rotating. However, there is a limiting outer rotation speed for the flow to remain laminar. By combining van Duuren's equation (12) for mean velocity gradient (Equation 25) and expression for limiting rotation frequency as a function of cylinder size (Equation 26), a plot of maximum shear stress attainable in a laminar flow versus inner cylinder radius can be

$$\tau_m = \frac{4\pi \mu R_1 R_2}{R_2^2 - R_1^2} f \qquad (25)$$

produced (See Figure 3.1).

$$f = 3.16 \times 10^5 \nu \frac{(R_2 - R_1)^{0.7}}{R_2^{2.7}} \qquad (26)$$

where τ_m is shear stress (dyne cm^{-2}), μ is viscosity (g cm^{-1} s^{-1}), f is rotation frequency, R_1 and R_2 are inner and outer cylinder radii (cm), and v is the kinematic viscosity (v = 0.1 cm^2 s^{-1} for a sediment suspension). For a narrow annulus width of 2 mm, Figure 3.1 demonstrates that an inner cylinder width of about 3.4 cm will give the maximum required laminar shear stress of about 6 dyne cm^{-2}.

Ideally, the cylinders should have infinite length to avoid end effects. Practically, a length of about 30 cm is sufficient. These concentric cylinders may be oriented vertically which limits end effects, but sedimentation effects on larger flocs are serious. To avoid

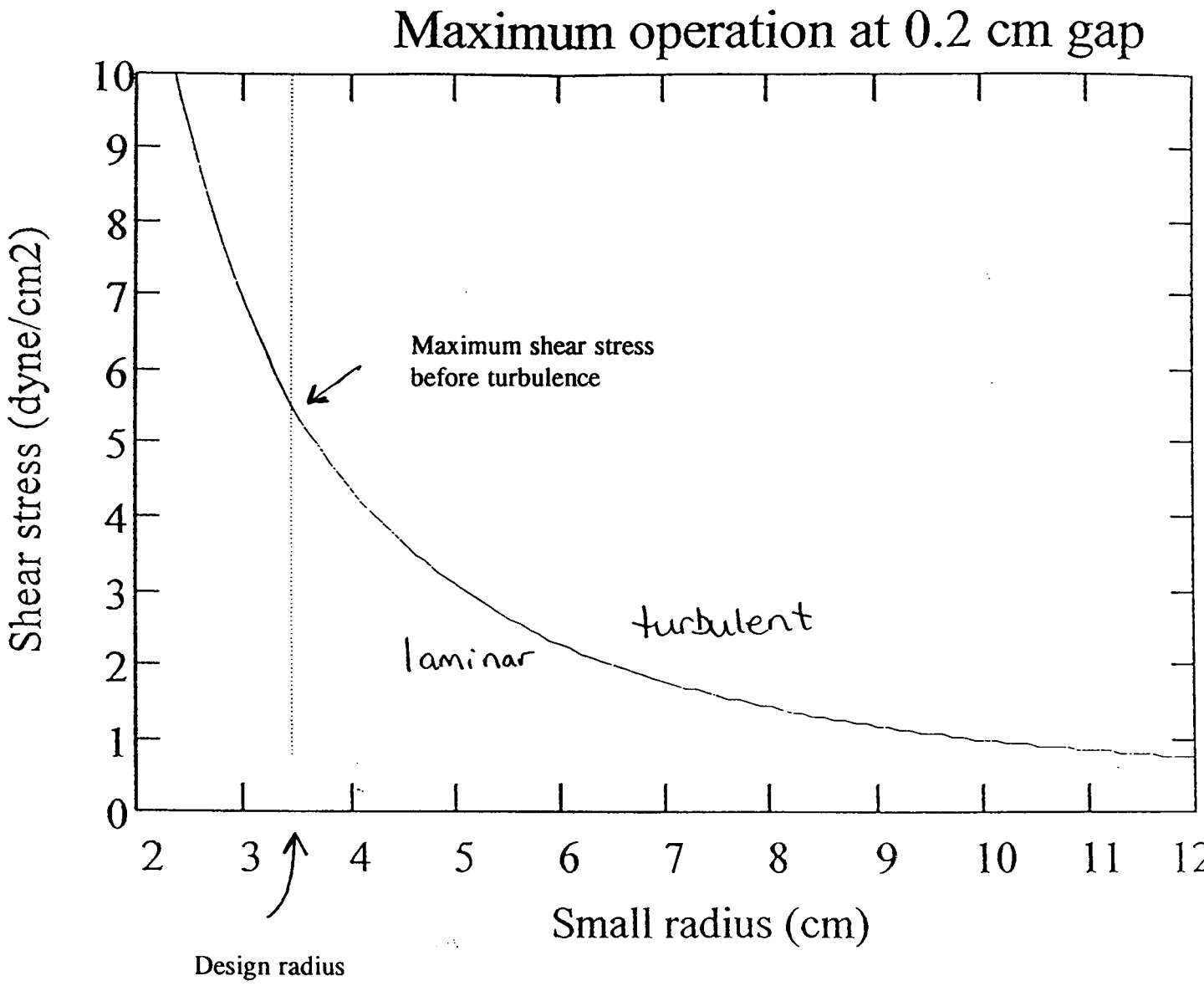

Figure 3.1: Effect of inner cylinder radius on maximum available shear stress for a 0.2 cm annulus.

sedimentation, the cylinders are mounted horizontally. Finally, it is desirable to be able to imprison a fluid within these moving walls and still be able to replace the suspension inside when necessary (12). A device which meets these criteria is called the Couette flocculator, and is pictured in Figure 3.2. For our flocculator design, inner and outer cylinder widths of 3.4 and 3.6 cm were chosen, leaving an annulus width of 2.0 mm (Figure 3.3). The length was 25 cm and the inner and outer cylinders were made of delrin and acrylic, respectively.

3.2 MATERIALS AND METHODS

3.2.1 The Couette Flocculator

Shear stress experiments were performed in a Couette flocculator (Figure 3.2), length 25 cm and annulus gap of 2.0 mm. The inner and outer cylinders were made of Delrin and acrylic, respectively. The inner cylinder was clamped horizontally to two anchored seats. Two end pieces were threaded and contained O-rings and bearings for easy removal, a good seal, and smooth rotation. A stopcock was built into one end for the removal of air bubbles. Four inlet/outlet ports were built in the inner cylinder. Polyethylene tubing was fed through each port to access the annulus volume. Two ports were widened into a shallow cone shape (diameter = 1.9 cm) on the inner cylinder surface, and were topped with a filter support to hold a 0.2 μm membrane (Nuclepore) (Figure 3.3). A large rubber O-ring (#250) was used as a belt and attached to the motor shaft in front

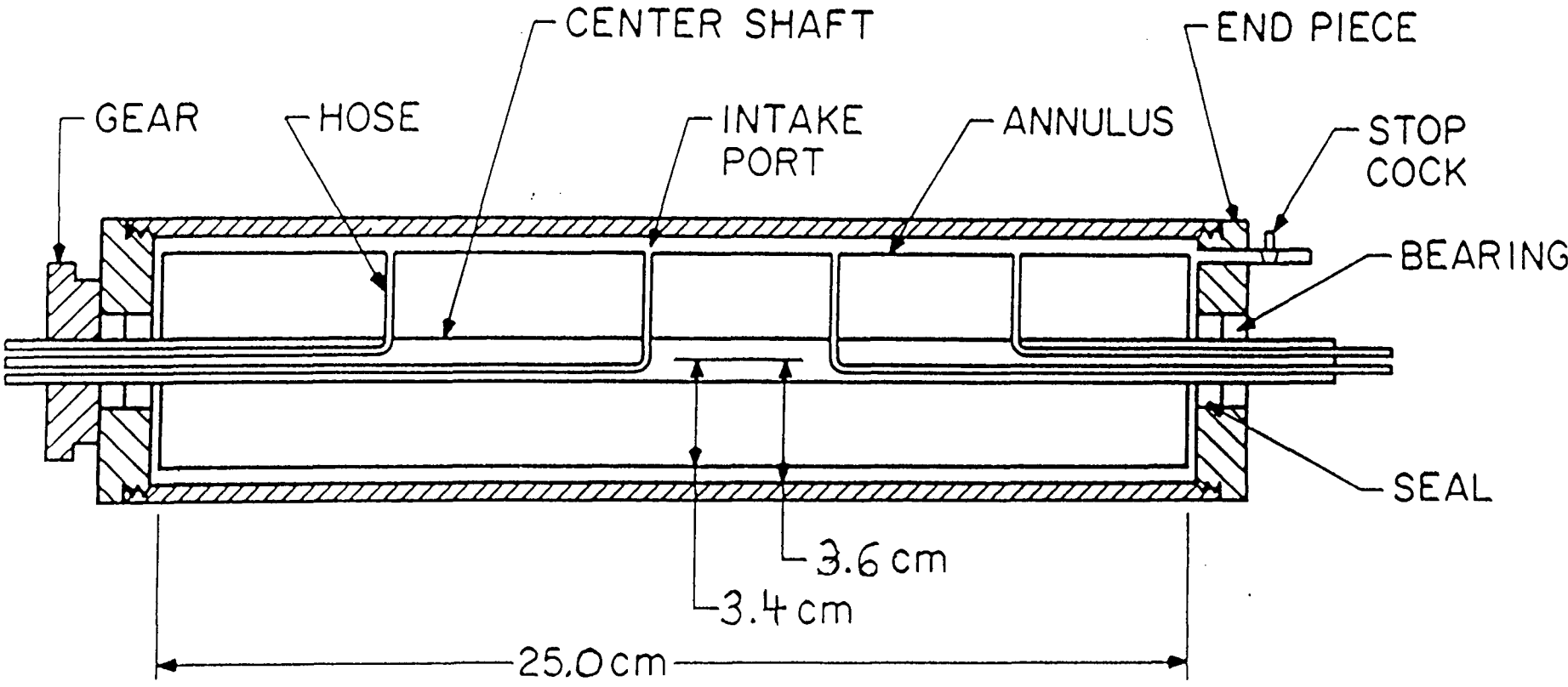

Figure 3.2: The Couette flocculator (Burban and Lick, 1989).

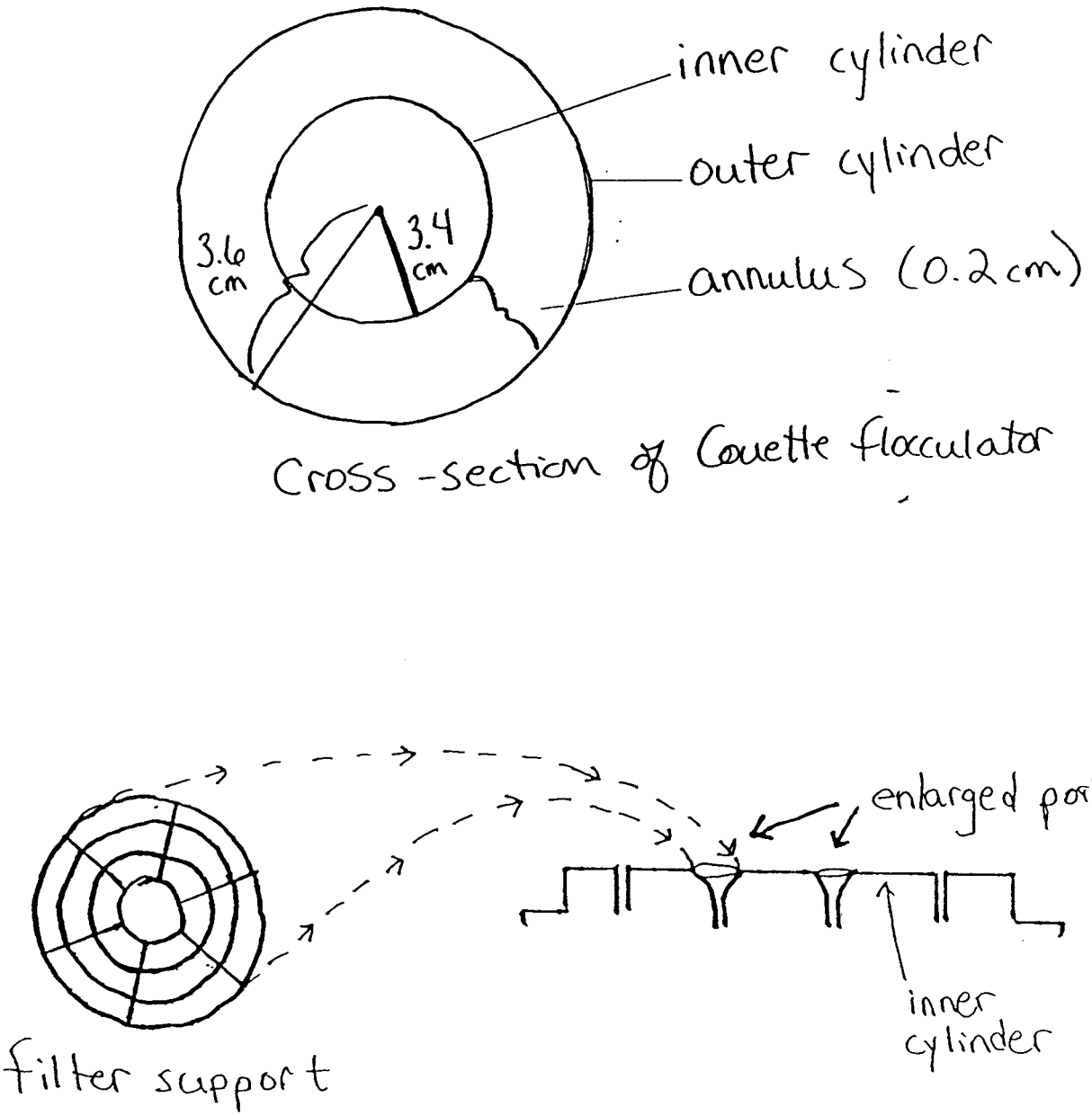

Figure 3.3: The Couette flocculator (cross-section and filtration ports).

in order to rotate the outer cylinder. The motor (Gerald K. Heller Company, Model # 2T60 1110, variable speed, reversible, direct current, shunt wound motor) was connected to a speed controller (Gerald K. Heller Company, Model # S10 Motor Controller, 115V AC Power). The outer cylinder was also fitted with a tachometer to measure the speed of rotation of the tube.

Floc size was measured by the Northern Reflections image analysis program (Empix Imaging). The flocculator was illuminated with a fibre optic ring illuminator (Cole Parmer, Model # 9741-50, Low-noise illuminator). A video camera (shutter speed 1/10000 sec), connected to both a microscope objective (2.5 X) and bellows, was suspended over the flocculator (Figure 3.4) and adjusted so that the camera field covered a 2 mm by 2 mm area. Five pictures of flocs were taken in rapid succession. Each photo was deinterlaced to produce two separate images, for a total of 10 photos for each time sample. A background image, taken at full speed, was subtracted, and a low pass filter was applied, before thresholding. The resulting image was analyzed to produce a data file containing the floc area, perimeter, long and short chords for each particle. The diameter was determined from the particle surface area and an average particle size was obtained for each group of photos at a given time.

3.2.2 Floc aggregation/disaggregation analysis

Procedures for analysing floc aggregation and disaggregation under a uniform shear stress are presented in Figure 3.5. Initially, a series of photos were taken at full

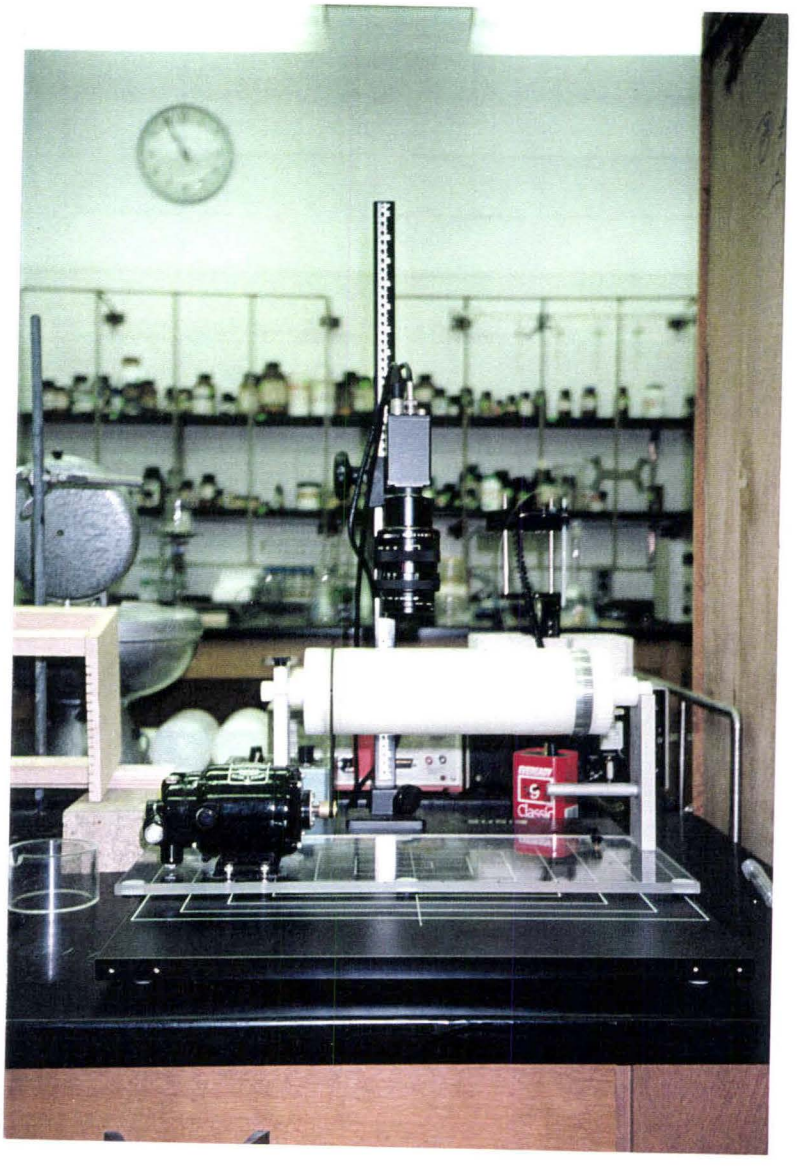

Figure 3.4: Image analysis configuration.

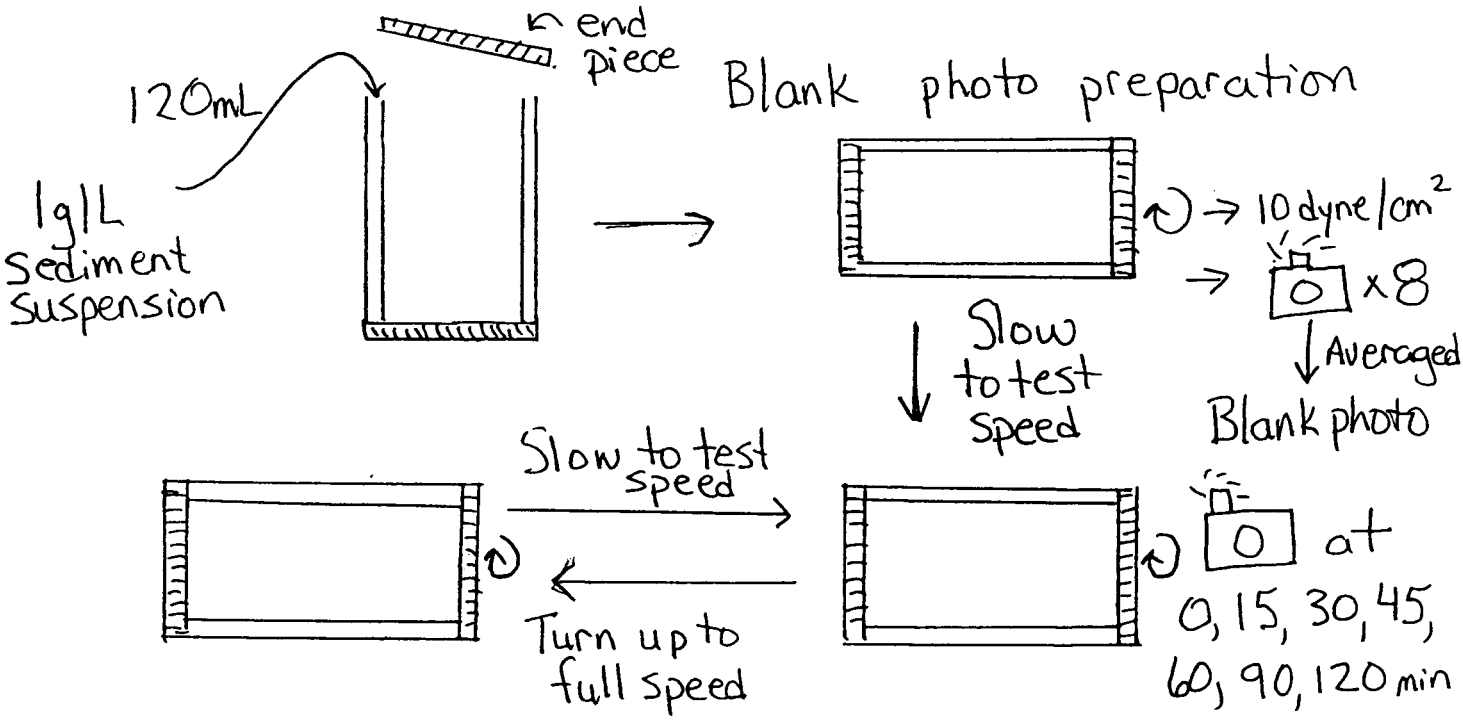

Figure 3.5: Procedure for analysis of floc aggregation/disaggregation under a uniform shear stress. Further details are presented in Appendix C.

speed and averaged to produce a background photo. Afterwards, the flocculator was set at several shear stresses. At each shear stress, seven sets of photos were taken over a period of two hours. Further details are presented in Appendix C.

3.2.3 Analysis of metal ion binding under shear stress

3.2.3.1 System calibration

Preparation: The flocculator was cleaned by removing all O-rings and soaking the inner and outer cylinders in a nitric acid bath (pH 2) for 24 hours. Sediment suspensions were prepared as described previously and metal ion cocktails at 100 and 50 ppb were prepared by diluting Plasmachem Associates, Inc. 1000 ppb, ICP-MS standards. The metal ion cocktails were prepared at a pH of about 2. When mixed with the sediment suspensions the resulting pH ranged from about 7 - 7.3.

Sediment metal ion background: Procedures for analysing background metal ions naturally existing in a sediment background under a uniform shear stress are presented in Figure 3.6. The flocculator was filled with a sediment suspension and rotated at several shear stresses. At each shear stress, supernatant samples were taken and a general ICP-MS scan was performed to determine the level of metal ions naturally present in the background. Further details are available in Appendix C.

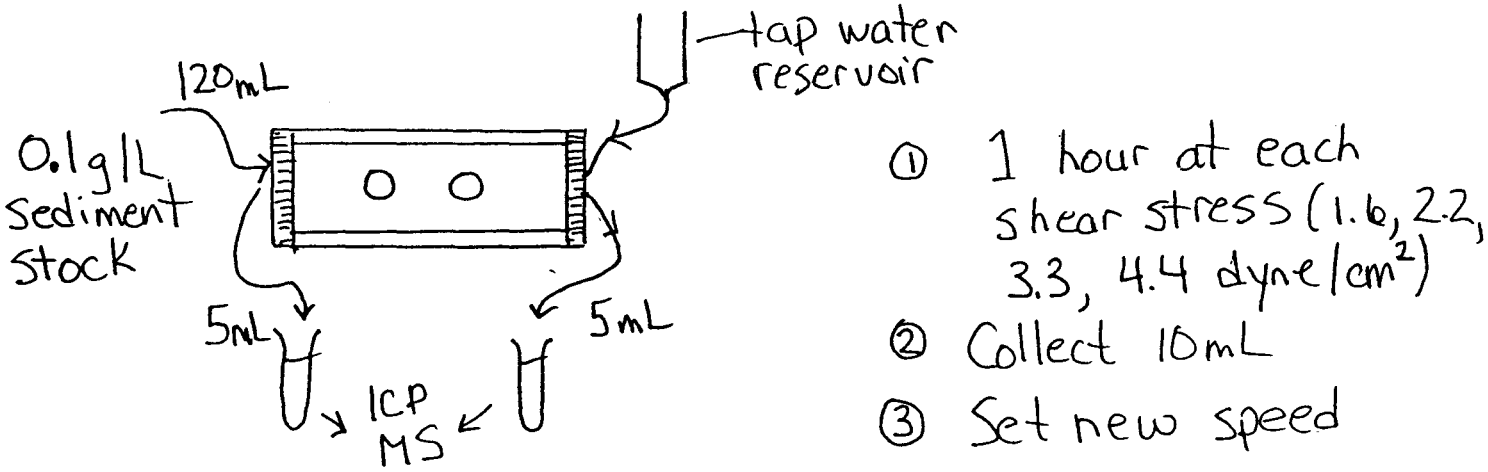

Figure 3.6 Procedure for analysing sediment metal ion background. Further details are presented in Appendix C.

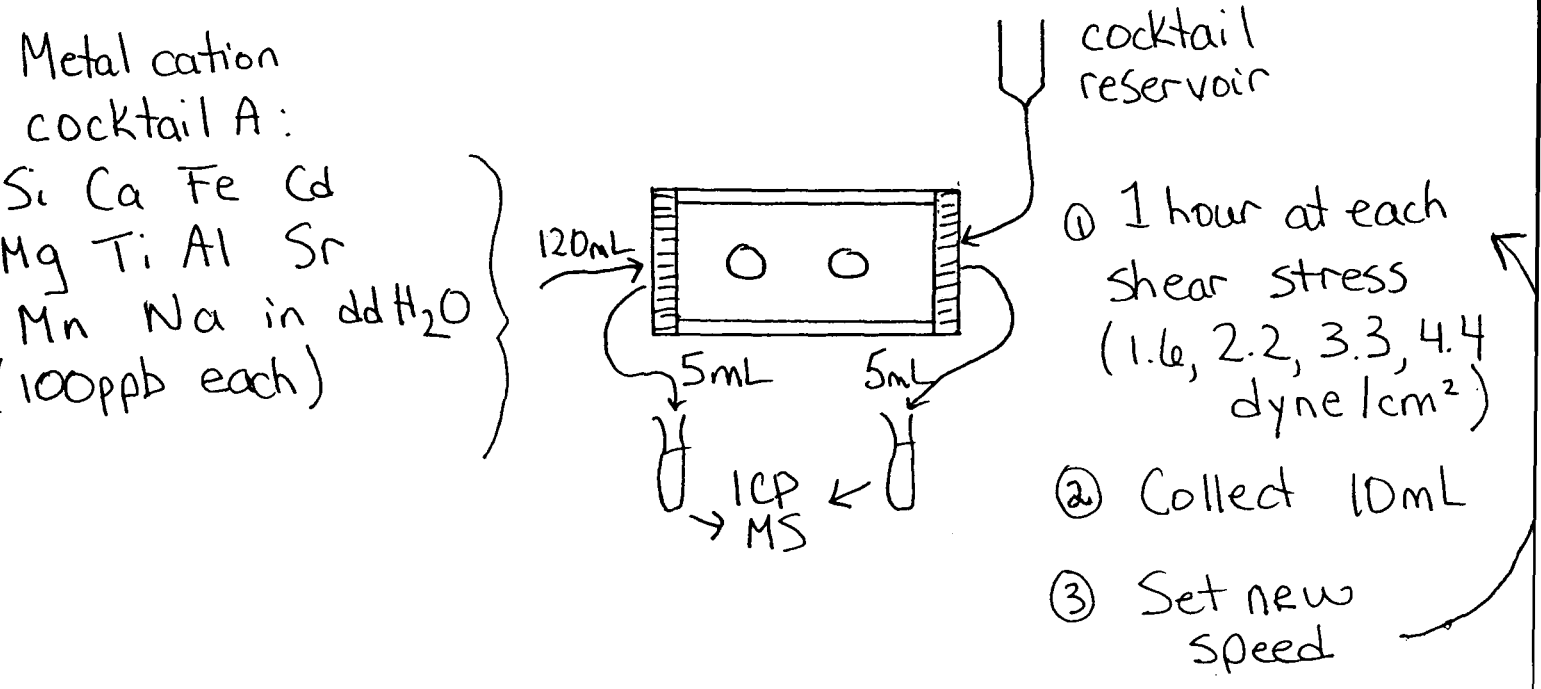

Figure 3.7: Procedure for determining metal ion concentration drift with speed. Further details are presented in Appendix C.

Metal ion concentration drift with shear stress: Procedures for analysing metal ion concentration drift with increasing shear stress are presented in Figure 3.7. The flocculator was filled with a metal ion cocktail and sampled after one hour of rotation at four different shear stresses. A semi-quantitative ICP-MS scan was performed. Further details are available in Appendix C.

Metal ion concentration drift with time: Procedures for analysing metal ion concentration drift with time under a uniform shear stress are presented in Figure 3.8. The flocculator was filled with a metal ion cocktail and set to rotate at a fixed shear stress. Samples were taken over 15 min intervals for 1.75 hours and after 4.5 and 24 hours. Further details are available in Appendix C.

3.2.3.2 Metal ion binding analysis

Procedures for analysing floc aggregation and disaggregation under a uniform shear stress and in the presence of metals are presented in Figure 3.9. The flocculator was filled with sediment suspended in a metal ion cocktail. After rotating at a fixed shear stress for two hours, a photo and an aliquot of the filtrate were taken. This process was repeated at several shear stresses. Further details are available in Appendix C.

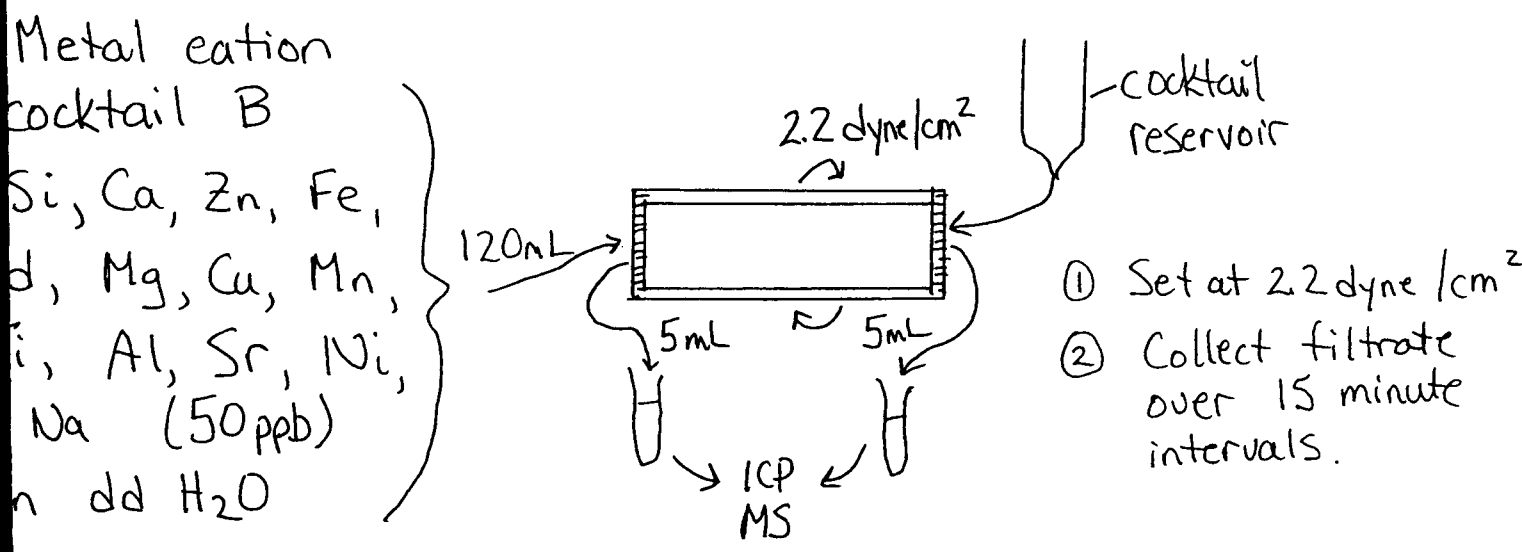

Figure 3.8: Procedure for determining metal ion concentration drift over time. Further details are presented in Appendix C.

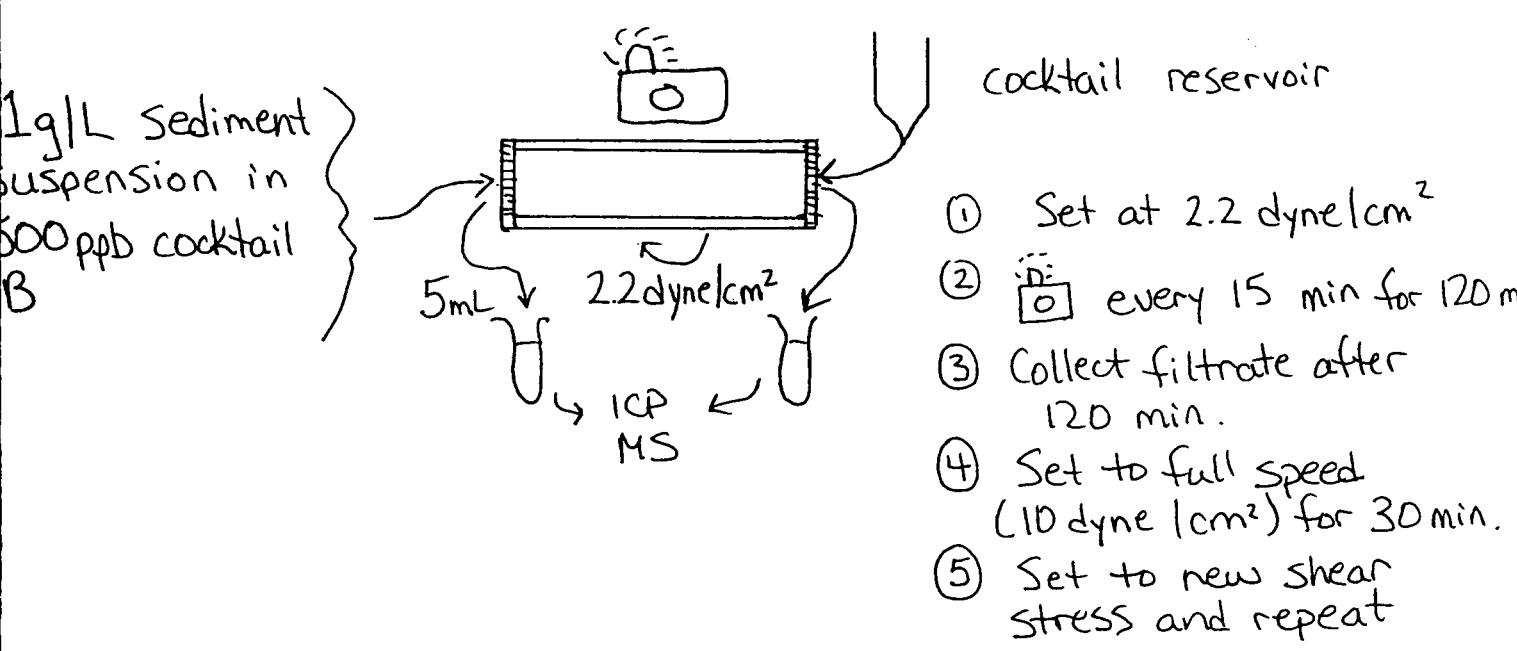

Figure 3.9: Procedure for analysing metal binding during sediment flocculation under a uniform shear stress. Further details are presented in Appendix C.

3.3 RESULTS AND DISCUSSION

3.3.1 Calibration of the apparatus

Figure 3.10 is an example of a typical particle size distribution for sediments in our Couette flocculator. When calculating a mean particle size for a distribution, for simplicity, a normal distribution was assumed, with one average size. The average was taken as a representative to estimate total particle surface and volume. Clearly the distribution is bi-model, which indicates that a single average may not be the most appropriate representation of the data. In the following discussion, mean particle size does assume a normal size distribution.

Several reports (10, 11, 13) describe work that studied the effects of fluid shear, and sediment concentration on the rates of aggregation and disaggregation of sediments. The results show that the median floc size decreases as the shear stress increases, and as the suspended sediment concentration increases. It follows that for a constant mass of sediment in a constant volume, the growth of larger particles leads to a decrease in particle number.

Data from our studies show that a plot of particle size and number versus time, at constant suspension loading and shear stress (Figure 3.11), demonstrates that steady state was reached in 30 minutes. When shear stress is increased by increasing the speed of the flocculator, the steady state particle size decreases. This effect is more pronounced as the particle concentration increases (Figure 3.12).

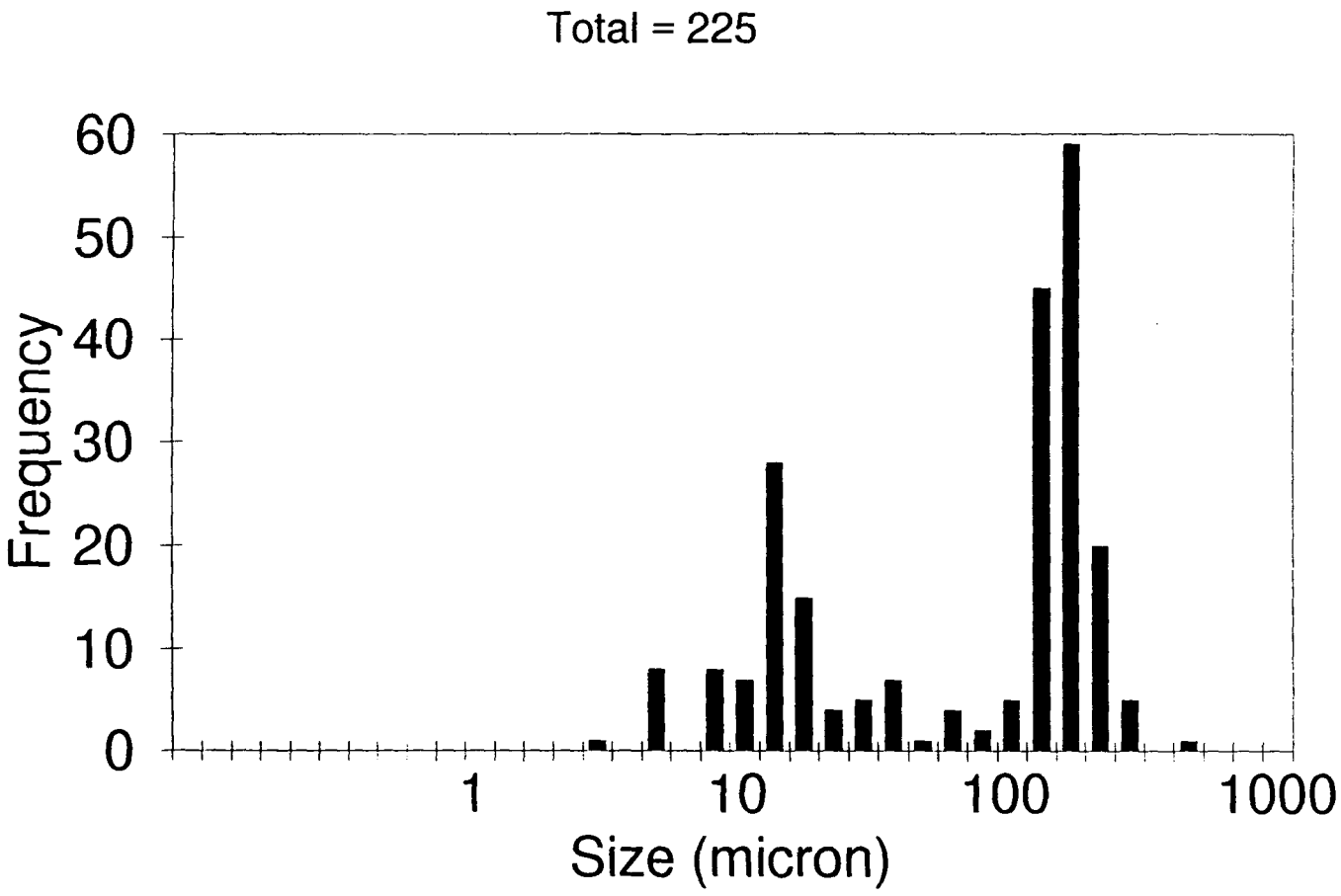

Figure 3.10: Typical particle size distribution taken from our Couette flocculator.

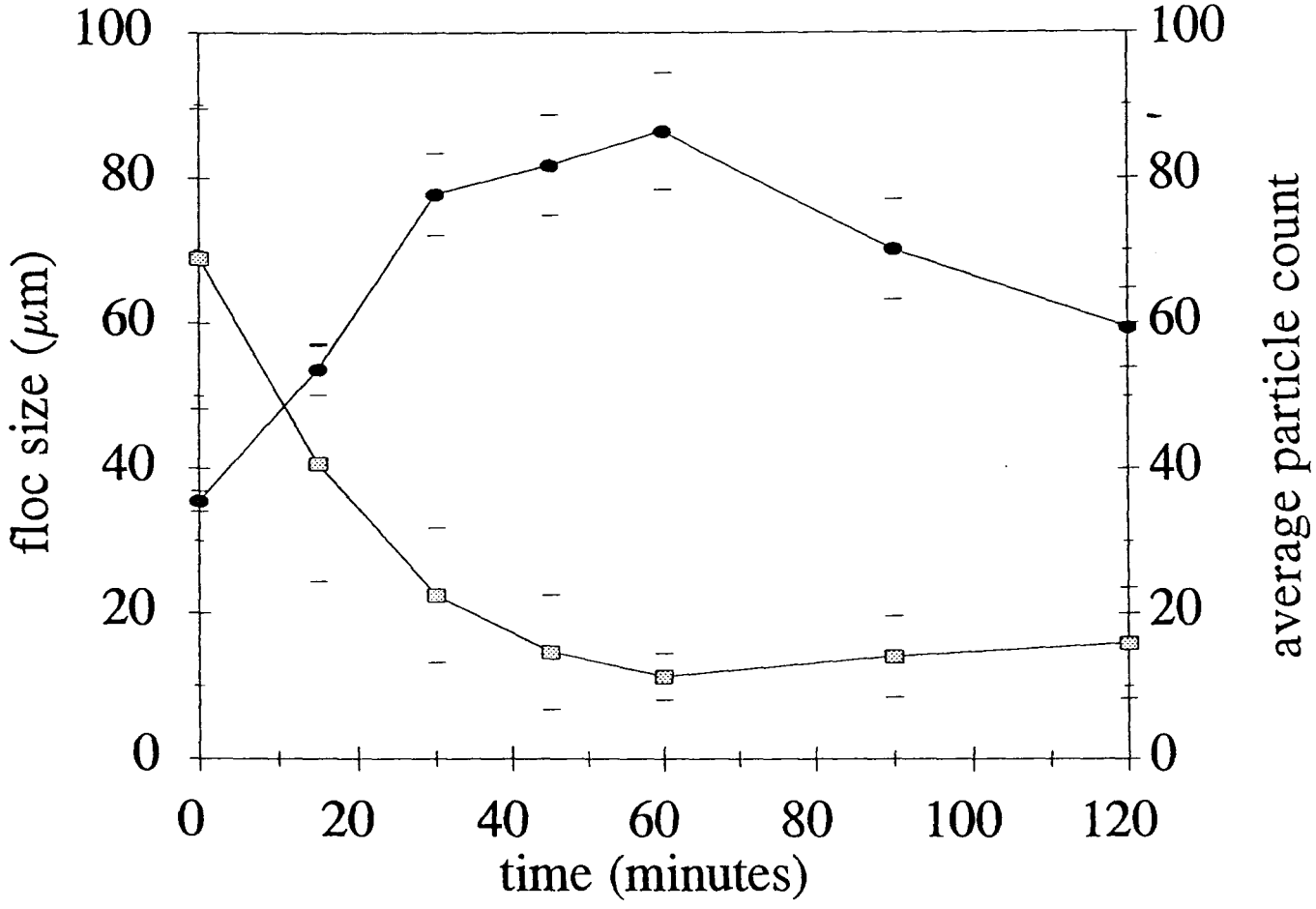

Figure 3.11: Floc size (μm)(●), and particle count (■), *versus* time for a 1 g/L sediment suspension at a shear stress of 1.6 dyne/cm^2.

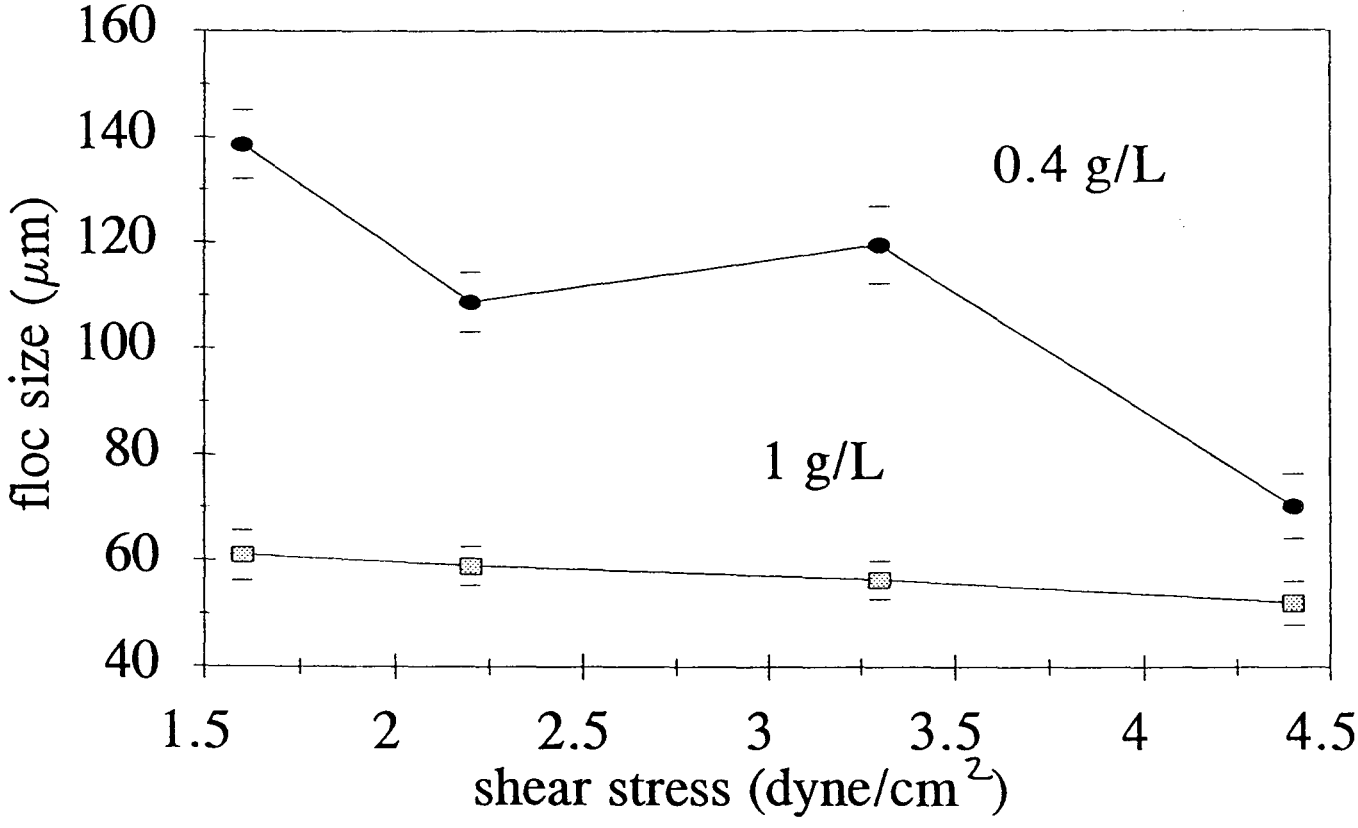

Figure 3.12: Steady state floc size (μm) *versus* shear stress (dyne/cm^2) for two suspension concentrations (●, 0.1 g/L; ■, 1.0 g/L).

We found a β value of 2.2 for the Coote's Paradise sediments (Figure 3.13), which agrees with Kavanaugh's range for low ionic strength environment. In our case, however, some deviation from the expected log-linear relationship occurs at both the low and high ends of the particle size range, which is explained by the limits of our camera system. Because our particle size analysis system does not see or count all particles less than 10 μm, fewer than expected small particles were detected. At the opposite end, too many large particles were counted which is due to the threshold function clumping particles together, which by eye, should not be. This produced an apparent higher count of particles larger than 100μm. Filella *et al* (37) have shown that a bimodal distribution tends to reduce to a unimodal one over time. Initially, small and large particles disappear very quickly, the former due to efficient Brownian coagulation and the latter because they settle down more quickly than they are formed by coagulation. Over time, these differences are reduced and a unimodal distribution is recovered. They attribute their bimodal distribution to a measurement artifact. This result suggests that the deviations at low and high particle sizes in Figure 3.13 could be due to insufficient equilibration time, and, that with further flocculation time, a unimodal distribution would be reached. This suggests that the scattered data (Figure 3.13) is due to the bimodal distribution. If true equilibrium had been reached, the scattered points would fall back to the expected values, thus we consider only the linear region.

3.3.2 Analysis of metal ion binding under shear stress

Sediments suspended in a fluid subjected to shear stress will collide with each

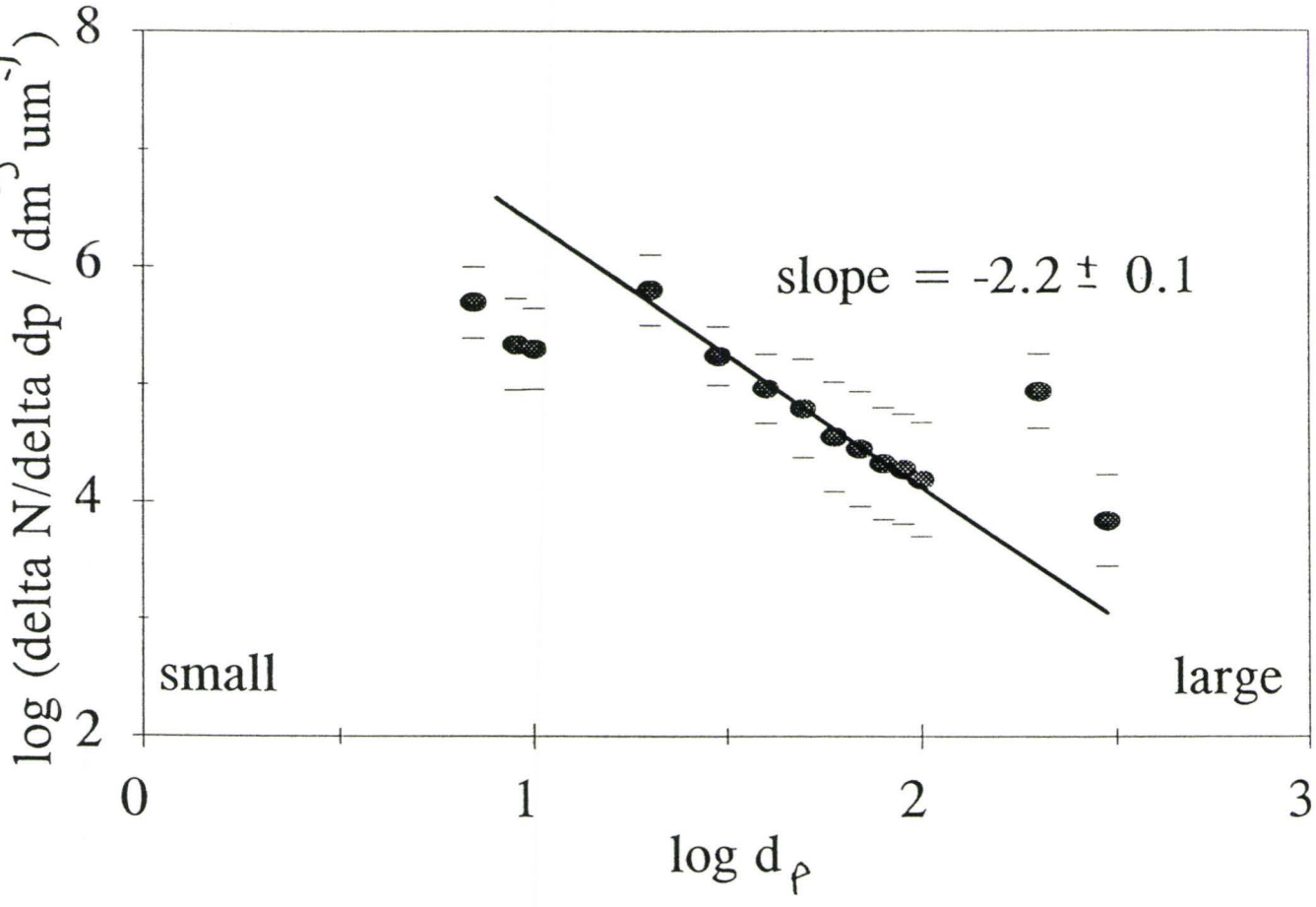

Figure 3.13: Particle size distribution analysis using the method of Hunt (15), Kavanaugh (16), and Filella (17) for a 1 g/L sediment suspension.

other, causing flocculation. Tsai (10) demonstrated that collisions due to shear stress contributed significantly to the overall collision frequency function. As aggregation occurs, particle surface area decreases and volume increases as the steady state particle size increases. It is expected that as floc size changes, the metal ion partitioning between the solution and sediment phases will change. If the binding of metal ions to the sediment surface is related to particle surface area, the total amount of bound metal ion should decrease with increasing floc size. If the metal ion binding is particle volume dependent, the opposite will occur; metal ion binding will increase with floc size.

3.3.2.1 System calibration

If accurate analysis of the metal ion content in the Couette flocculator is to be made, it is essential to know the background metal ion level arising from sediment suspensions in the flocculator, or from operation of the flocculator itself.

Sediment metal ion background determination: As the shear stress increased, in all cases except for iron, the metal ion intensity remained constant. This indicates that no metal ions we considered would be released from the sediment in the flocculator as it rotates, under typical experimental conditions. The metal ions which are expected to bind to sediment when added to the system (nickel, copper, zinc, and cadmium), were naturally present at, or below 15 ppb. The increase in iron metal ions is likely due to the continual rusting of the bearing casings in the ends of the flocculator tube. This will be minimized by the dismantling, cleaning, and lubrication of the inside workings of the end pieces with silicon grease before each experiment.

Metal ion concentration drift with shear stress changes (no sediments): The data is presented in Appendix D. As the shear increased, slight variations in the original metal ion cocktail concentration of 100 ppb occurred. Iron ions approximately doubled at the highest shear stress of 10 dynes/cm^2. Appendix D demonstrates that, at shear stresses ranging from 1.6 to 4.4 dyne/cm^2, the majority of the remaining metal ions varied within 6% of their average concentration. The average concentrations for calcium and sodium are not an accurate reflection of the flocculator system because the ICP-MS analysis proved to be extremely variable for these elements, due to memory effects from previous samples.

Metal ion concentration drift with time (no sediments): Appendix E presents the ICP-MS data obtained when cocktail B in the flocculator was sampled over time at a shear stress of 2.2 dyne/cm^2. Of the metal ions in cocktail B, cadmium, copper, nickel, and zinc are expected to bind most significantly to sediments. With no sediments present, over time cadmium, copper, and nickel remained constant for 24 hours (Figure 3.14). However, the zinc started to increase after about five hours from 50 ppb to a maximum of 300 ppb at 24 hours. Appendix E demonstrates that, for the average concentration over 24 hours, a relative error of less than 9% was accumulated for each of cadmium, copper, nickel, and zinc. The remaining metals all had relative errors less than 13 % after 24 hours. These errors tended to significantly increase over the final 20 hours of the experiment. If an experiment was designed such that its duration would be no longer than 4 hours, relatively insignificant drift would occur over the time period.

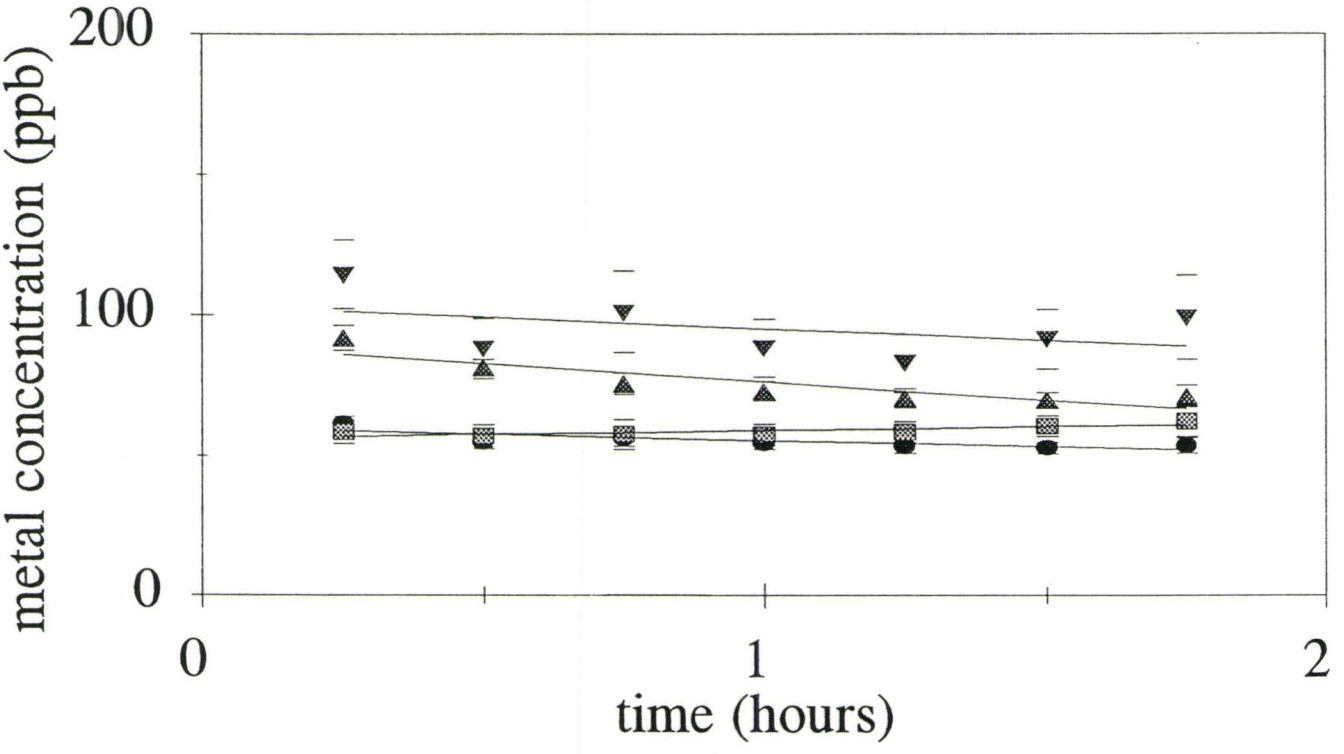

Figure 3.14: Variation of 50 ppb metal ion cocktail B with time: cadmium (●), copper (■), nickel (▲), zinc (▼). Error bars represent deviation from the mean.

3.3.2.2 Metal ion binding analysis

Data from our studies show that, over time at each shear stress tested, the floc size increased while the particle count decreased as equilibrium was approached (Figure 3.15). Larger floc sizes were obtained at slower rotation speeds (Figure 3.16). In general, the floc size increased at lower rotation speeds more significantly when metal ions were added to the system (Figure 3.17) than when no metal ions were present. This strongly suggests that the presence of the metal ions on the sediment surface neutralizes the charge, thereby decreasing colloidal stability and increasing flocculation. A small amount of metal ion added to the system caused a relatively large change in the properties of the flocs formed, without significantly changing the double layer properties of the particles.

Hunt, Kavanaugh and Filella's beta value analysis of our floc size distribution in a metal ion cocktail ($\beta = 2.5$) was comparable to our system with no metal ions (Figure 3.18). This indicates that the same collision mechanics occurred in both experiments, which is expected since all experiments were performed in the same apparatus under a uniform shear stress. Similar outliers at low and high particle sizes were apparent. Again, we attribute these deviations to artifacts of our particle size analysis system.

Of the metal ions present at 500 ppb in cocktail B, cadmium, copper, nickel, and zinc were expected to bind to sediments. The extent of binding increased as follows: nickel, cadmium, zinc, copper, ranging from about 100 ppb bound to the sediment to 490 ppb bound to the sediment (Figure 3.19). In order to compare the affinity of metal ions to Cootes Paradise sediment to other sediments, a distribution coefficient (K_D) can be

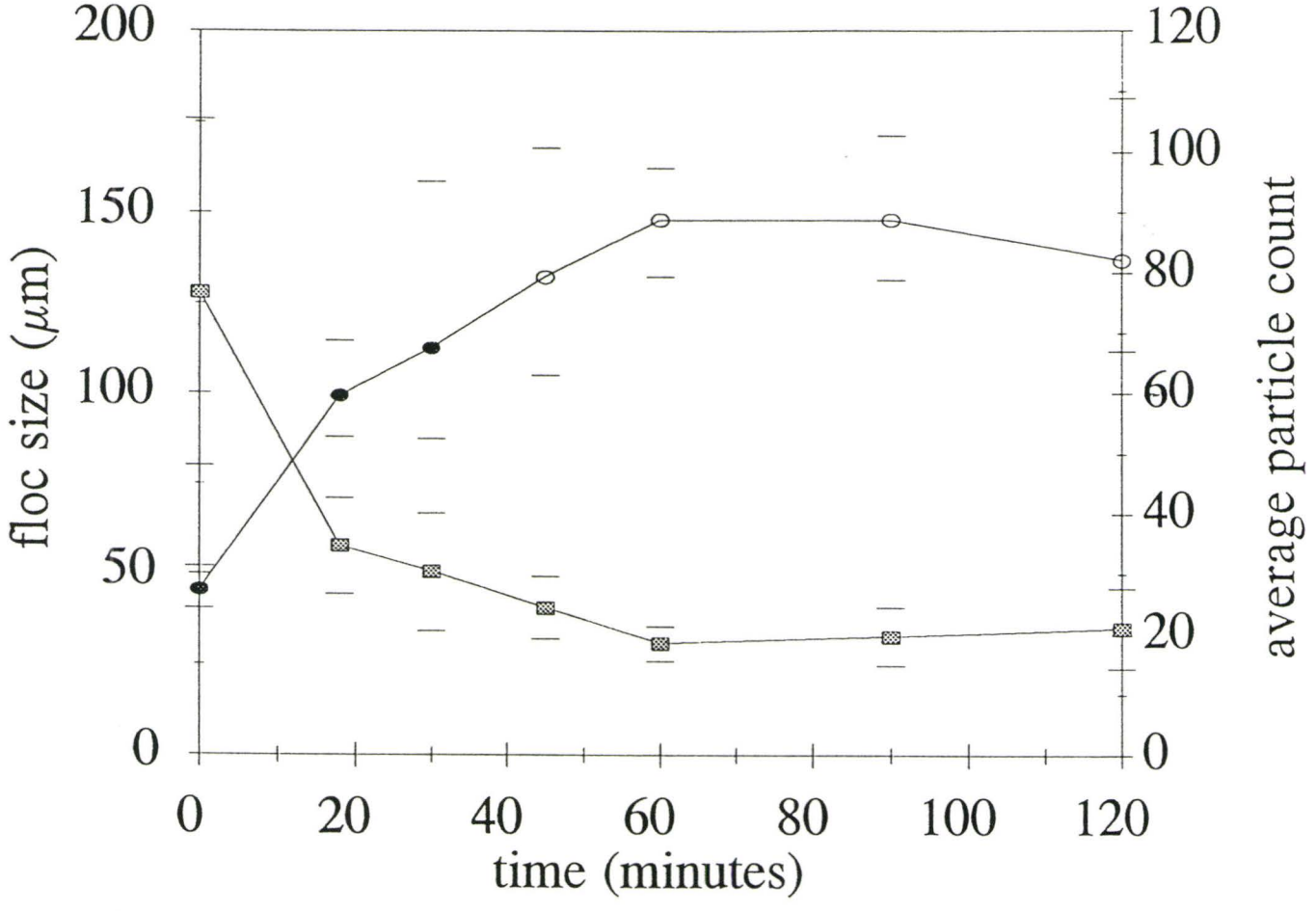

Figure 3.15: Floc size (μm)(●), and particle count (■), variations with time for a 1 g/L sediment suspended in 500 ppb metal ion cocktail B, at a shear stress of 2.2 dyne/cm^2. Error bars represent deviation from the mean.

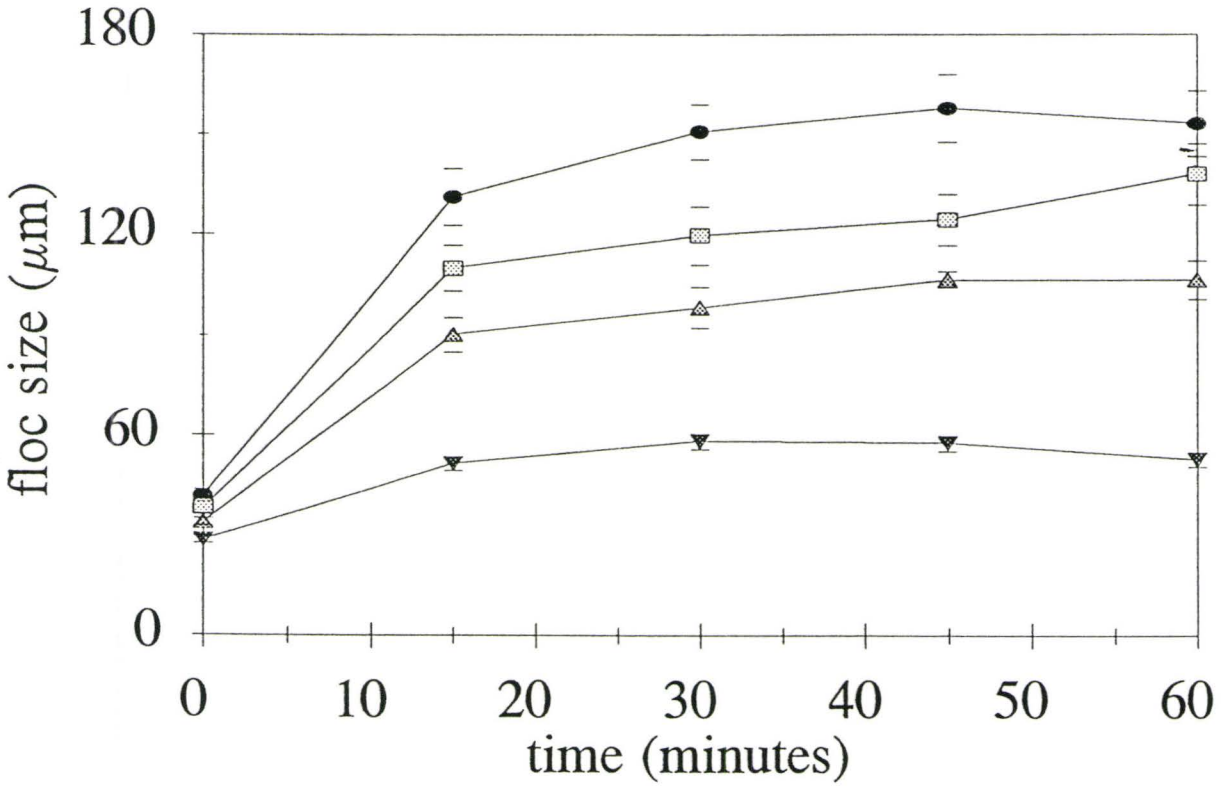

Figure 3.16: Floc size (μm) variations with shear stress (1.6 dyne/cm^2 (●), 1.9 dyne/cm^2 (■), 2.2 dyne/cm^2 (▲), 4.4 dyne/cm^2 (▼), for a 1 g/L suspension.

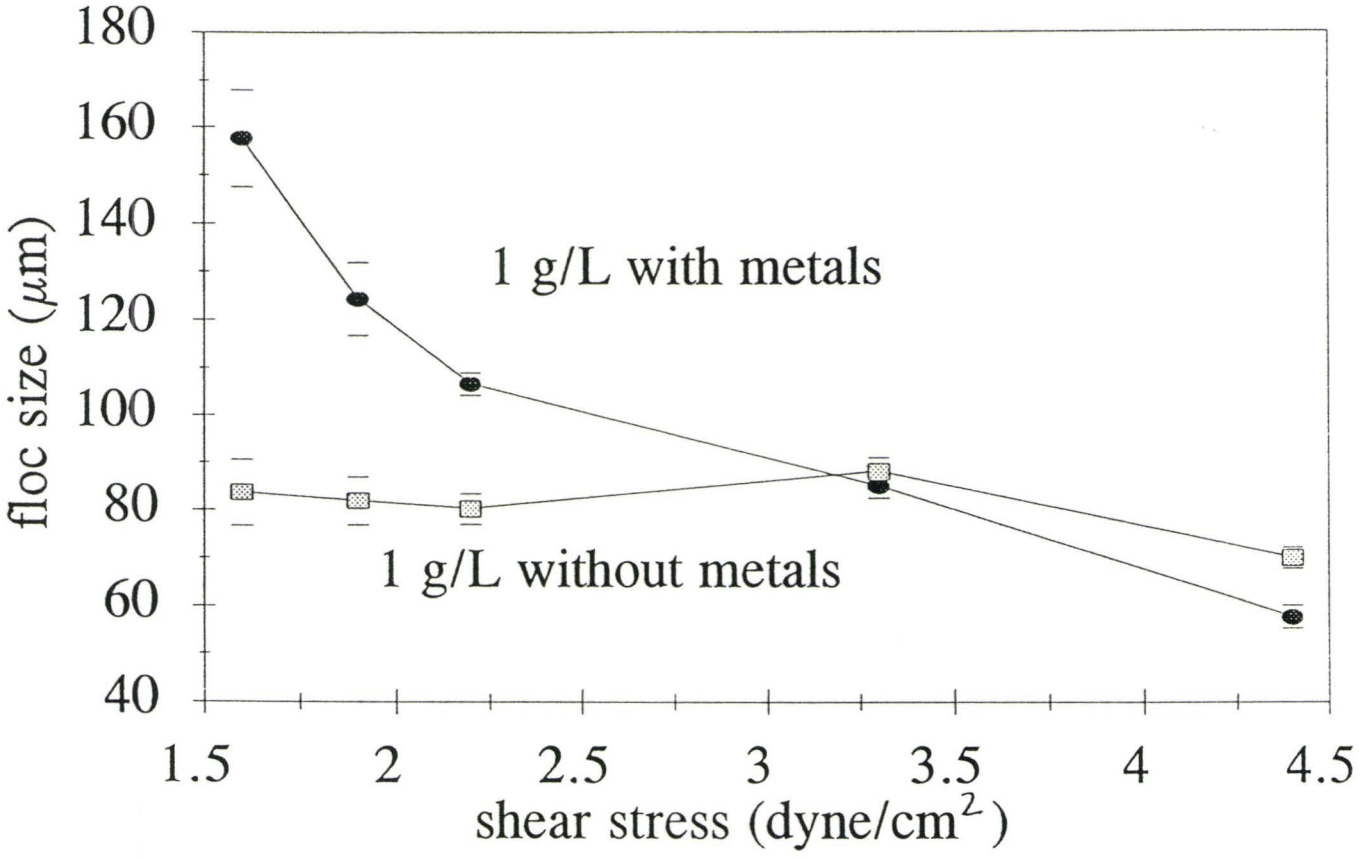

Figure 3.17: Comparison of steady state floc size with and without metal ions present (with metal ions, ●; without metal ions, ■).

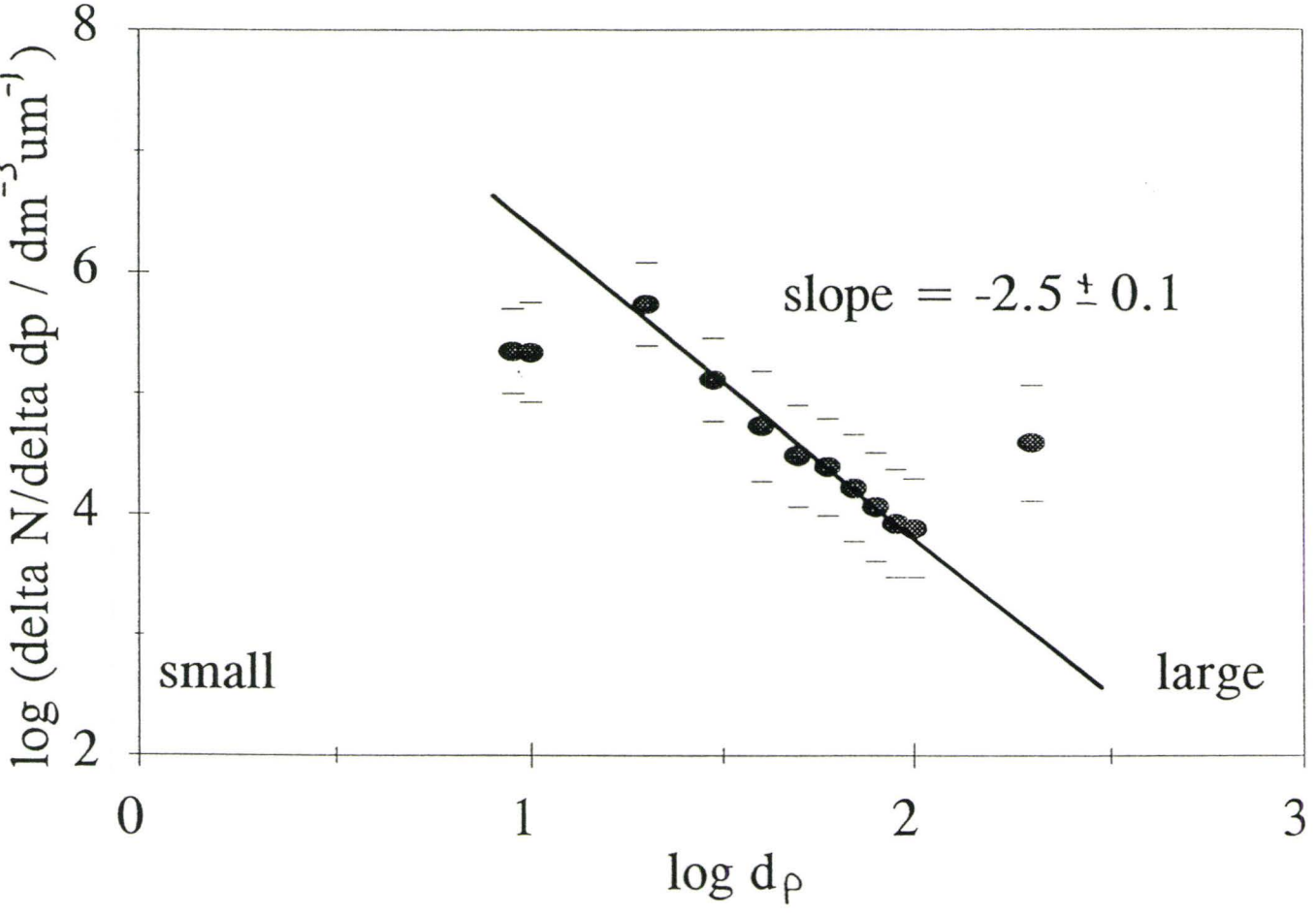

Figure 3.18: Particle size distribution analysis by Hunt, (15), Kavanaugh (16) and Filella (17) for a 1 g/L sediment suspension in 500 ppb of metal ion cocktail B.

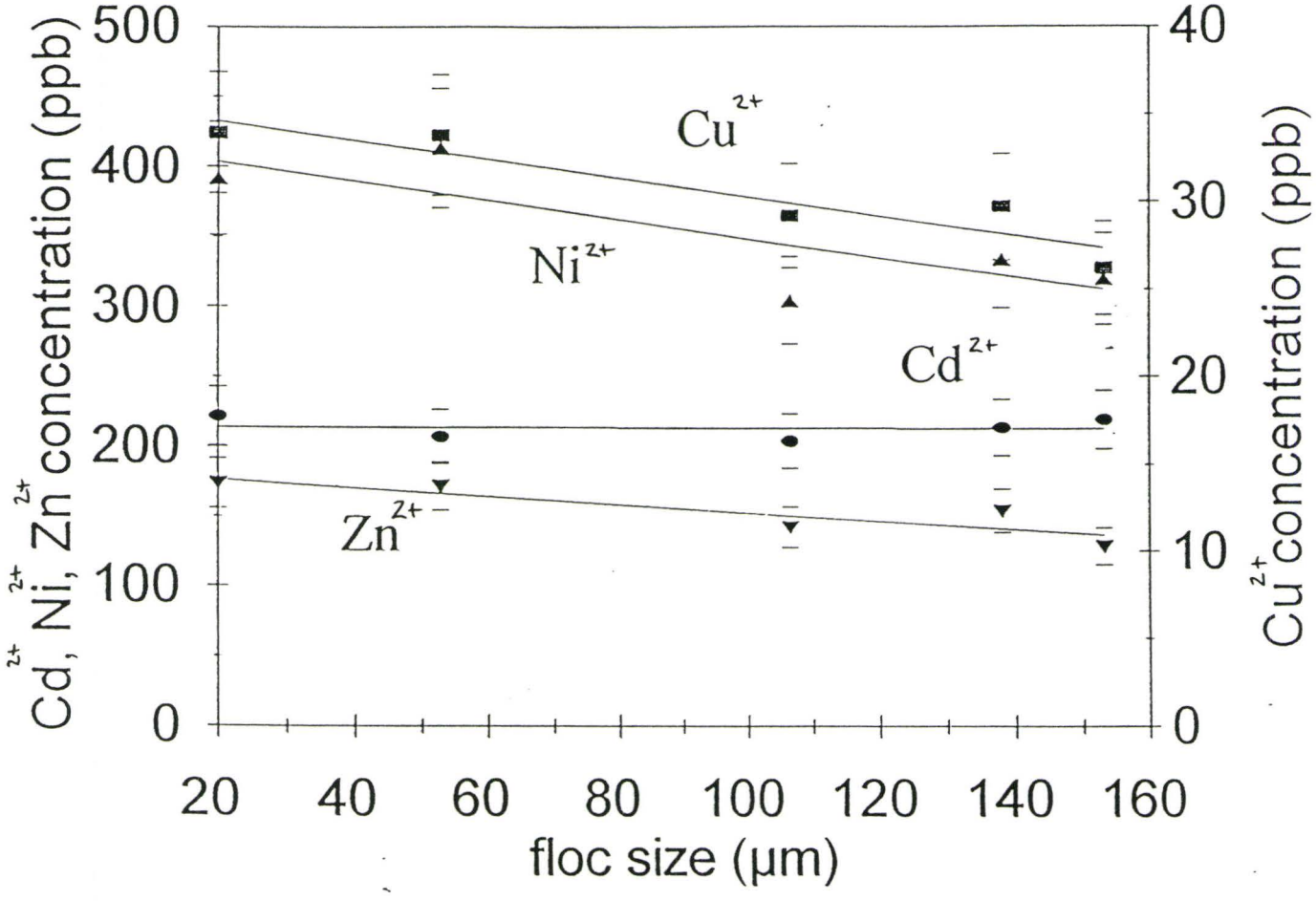

Figure 3.19: Change in free metal ion concentration with increasing floc size for a 1g/L sediment suspension in 500 ppb of metal ion cocktail B, at a shear stress of 2.2 dyne/cm^2.

calculated. Tessier (38) expresses partitioning of metal ions between solution and sediment using this distribution coefficient, K_D (L/g):

$$K_D = \frac{[M_p]}{[M_d]} \frac{1}{C_p} \qquad (27)$$

where M_p is the concentration of metal ion bound to particles in μg/L, M_d is the free concentration of the metal ion in μg/L, and C_p is the particle concentration in mg/L.

Values of log K_D were calculated for each of cadmium, copper, nickel, and zinc from the metal ion partitioning data under uniform shear stress (Figure 3.19) and are presented in Table 3.1 and plotted on Figure 3.20:

Metal ion	log K_D	First hydrolysis constant (log K)
Cd	3.2	-10
Cu	4.2	-8
Ni	2.6	-10
Zn	3.4	-9

Table 3.1: Metal ion distribution coefficients

K_D values have been related to the first hydrolysis constant for the metal ion in seawater

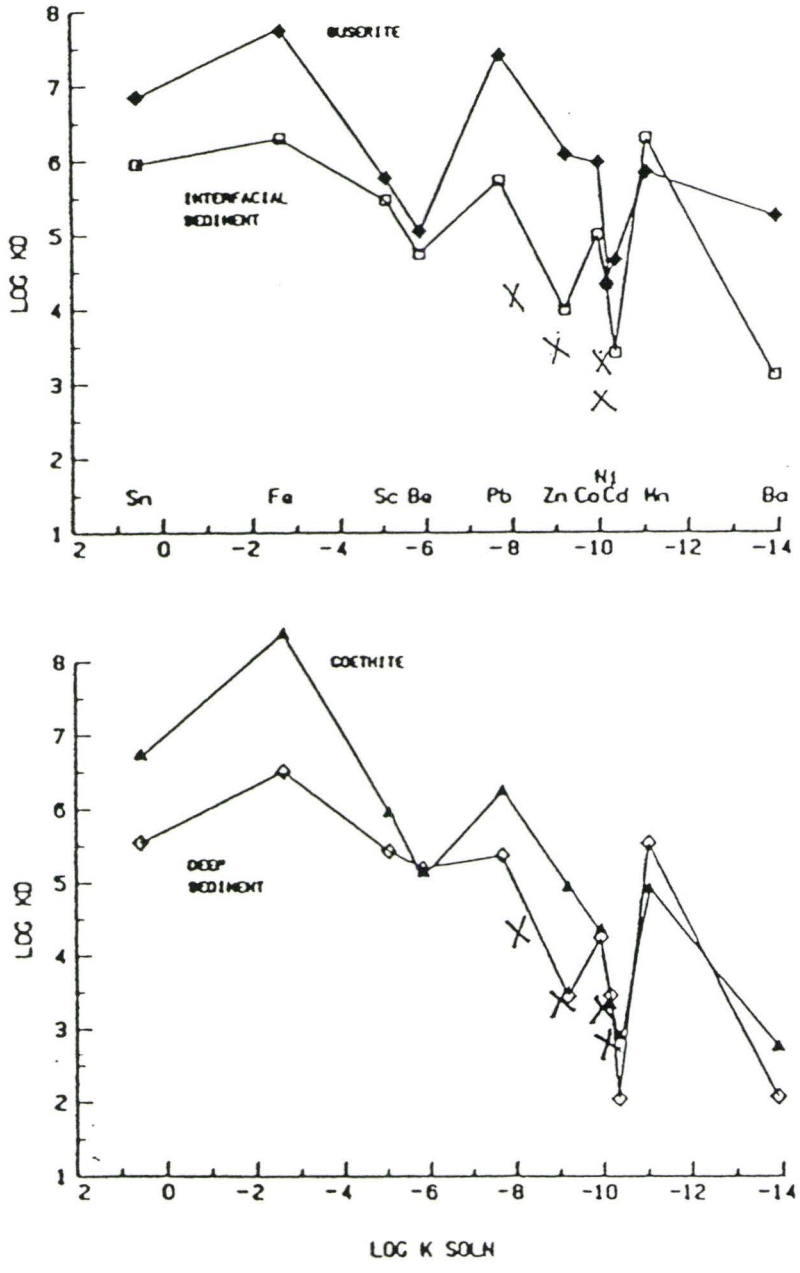

Figure 3.20: Log K_D values *versus* the first hydrolysis constant of the metal ion in seawater (39) for interfacial (0.5 - 3 cm) and deep sediment (15 - 19 cm) from the Panama Basin and for goethite (α-FeOOH) and buserite ($MnO_{1.59}$) (38). Log K_D values were added for cadmium, copper, nickel, and zinc binding to 1 g/L Coote's Paradise sediments.

(39). Figure 3.20 compares our results with experimental data from Balistrieri *et al* (39) and Baes *et al* (40) (Figure 4 in 38). A correlation between log K_D and log K (hydrolysis constant) is apparent and our data is consistent with the reported metal ion binding to both sediments and artificial surfaces. Although falling in the same order of magnitude, Figure 3.20 also demonstrates the widely varying affinity of different sediments for one metal ion. A simple assumption that log K_D is related to log K does not explain all the binding of metal ions to different surfaces.

Changes in metal sorption with particle size indicate what part of the floc is important for metal exchange. Assuming flocs to be incompressible volumes, the total surface area should increase with smaller floc sizes while the volume of individual flocs should decrease. It follows that the decrease in metal ion sorption in Figure 3.19 is due to processes occurring int he volume of the flocs, not on the surface as proposed by surface complexation models.

Balistrieri *et al* (41) found that values of K_D tend to decrease with increasing particle concentrations. Since K_D is a ratio of particle bound metal ion to dissolved metal ion, the actual amount of metal ion binding is decreasing with increasing particle concentration. Honeyman and Santschi (42) propose that the increase in K_D is caused by a filtration artifact. We propose that the decrease in metal ion binding with increasing particle concentration is due to a polyelectrolyte effect. Increasing concentration has been shown to result in more collisions and decreased particle size as show by Burban *et al*, Tsai, *et al*, and Lick *et al* (10, 11, 13) and by the results in our Couette flocculator. According to

the polyelectrolyte theory, this would result in a decrease of metal ion binding, due to a volume decrease in each particle.

SUMMARY

Binding sites for a constant particle size distribution were characterized with pH edge titrations. A proton binding site and a cadmium-proton exchange site were identified.

Two significant causes of aggregation and disaggregation in natural waters are differential settling and shear. A batch titration of both settled and resuspended sediments demonstrated that metal ion binding increased with the size of organic colloids and therefore with floc volume. This behaviour is contrary to surface complexation theory which assigns binding to the surface of particles. This leads to the proposal that, as agglomeration occurs, the organic material acquires a polyelectrolyte property with a greater affinity for metal ions.

FUTURE WORK

Further experiments with the Couette flocculator could provide further evidence of the polyelectrolyte model. Marinsky (43) determined that a change in ionic strength results in a change in the indifferent ion concentration (See equation 28). This affects the proton concentration inside the polyelectrolyte domain which, in turn, affects the apparent stability constant.

$$p\{H^+\} + p\{Cl^-\} = p\{H^+\} + p\{Cl^-\} \qquad (28)$$

The polyelectrolyte model predicts a dependence of binding on ionic strength and a retardation of binding equilibrium due to diffusion inside the floc.

It would be useful to examine the binding in a polyelectrolyte for varying size and ionic strength. The basic procedure required is presented in a flow chart (See Figure III). We hypothesize that a decrease in binding with increasing ionic strength will occur. In addition, as the particles/polyelectrolyte increase in size, equilibrium will be further delayed. It is also expected that as the particle size increases, increased adsorption will occur due to larger particles.

A sediment suspended in a metal ion cocktail would be prepared at three different ionic strengths: low, medium, and high. The flocculator would be filled with one of the sediment suspensions and rotated at several different shear stresses. At each shear

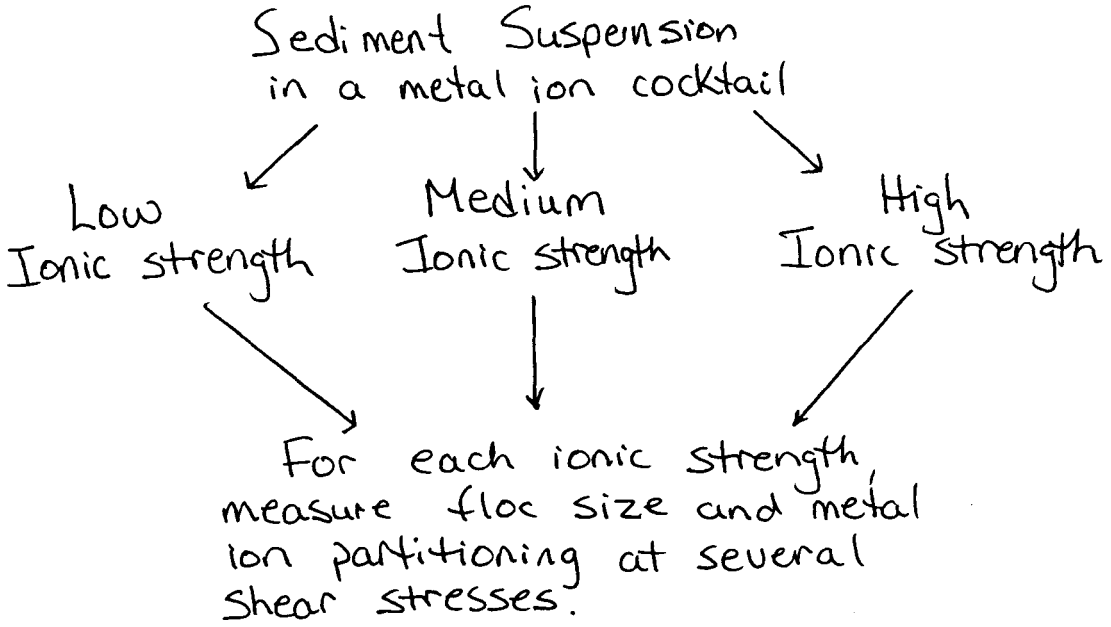

Figure III: Flow chart describing the procedure required to examine binding in a polyelectrolyte under varying size and ionic strength.

stress, photos and an aliquot of the filtrate would be taken at fixed time intervals for a fixed period of time. The photos would be used to determine the particle size distribution and ICP-MS analysis of the aliquots would be used to determine when equilibrium in the Couette flocculator was reached and at what metal ion concentration. The entire experiment would be repeated with the remained sediment suspensions at varying ionic strengths.

REFERENCES

(1) O'Melia, C. R. and Tiller, C. L. Physicochemical aggregation and deposition in aquatic environments. In: *Environmental particles, Volume 2.* J. Buffle, H. P. van Leeuwen (eds.) Lewis (publ.), **1993**, 353-386.

(2) Hunter, K. A., Microelectrophoretic properties of natural surface-active organic matter in coastal seawater. *Limnol. and Oceanogr.*, **1980**, 25(5), 807-822.

(3) MacCarthy, P., *Introduction: Aquatic humic substances and their influence on the fate and treatment of pollutants.* I. H. Suffet, P. MacCarthy (eds.) American Chemical Society (publ.), **1989**, xvii-xxx.

(4) Tipping, E. and Higgins, D. C., The effect of adsorbed humic substances on the colloid stability of haematite particles. *Colloids and Surfaces*, **1982**, 5, 85-92.

(5) Neihof, R. A. and Loeb, G. I., The surface charge of particulate matter in seawater. *Limnol. and Oceanogr.*, **1972**, 17(1), 7-16.

(6) Neihof, R. A. and Loeb, G. I., Dissolved organic matter in seawater and the electric charge of immersed surfaces. *J. Marine Res.*, **1974**, 32, 5-12.

(7) Davis, J. A. and Gloor, R., Adsorption of dissolved organics in lake water by aluminum oxide. Effect of molecular weight. *Environ. Sci. and Technol.*, **1981**, 15(10), 1223-1229.

(8) Tipping, E. and Cooke, D., The effects of adsorbed humic substances on the surface charge of goethite (α-FeOOH) in freshwaters. *Geochimica et Cosmochimica Acta,* **1982**, 46, 75-80.

(9) Loder, T. C. and Liss, P. S., Control by organic coatings of the surface charge of estuarine suspended particles. *Limnol. Oceanogr.*, **1985**, 30(2), 418-421.

(10) Tsai, C. H., Iacobellis, S., and Lick, W., Flocculation of fine-grained lake sediments due to a uniform shear stress. *Internat. Assoc. Great Lakes Res.*, **1987**, 13(2), 135-146.

(11) Lick, W. and Lick, J., Aggregation and disaggregation of fine-grained lake sediments. *J. Great Lakes Res.*, **1988**, 14(4), 514-523.

(12) van Duuren, F. A., Defined velocity gradient model flocculator. *Journal of the Sanitary Engineering Division*, **1968**, 94(SA4), 671-682.

(13) Burban, P. Y., Lick, W., and Lick, J., The flocculation of fine-grained sediments in estuarine waters. *Journal of Geophysical Research*, **1989**, 94(C6), 8323-8330.

(14) Smoluchowski, M., Versuch einer Mathematischen Theorie der Koagulations-Kinetik Kolloid Losungen. *Zeitschrift fur Physikalische Chemie*, 1917, 92 129-168.

(15) Hunt, J. R., Prediction of oceanic particle size distributions from coagulation and sedimentation mechanisms. In: *Particulates in water. Advances in Chemistry Series #189,* M. C. Kavanaugh, J. O. Leckie (eds.), American Chemical Society (publ.), **1980**, 243-257.

(16) Kavanaugh, M. C., Tate, C. H., Trussell, A. R., Trussell, R. R., Treweek, G., Use of particle size distribution measurements for selection and control of solid/liquid separation processes. In: *Particulates in water. Advances in Chemistry Series #189* M. C. Kavanaugh, J. O. Leckie (eds.), American Chemical Society (publ.), **1980**, 306-328.

(17) Filella, M. and Buffle, J., Factors controlling the stability of submicron colloids in natural waters. *Colloids and Surfaces A: Physicochemical and Engineering Aspects*, **1993**, 73, 255-273.

(18) Fu, G. and Allen, H.E., Cadmium adsorption by oxic sediment. *Water Research*, **1992**, 26, 225-233.

(19) Bourg, A.C.M. and Mouvet, C. A Heterogeneous Complexation Model of the Adsorption of Trace Metals on Natural Particulate Matter, in C.J.M. Kramer, J.C. Duinker (eds.), Complexation of trace metals in natural waters, Martinus Nijhoff/Dr. W. Junk, **1984**, pp. 267-278.

(20) Brassard, P., Macedo, E., and Fish, S. Diffusion and binding of protons in sediments. Submitted to *Environ. Sci. Tech.* (**1996**).

(21) Schindler, P. W., and Stumm, W., The surface chemistry of oxides, hydroxides, and oxide minerals. In: *Aquatic surface chemistry: chemical processes at the particle-water interface*. W. Stumm (ed), John Wiley and sons, **1987**, 83-107.

(22) Marinsky, J. A., A two-phase model for the interpretation of proton and metal ion interaction with charged polyelectrolyte gels and their linear analogs. In: *Aquatic surface chemistry: chemical processes at the particle-water interface*. W. Stumm (ed), John Wiley and sons, **1987**, 83-107.

(23) Marinsky, J. A., and Ephraim, J., A unified physicochemical description of the protonation and metal ion complexation equilibria of natural organic acids (humic and fulvic acids). 1. Analysis of the influence of polyelectrolyte properties on protonation equilibria in ionic media: fundamental concepts. *Environ. Sci. Technol.*, **1986**, 20, 349-354.

(24) Plese, T., and Zutic, V. J., Irregular patterns of polarographic maxima in surfactant dispersions. *Electroanal. Chem.*, **1984**, 175, 299-312.

(25) Ochs, M., Cosovic, B., and Stumm, W., Coordinative and hydrophobic interaction of humic substances with hydrophillic Al_2O_3 and hydrophobic mercury surfaces. *Geochimica et Cosmochimica Acta*, **1994**, 58(2), 639-650.

(26) DeMarco, R., Cattrall, R. W., Liesegang, J., Nyberg, G. L., and Hamilton, I. C., Surface studies of the silver sulfide ion selective electrode membrane. *Analytical Chemistry*, **1990**, 62, 2339-2346.

(27) Gulens, J., and Ikeda, B., Effects of surface heterogeneity on the sensitivity of sulfide ion-selective electrodes. *Analytical Chemistry*, **1978**, 50(6), 782-787.

(28) Bu, H., Mikkelsen, S. R., and English, A. M., Characterization of a ferrocene-containing polyacrylamide-based redox gel for biosensor use. *Analytical Chemistry*, **1995**, 67, 4071-4076.

(29) Brassard P., Kramer, J., and Collins P. V., Dissolved metal concentrations and suspended sediment in Hamilton Harbour. Submitted to *Journal of Great Lakes Research* (**1996**).

(30) Sekerka, I., and Lechner, J. F., Preparation and evaluation of halide ion-selective electrodes based on HgS matrices. *Journal of Electroanalytical Chemistry*, **1976**, 69, 339-344.

(31) Sekerka, I., and Lechner, J. F., Behaviour of ion selective electrodes based on silver or mercuric sulfide selenide and telluride matrices. *Analytical Letters*, **1976**, 9(12), 1099-1110.

(32) Hunter, K. A., and Liss, P. S., The surface charge of suspended particles in estuarine and coastal waters. *Nature*, **1979**, 282, 823-825.

(33) Davis, J. A., Complexation of trace metals by adsorbed natural organic matter. *Geochimica et Cosmochimica Acta*, **1984**, 48, 679-691.

(34) Fu, G., Allen, H. E., and Cowan, C. E., Adsorption of cadmium and copper by manganese oxide. *Soil Science*, **1991**, 152(2), 72-81.

(35) Milne, C. J., Kinniburgh, D. G., De Wit, J. C. M., Riemsduk, W. H., and Koopal, L. K., Analysis of proton binding by a peat humic acid using a simple electrostatic model. *Geochimica et Cosmochimica*, **1995**, 59(6), 1101-1112.

(36) Taylor, G. I., Stability of a viscous liquid contained between two rotating cylinders. *Philosophical transactions*, Royal Society, Series A, **1923**, 223, 289. In: van Duuren, (12).

(37) Filella, M., Buffle, J., and Leppard, G. G., Characterization of submicrometre colloids in freshwaters: Evidence for their bridging by organic structures. *Water Science and Technology,* **1993**, 27(11), 91-102.

(38) Tessier, A., Sorption of trace elements on natural particles in oxic environments. In: *Environmental Particles, Volume 1.* J. Buffle and H. P. van Leeuwen (eds), Lewis (publ.), **1992**, 425-453.

(39) Balistrieri, L. S., and Maare, J. W., The surface chemistry of sediments from the Panama Basin: The influence of M oxides on metal adsorption. *Geochimica et Cosmochimica Acta*, **1986**, 50, 2235-2243.

(40) Baes, C. F., and Mesmer, R. E., *The hydrolysis of cations.* John Wiley and Sons-(publ.), **1976**, 489 p.

(41) Balistrieri, L. S., Maare, J. W., and Paul, B., The geochemical cycling of trace elements in a biogenic meromictic lake. *Geochimica et Cosmochimica Acta*, **1994**, 58(19), 3993-4008.

(42) Honeyman, B. D. and Santschi, P. H., A Brownian-pumping model for oceanic , trace metal scavenging: evidence from Th isotopes. *J. Mar. Res.*, **1989**, 47, 951-992.

(43) Marinsky, J. A., Alternate interpretation of the change observed in H^+ ion concentration levels of the aqueous medium of metal oxide suspensions in resonse to change in the electrolyte concentration levels of the aqueous medium. *J. Phys. Chem.*, **1996**, 100, 1858-1866.

APPENDICES

Appendix A: **Slope and y-intercept values for cadmium ISE calibration without a membrane.**

Exposure conditions	slope (stnd error)	y-intercept (stnd err)
no exposure, no membrane	29.5 (0.8)	-79.6 (1.6)
no exposure, membrane	27.8 (0.4)	-85.4 (0.8)
pH 5, 5 minutes	28.7 (0.7)	-83.2 (1.4)
pH 4, 1.25 hours	25.3 (1.2)	-82.4 (2.4)
pH 5, 2.0 hours	20.4 (3.1)	-96.7 (6.4)
pH 6, 3.0 hours	12.5 (5.6)	-116.8 (11.7)
pH 4, 3.5 hours	5.0 (5.2)	-127.5 (10.8)

Appendix B: Experimental details for batch settling and resuspension experiments

Sediment stock was diluted to 3 g L^{-1} in 0.01 M $NaNO_3$, and spiked with 10^{-4} M Cd^{2+}. 100 mL portions were acidified with 0.1 N HCl over a range of pH from 3 to 8. Similar solutions containing 0.01 M $NaNO_3$, 10^{-4} M Cd^{2+}, and dd H_2O (in place of sediment) were also prepared as blanks. Two sets of 15 sediment solutions and 7 blanks were mixed well on a rotary shaker for 20 min and allowed to settle for 24 hours. The supernatant was decanted from one set and the second set was resuspended for 8 hours. The pH and Cd of both the supernatant and the resuspended solutions were measured with electrodes. An aliquot was collected by reverse filtration. The free and organic cadmium were determined for both sets of filtrates, in duplicate, by atomic absorption spectroscopy (AAS) and the dissolved organic carbon (DOC), in triplicate, by perchloric acid digestion followed by IR adsorption of carbon dioxide.

APPENDIX C: Experimental details for Couette flocculator experiments

Floc aggregation/disaggregation analysis

The flocculator was filled with 120 mL a 1 g L^{-1} sediment suspension and was then operated at full speed (10 dynes/cm^2) for at least 15 minutes. A series of 8 photos was taken. The intensity of corresponding pixels from each photo were averaged to produce a background photo. Next, the flocculator was slowed to the test shear stress. Photos were taken over a period of two hours at 0, 15, 30, 45, 60, 90, and 120 minutes. When the photos were completed, the flocculator was increased to full speed again to break up the flocs, then slowed to the new test speed. This entire process was repeated for four shear stresses: 1.6, 2.2, 3.3, 4.4 dyne/cm^2.

Analysis of metal ion binding under shear stress

System calibration

Sediment metal ion background determination: The flocculator was filled with 120 mL of a 0.1 g/L sediment stock. After running the flocculator at several shear stresses (1.6, 2.2, 3.3, 4.4 dyne/cm^2) for 1 hour, samples were taken from each port, with Hamilton city tap water as the replacement fluid. 10 mL of replacement fluid was allowed to flow into the flocculator and 5 mL was collected from each exit port. A general ICP-MS scan was

performed in order to determine the levels of metal ions naturally present in the sediment suspension and the Couette flocculator background.

Metal ion concentration drift with speed: Next, the flocculator was filled with a metal ion cocktail. Each metal was at 100 ppb in deionized, distilled water (Cocktail A: Si, Ca, Fe, Cd, Mg, M, Ti, Al, Sr (100 ppb), Na (160 ppb)). The flocculator was sampled after one hour of rotation at four different shear stresses: 1.6, 2.2, 3.3, and 4.4 dyne/cm^2. At each speed, both filter ports were sampled independently. 10 mL of replacement cocktail was allowed to flow into the flocculator and 5 mL was collected from each exit port. A semi-quantitative ICP-MS scan was performed.

Metal ion concentration drift with time: The flocculator was filled with a metal ion cocktail containing 50 ppb of Si, Ca, Zn, Fe, Cd, Mg, Cu, M, Ti, Al, Sr, and Ni, and 80 ppb of Na (Cocktail B) in deionized distilled water. The flocculator was set to rotate with a shear stress of 2.2 dyne/cm^2, and both filter ports were sampled separately over 15 minute intervals for 1.75 hours by allowing fresh cocktail to be pulled by gravity into the flocculator as the filtrate dripped out of each hole over the time interval. A sample from each hole was also collected after 4.5 and 24 hours of rotation at this speed. A quantitative ICP-MS scan was performed.

Metal ion binding analysis

The flocculator was filled with 120 mL of a 1 g L^{-1} sediment suspension in a matrix

of metal ion cocktail B at 500 ppb at pH 7.3. The flocculator was rotated at a shear stress of 2.2 dyne/cm^2 for 120 minutes. Then, a picture and a 5 mL aliquot of the filtrate were taken as described previously, the first to determine floc size, the second to determine metal ion partitioning. Filtration proceeded slowly (10 mL/hr) to minimize particle entrapment on the filter surface. This filtrate was simultaneously replaced with deionized, distilled water. After each experiment, the shear stress was increased to 10 dyne/cm^2, and then lowered to the new shear stress. This process was repeated at 1.6, 1.9 and 4.4 dyne/cm^2.

APPENDIX D: **Metal ion concentrations and relative error for cocktail A for six different shear stresses.**

Metal ion	0.7 dyne cm^2	1.1 dyne cm^2	1.6 dyne cm^2	2.2 dyne cm^2	3.3 dyne cm^2	4.4 dyne cm^2	Avg. Conc. (ppb)	Relative Error %
Al	100	99	112	111	102	113	106	6.1
Ca	120	98	143	122	112	539	189	5.7
Cd	89	87	83	88	80	114	90	6.0
Fe	87	78	182	229	226	227	171	4.8
Mg	100	93	104	104	99	179	113	5.7
M	96	93	94	86	93	88	91	5.3
Na	205	144	267	142	68	739	261	8.3
Si	98	135	116	114	105	144	119	28.7
Sr	88	91	87	89	85	93	89	5.1
Ti	83	80	68	70	69	80	75	6.1

Appendix E: **Meal ion concentrations and relative error for cocktail B over 24 hours.**

Metal ion	Time: 15 min	Time: 30 min	Time: 45 min	Time: 60 min	Time: 75 min
Al	64	63	67	64	67
Ca	397	233	285	299	366
Cd	64	57	61	56	58
Cu	60	59	57	58	58
Fe	41	42	38	43	45
Mg	75	64	63	74	84
M	48	51	55	53	54
Na	322	153	151	155	149
Ni	92	86	87	84	83
Si	95	92	73	82	82
Sr	48	53	56	50	51
Ti	39	41	39	40	39
Zn	120	95	128	98	108

Appendix E continued...

Metal ion	Time: 90 min	Time: 105 min	Time: 4.5 hours	Time: 24 hours	Average Conc. (ppb)	Relative Error %
Al	66	71	78	88	66	9
Ca	447	481	556	630	316	12
Cd	56	56	61	58	56	7
Cu	62	63	72	35	59	8
Fe	51	57	111	460	87	13
Mg	97	97	121	130	79	9
M	56	56	57	62	53	8
Na	145	119	240	194	138	13
Ni	83	81	91	99	80	9
Si	78	67	72	103	78	10
Sr	52	53	55	55	52	8
Ti	36	33	26	13	35	9
Zn	124	138	178	332	131	9